ITTC2024

30TH INTERNATIONAL TOWING TANK CONFERENCE
22–27 SEPTEMBER 2024 | HOBART TASMANIA AUSTRALIA

Report of the Seakeeping Committee

SEAKEEPING COMMITTEE

1. INTRODUCTION

1.1 Membership and meetings

The Committee appointed by the 29th ITTC consisted of the following members:

- Frederik Gerhardt (Chairman), RISE, Gothenburg, Sweden;
- Ole Andreas Hermundstad (Secretary), SINTEF Ocean, Trondheim, Norway;
- Benjamin Bouscasse, École Centrale de Nantes (ECN), Nantes, France;
- Kay Domke, Schiffbau Versuchsanstalt Potsdam (SVA), Potsdam, Germany;
- WenYang Duan, Harbin Engineering University (HEU), Harbin, China;
- Bertrand Malas, École Centrale de Nantes (ECN), Nantes, France;
- Munehiko Minoura, Osaka University, Osaka, Japan;
- Bo Woo Nam, Seoul National University, Seoul, Korea;
- Yulin Pan, University of Michigan, Ann Arbor, USA;
- Antonio Souto-Iglesias, Universidad Politécnica de Madrid (UPM), Madrid, Spain.

Two in-person meetings were held:

- SSPA Maritime Center, Gothenburg, Sweden, June 2023
- Escuela Técnica Superior de Ingenieros Navales (ETSIN), Madrid, January 2024

In addition, 12 video teleconferences were held in the time-period of November 2021 to June 2024.

1.2 Terms of Reference given by the 29th ITTC

The Seakeeping Committee is primarily concerned with the behaviour of ships underway in waves. The Ocean Engineering Committee covers moored and dynamically positioned ships. For the 30th ITTC, the modelling and simulation of waves, wind and current is the primary responsibility of the Specialist Committee on Modelling of Environmental Conditions, with the cooperation of the Ocean Engineering, the Seakeeping and the Stability in Waves Committees.

1. Update the state-of-the-art for predicting the behaviour of ships in waves, emphasizing developments since the 2021 ITTC Conference. The committee report should include sections on:
   - the potential impact of new technological developments on the ITTC new experiment techniques and extrapolation methods
   - new benchmark data

- the practical applications of numerical simulation to seakeeping predictions and correlation to full scale
- the need for R&D for improving methods of model experiments, numerical modelling and full-scale measurements.

2. Review ITTC Recommended Procedures relevant to seakeeping procedures, and
   - identify any requirements for changes in the light of current practice, and, if approved by the Advisory Council, update them
   - identify the need for new procedures and outline the purpose and contents of these.
3. Create a new guideline on verification and validation of the CFD methods for seakeeping analysis. For example, finite-volume-based methods and particle methods which solve RANS and LES, for seakeeping procedures, collaborating with the Specialist Committee on Combined CFD/EFD Methods and taking existing procedures for verification and validation of CFD methods into account.
4. Investigate the functionality of Procedure 7.5-02-07-02.8, Calculation of the Weather Factor *fw*, when applied to ships smaller than 150 m in length, and provide any method to improve the current procedure for small ships.
5. Investigate if there is any practical problem in the application of MEPC.1/Circ.850/ Rev.2 for minimum power requirement, and develop a new ITTC guideline, if needed.
6. Develop a guideline for wind loads for ships, collaborating with the committees related to this issue, particularly the Ocean Engineering Committee, the SC on Renewable Ocean Energy, Manoeuvring Committee and the Full-Scale Performance Committee.
7. Organize a benchmark experimental campaign, including the added resistance measurement in oblique seas and different loading conditions, and the characterization of the uncertainty in the measurement of added resistance.
8. Survey the state of the art for the acquisition and analysis in on-board and/or real-time seakeeping data, and investigate the need of ITTC activities, including future issues related to autonomous vessels.
9. Collaborate with Manoeuvring Committee for the development of guidelines related to manoeuvring in waves.

2. STATE OF THE ART

2.1 New Experimental Facilities

2.1.1 Boldrewood Towing Tank, Southampton

The University of Southampton Boldrewood Towing Tank became fully operational in February 2022, as reported by Malas et al. (2024). The tank, which is used for teaching, research and commercial activities, is 138 m long, 6 m wide and 3.5 m deep and equipped with a 12 paddle HR Wallingford wavemaker capable of generating regular and irregular waves with a maximum height of 0.70 m and a significant wave height of 0.37 m respectively. It also has the capability of generating oblique waves and to run in active absorption mode.

The tank carriage is driven by two winches and two cables located at both ends of the facility and is capable of speeds up to 10 m/s and 8 m/s in the East/West and West/East directions respectively.

The tank is also equipped with a parabolic end beach for waves absorption and an automatic side beach that can be deployed within seconds after pressing the on/off button on the side of the tank or on the carriage. The side beach is left deployed for calm water experiments and is deployed and retracted between seakeeping runs to reduce the waiting time and therefore increase the facility productivity.

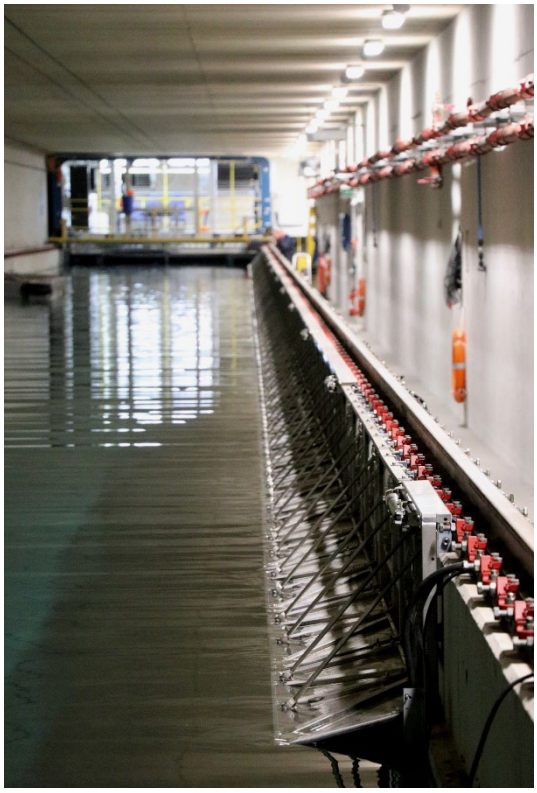

Figure 1: View of the deployed automatic side beach at Boldrewood towing tank (Malas et al. 2024).

The facility is also equipped with an underwater 500 kg lifting platform located at 10 m from the wavemaker. This can be used for static moored experiments where the quality of waves is best and available experimental time is optimum.

2.1.2 Coastal and Ocean Basin (COB), Ostend

The basin, part of the Flanders Maritime Laboratory in Ostend, and with ties to Ghent University, was fully commissioned in 2023. The facility is 30x30 m, with a variable water depth ranging from 0 to 1. 4 m. A 4 m deep central pit is also present. The facility is equipped with a 20x20 m Van Halteren L-shaped piston wavemaker capable of generating waves up to 0.55 m in multiple directions. On the opposite sides are located rock-based absorption beaches. A current generation system is also scheduled to be installed, with a speed up to 0.4 m/s.

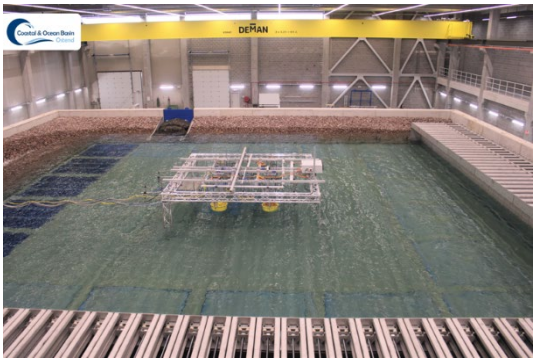

Figure 2: View of the COB (https://www.ugent.be/ea/civil-engineering/en/research/coastal-bridges-roads/coastal-engineering/cob-ugent/wecfarm-1).

2.1.3 Technology Centre for Offshore and Marine (TCOMS), Singapore

The TCOMS large ocean basin was open in July 2022. The basin is 60x48 m with a depth of 12 m and a 10 m diameter central pit reaching a depth of 50 m. The facility is equipped with 180 flaps L-shaped Edinburgh Design wavemaker on two sides, capable of generating waves up to 1.0 m. On the other sides are located deployable absorption beaches. An X/Y instrumented carriage is also present. This carriage can reach speeds up to 2 m/s and 4 m/s in the longitudinal and transverse directions respectively. A current generation system can produce six layers of inflow with maximum near surface current of 0.5 m/s and has the capability to produce variable current profiles such as uniform and shear currents. The water depth of the basin can be varied from 0 to 12 m, as required based on the test set-up to cater to deep-water or shallow-water studies, by adjusting the elevation of the movable floor.

Figure 3: View of the TCOMS ocean basin (https://news.nus.edu.sg/tcoms-opens-ocean-basin-facility/).

2.1.4 Virginia Tech Towing Tank

The Virginia Tech towing tank was commissioned in the 1960s. The facility is 30 m long, 1.8 m wide and 2.7 m deep. As reported by Gilbert et al. (2023), the original Kempf and Remmers carriage was recently replaced by a modern one supplied by Edinburgh Design with the support of Donald L. Blount Associates. The new carriage is driven by electric motors and belts and is capable of a maximum speed of 7.0 m/s (compared to the original 3.0 m/s).

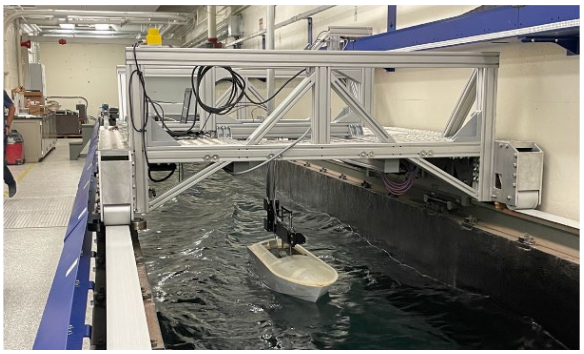

Figure 4: View of the new towing carriage at Virginia Tech (Gilbert et al. 2023).

Comparative resistance experiments were performed against past experiments and showed that measured resistance, heave and pitch are higher than previous results. Investigations are ongoing.

A Vertical Planar Motion Mechanism (VPMM) is planned to be installed allowing to perform controlled slamming as well as vertical motions manoeuvring experiments. The facility wavemaker is also anticipated to be replaced in the coming years.

2.1.5 CSSRC Seakeeping and Manoeuvrability Basin

The new Seakeeping and Manoeuvring Basin (SMB) at CSSRC was opened in late 2021, Figure 5. With dimensions of 170×47×6 m (length × width × water depth), it is typically used for manoeuvring and seakeeping tests. The carriage spanning the basin can move in the X direction at a maximum speed of 5.0 m/s and in the Y direction at a maximum speed of 4.0 m/s. The basin is equipped with flap-type wave makers along two adjacent sides and adjustable wave-absorbing beaches along the two opposite sides. Regular waves can be generated with periods ranging from 0.5 to 5.0 seconds and a maximum wave height of 0.58 m, while irregular waves can reach a significant wave height of 0.45 m.

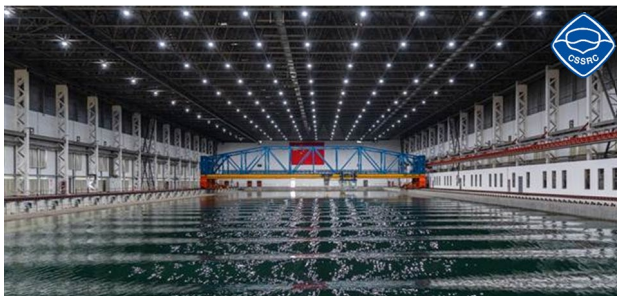

Figure 5: V The new Seakeeping and Manoeuvring Basin at CSSRC (Photo: CSSRC).

2.2 Experimental Techniques

2.2.1 Measurement of roll motion

Subramaniam et al. (2021) investigated trapped deck water and its effect on the roll dynamics of an offshore supply vessel by free-running model tests. The test setup combines measurements with pressure sensors and of motions by an optical fibre gyroscope. Additionally, cameras were used to monitor the deck water motion. The pressure sensor and camera setup is shown in Figure 6. Roll damping is evaluated by determining the phase difference between the ship roll and the deck water motion. Therefore, frequency-domain analysis is best suited for irregular wave situations, where the spectra of the signals from the gyroscope and the pressure sensors are compared to identify the phase relationship between peaks in the spectrum. The analysis of the ship roll and deck water motion points to damping within the operational speed range in regular as well as irregular waves. Furthermore, the investigations show that at higher Froude numbers the positive damping effect is reduced.

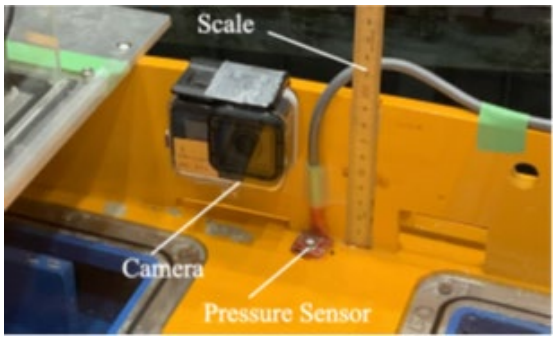

Figure 6: Arrangement of the pressure sensor and camera (Subramaniam et al. 2021).

Wang et al. (2023d) investigated the sloshing effect at model scale tests by a large LNG carrier model outfitted with three partially filled prismatic tanks. They analysed sloshing behaviour and model motions for different equal filling levels as well as different filling levels inside the tanks at different exciting wave periods. The roll, pitch and heave motions were measured by an attitude and heading reference system with 50 Hz and an error tolerance of 0.04° in normal temperature. It is pointed out that using different tank fillings at the same time will lead to a strong reduction in roll amplitude especially at the roll natural period of the ship motion. This effect is caused by one more natural period of sloshing inside the tanks.

For investigating extremes on a floating hinged raft wave energy converter Jin et al. (2022) used the application of short design waves. A 1:50 scale two-body hinged raft wave energy converter model was built. The test setup is presented in Figure 7. The main objective of measuring the relative hinge angle was demonstrating the application of short design wave on the floating structure. This was measured with a rotary sensor. The aim was to investigate four types of short design waves experimentally. They pointed out that response conditioned design waves have a good performance for generating extremes on a floating structure and that the setup used is suitable for further investigations.

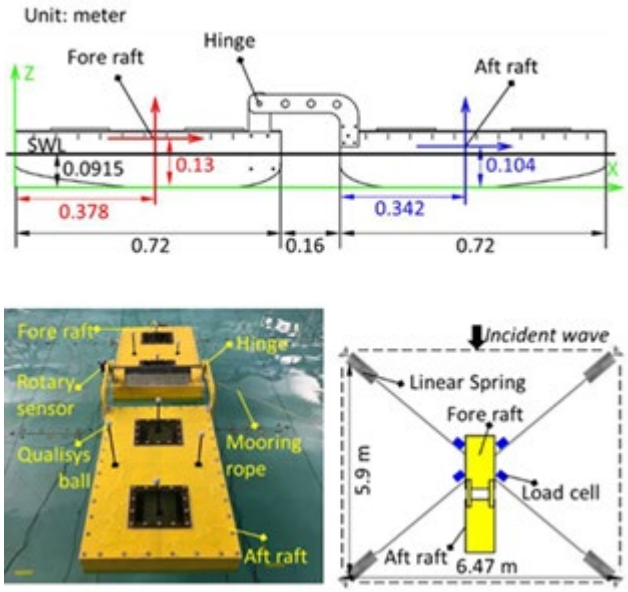

Figure 7: Test setup and arrangement for investigations on a wave energy converter (Jin et al. (2022).

2.2.2 Instrumentation, measurement technologies and machine learning support

Suzuki et al. (2023) developed a method for measuring and analysing the spatial pressure distribution over the ship-hull surface using many Fibre Bragg Grating (FBG) pressure sensors to obtain experimental data on the details of the flow induced by the ship disturbance. In their work they analysed the improvements installed in version 7 of the sensor, which are increase of rigidity of the ring frame, the installation of a stainless steel-frame on the diaphragm and the adoption of the glass soldering method at both ends of the optical fibres in the pressure sensitive part. FBG is a diffraction grating embedded into a fibre core that reflects a particular wavelength of light. The reflected wavelength is called the Bragg wavelength. Deformation resulting from pressure leads to spacing between the reflectors and so the Bragg wavelength changes, too. The amount of change in this Bragg wavelength is used to estimate the pressure. The principle of FBG and of the FBG pressure sensor is shown in Figure 8. The authors have shown that version 7 of the FBG pressure sensors was significantly improved in respect to temperature interference

effects compared to version 6. Furthermore, they showed that the effect of temperature interference depends on the material of the ship model and recommend material with low thermal conductivity. It was also pointed out that the measurement accuracy of steady pressures is not as good as that of the strain-type pressure sensor due to the sensor thickness.

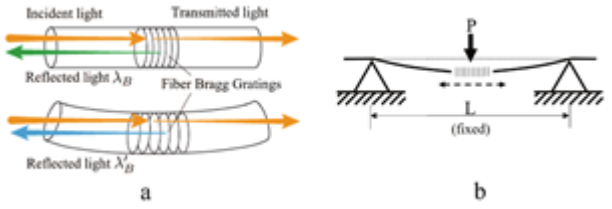

Figure 8: Schematic representation of a) Principle of FBG, b) Principle of the FBG pressure sensor used by Suzuki et al. (2023).

Ma et al. (2023) measured and illustrated the wet deck slamming for a SWATH cross-section model using PIV and pressure measurements. The instrumentation with a sampling frequency of 20 kHz at overall 15 positions and 3 different kind of pressure sensors regarding the measurement range as well as 1 kHz PIV measurement with adjustable camera exposure time was used. The measurement was started by a trigger impulse-based release of the model, which was held by a steel truss attachment at the model and an electromagnet. The analysis of three initial water-entry velocities focused on the fluid field, slamming pressure, and air cushion effect during the wet deck slamming.

For the investigation of turning circles in waves, Stern et al. (2022) analysed CFD and experimental data. For a detailed comparison of the investigated tuning circles, they introduced a transformation which uses the wave drift distance H_D and direction μ_D. This leads to a collapse of the trajectories onto a single circle.

The application of Machine Learning (ML) and Artificial Intelligence (AI) techniques has recently become a contentious issue. Current publications show promising application possibilities and only hint at the extent to which their influence will increase in the upcoming years.

Nielsen et al. (2023) used ML-based methods to explore and determine the relation between waves and wave-induced ship responses entirely through data. This method was compared to an experimental physics-based data evaluation. The advantage of the ML-method is that transfer functions are not needed, and all associated uncertainties are thus removed. On the other hand, the data input values need to be as good as possible which requires very high-quality sensors. The authors present a good correlation between ML and physics-based method. Furthermore, they show that ML-based methods have wide and large potential but the complexity of the system being considered makes the use of ML delicate, and the generalisation of the results must be made with care. As part of the problem, the quality of ship telemetry data is low. A fallback framework is recommended from the actual point of view.

2.2.3 Hydroelastic ship models and structural loads

Kim et al. (2023b) investigated the influence of mooring lines at an experimental setup with a 9-segmented model in -120° oblique regular waves without forward speed. Experiments with and without a mooring system under the same wave condition were conducted; see Figure 9. They qualitatively confirmed that the mooring system's restoring moment correlates with the asymmetric horizontal bending moment and average yaw movement change.

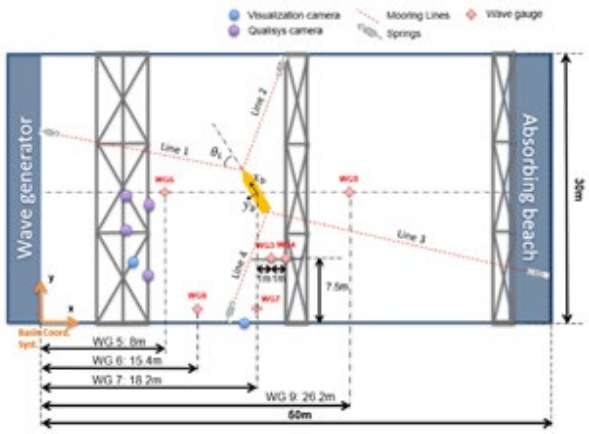

Figure 9: Experimental setup for segmented model tests with mooring lines used by Kim et al. (2023b).

Tang et al. (2022) used a segmented model with the backbone of an ultra large container ship over 300 m. They presented the design and calibration procedure of the segmented ship model with a variable cross-section backbone beam. They introduced the application and the conversion from the signals of strain to the bending moments by calibration. With the setup they investigated the transfer function of vertical bending moments at different Froude numbers and wave headings as well as analysing phase differences between wave frequency and high-order harmonics in extreme waves.

2.3 Numerical Methods

The research of recent years numerical methods on ship seakeeping can be divided into three aspects. The potential flow numerical method, viscous flow numerical method and potential flow viscous flow coupled numerical method.

2.3.1 The Potential flow numerical method

2.3.1.1 Linear free surface potential flow BEM method

The boundary element method (BEM) based on the potential flow theory is the main computational method to linear free surface ship seakeeping problem.

Chen et al. (2021a) proposed a three-dimensional unsteady potential flow numerical method to solve the seakeeping of ships in waves. The flow field is divided into inner and outer regions by artificial matching surface. The inner domain includes the wet body surface, the matching surface and the free surface of the inner region near ship; The outer region includes matching surface, outer region free surface and far field boundary. Using impulse response function, the boundary integral equation of the inner and outer domains is established and solved by Taylor expansion boundary element method (TEBEM). The hydrodynamic coefficients of different ships at different forward speeds are calculated, and the accuracy of the numerical results is verified by the experimental data. TEBEM method has also been used to study propeller propulsion performance in waves. Duan et al. (2022a) proposed a fast and effective calculation method for predicting ship speed and power in head waves based on TEBEM.

Song et al. (2022) developed a 3D time-domain desingularized Rankine panel (DRP) method based on near-field and mid field theories to calculate the wave added resistance of ships in regular waves. By comparing with experimental data, it is shown that the numerical method can accurately calculate the ship wave added resistance.

Li et al. (2023b) established a numerical model of multi-ship hydrodynamic interaction in waves based on the Rankine source element method in the time domain. He et al. (2023) proposed a set of boundary integral methods for wave diffraction-radiation problems applicable to offshore structures or ships sailing in regular waves. It can effectively calculate the influence coefficients in the Rankine source and Fourier component.

Zhang et al. (2023c) established a three-dimensional frequency domain seakeeping calculation model based on Rankine surface element method and calculated the wave drift force and moment acting on a ship with forward

speed. Chen et al. (2022) proposed a numerical simulation method for the hydroelastic response of very large floating structures (VLFS) in focused waves. The modal expansion method is used to decouple the fluid-structure coupling problem. The high order boundary element method for the fluid dynamics problem is solved in the frequency domain and a finite element model is used for the structural analysis.

Lu et al. (2023) proposed a time-domain hydroelastic analysis method considering the asymmetric slamming on ships and adopted the three-dimensional Rankine surface element method to solve the problem of ship seakeeping, and the modified Logvinovich model (MLM) is used to calculate the asymmetric slam load of a 21000 TEU container ship.

2.3.1.2 Nonlinear potential flow numerical method

When the incident wave is highly nonlinear, it is necessary to develop the corresponding nonlinear potential flow calculation method to calculate the motion response more accurately.

Tang et al. (2021b) calculated the motion characteristics of container ships in irregular waves based on the fully nonlinear time-domain potential flow theory. Lin et al. (2021) established a fully nonlinear potential flow (FNPF) numerical model to simulate nonlinear water wave interaction problems. Wang et al. (2021a) simulated irregular sea waves with different breaking strength based on the FNPF program. Irannezhad et al. (2022) calculated ship motion response and resistance based on FNPF. The ship motion characteristics near resonant frequencies in waves are studied.

Liang et al. (2023) established a two-dimensional fully nonlinear numerical wave tank based on the higher-order boundary element method. The second order harmonic displacement of large-scale elastic plate near the second order natural frequency is calculated. Zhang et al. (2023b) developed a fully nonlinear potential flow theory based on the Rankine source method to calculate the motion response and wave added resistance of ships. By calculating the radiation, diffraction and motion responses of Wigley hull and S-175 container ship, it is shown that the fully nonlinear method can better predict the peak of ship motion response and wave added resistance.

In the calculation of potential flow problem, the singularity at the corner of the body surface will lead to the wrong pressure integral. In nonlinear potential flow problems, the singularity occurs at corner points for the higher order derivatives. Qian and Teng (2023) proposed a coupling method combining scaled boundary finite element method (SBFEM) and finite element method (FEM) to solve this problem. SBFEM can provide an accurate and effective direct pressure integral for second-order wave forces.

Hanssen and Greco (2021) propose a fully nonlinear numerical method based on potential flow theory to study the two-dimensional interaction between water waves and body. The velocity potential and its time derivatives are calculated by solving Laplace equation with Harmonic Polynomial Cell (HPC) method. At the same time, it uses the immersion boundary method to simulate moving boundaries. The method is verified and analysed for wave propagation, forced heave motion of semi-submersible cylinders, and stationary and free-moving floating bodies in beam waves.

Xu et al. (2023b) developed a fully nonlinear potential flow solver based on high order finite difference to calculate nonlinear wave loads on ocean structures. All boundary conditions were treated by immersion boundary method. The nonlinear wave load on a cylinder with forced heave motion on the water surface is analysed.

Takami et al. (2023) combined the HOS (High-Order Spectral) method with the first-order Reliability method (FORM) and applied it to the prediction of the linear and nonlinear wave response of ships in nonlinear waves. Chen et al. (2023a) used a HOS method coupled

with a fully nonlinear hydrodynamic solver (HOS-FNL) to simulate the interaction between waves and structures in nonlinear waves.

Shi and Zhu (2023) proposed a nonlinear time-domain simulation method. In this method, the overlapping grid method is used to track the ship motion. The hydrodynamic characteristics of Wigley and Series 60 sailing at different speeds were calculated. Zhang et al. (2024) studied the motion response and wave loads on semi-submersible platforms under different wave steepness by using a fully nonlinear potential flow calculation method.

2.3.2 The viscous flow numerical method

2.3.2.1 Free surface flow algorithm

For the seakeeping problem, how to accurately and effectively capture the water-gas interface with a large density ratio, especially the interaction between strong nonlinear waves and ships involves complex physical phenomena such as wave slamming and breaking, and droplet splashing, are the difficulty of viscous flow numerical method research problem.

Li et al. (2022a) used the hybrid method of THINC/QQ-SF and HRIC to capture the details of wave breaking around a forward speed ship. This method can calculate ship resistance with less numerical dissipation.

Ferro et al. (2022) developed a solver (MarineFOAM) that combines the VOF method with the Ghost Cell method to deal with the discontinuity of the free surface. It is shown that this method can be used for larger Courant number in numerical simulation, while avoiding the free surface oscillation.

Chatzimarkou et al. (2022) proposed the coupled Level-set and VOF method (CLSVOF). The VOF method is used to track and reconstruct the free surface, which guarantees the conservation of mass. At the same time, Level Set function is used to calculate the geometric parameters (normal vector, curvature, etc.) of the free surface, so that the surface tension can be calculated accurately. The free surface turbulence damping (FSTD) boundary conditions are added to limit the overprediction of turbulence near the free surface. Simulations of wave breaking are in good agreement with experimental results. Chen and Chen (2023) improved CLSVOF to solve the problem of non-uniform interface on the boundary. It is shown that the improved method can better simulate the green water and droplets splashing phenomena.

Meshless methods are based on Lagrange description, which is very suitable for dealing with large deformation problems. The movement of particles along with the interface makes it possible to automatically track the multiphase interface. The advantage is that it can accurately capture the droplet phenomenon caused by breaking waves. Zhong et al. (2023) show that an SPH method can accurately calculate the hydrodynamic characteristics of a ship hull and can better track droplet splash details. Salis et al. (2024) studied the dynamic interaction between focused waves and mooring and structural based on a three-dimensional SPH method coupled with multi-body solvers.

To improve computational efficiency of the SPH method, Liu et al. (2023a) proposed a coupling algorithm based on SPH and finite difference. Through the calculation domain decomposition, the near field adopts SPH method to simulate the flow with severe deformation of the free surface, while the far field adopts the finite difference method to reduce the calculation load of SPH and increase its calculation efficiency. The Euler solution and Lagrange solution are coupled to each other by interpolating in the near and far field overlapping region. The algorithm has good accuracy, convergence and applicability. Di Mascio et al. (2021) conducted a three-dimensional simulation based on the coupling of SPH and finite volume method, for ship's bow waves breaking.

Zhang et al. (2021c) developed an ISPH_QSFDI solver based on the second order semi-analytic finite difference interpolation scheme (QSFDI) to discrete Laplacian operator and applied it to the simulation of wave propagation and wave impact on structures. The results show that ISPH_QSFDI is more accurate and requires less computation time compared to alternative schemes but at slower convergence. Zhang et al. (2023a) combined convolutional neural network (CNN) with ISPH method to calculate fluid pressure without solving Poisson equation. Through the parameter training, the calculation results show that the solver can maintain high calculation accuracy with large particle number.

Chen et al. (2024) proposed an adaptive SPH algorithm based on multi-GPU acceleration. Through a series of optimization algorithms, the computational efficiency of SPH method in multi-GPU parallel computing is improved.

2.3.2.2 Fluid structure interaction

Ship hydroelasticity simulation by coupling the viscous flow numerical algorithm with the finite element analysis method is the typical fluid structure interaction problem in seakeeping research.

Jiao et al. (2021a, 2021b) and Wei et al. (2023) proposed a CFD and FEA two-way coupling numerical method for calculating the nonlinear hydroelasticity response of ships sailing in waves. The external fluid pressure derived from the CFD simulation is used to calculate the structural response in the FEA structure solver, while the structural deformation is transferred to the CFD solver to deform the mesh. By calculating the hydrodynamic characteristics of the container ship S175, it is shown that the coupling method can accurately simulate seakeeping and hydroelasticity characteristics.

2.3.3 Potential flow and viscous flow coupled numerical method

The advantage of the potential flow method is that the calculation speed is fast. However, the effect of fluid viscosity is ignored in the potential flow formulation, so the computational accuracy for seakeeping problem is limited. The viscous flow numerical method can simulate the real flow field environment considering viscosity, and the calculation accuracy is high. But the computing speed is slow.

Therefore, the potential flow and viscous flow coupled numerical method has been developed in recent years. The coupling of potential flow and viscous flow algorithm expands the engineering application range of potential flow algorithm, saves more computing resources and speeds up the calculation compared with viscous flow algorithm.

Li et al. (2021) investigated SWENSE (Spectral Wave Explicit Navier-Stokes Equations) method which was coupled with HOS method through wave velocity decomposition in OpenFOAM and applied to the numerical simulation of wave-structure interaction. Zhang et al. (2021d) used SWENSE method to study the wave added resistance and seakeeping of KVLCC2. The calculation results show that this method can predict the wave added resistance and seakeeping of ships in irregular waves. Yu et al. (2023b) developed a new solver, HUST-SWENSE, which uses dynamic structure grid superposition technology to deal with four-DoF motion of ship. The motion of surge, heave, roll and pitch of KCS ship in regular oblique waves are numerically simulated.

Zhuang and Wan (2021) proposed a method by coupling the potential flow HOS method with the viscous flow solvers naoe-FOAM-SJTU. The parameters of nonlinear wave propagation are studied, and the wave response of an LNG ship is solved. Also based on the coupling of HOS and SPH, Xie et al. (2023) proposed a new algorithm for solving the strong

nonlinear wave-structure interaction. This method combines the advantages of the HOS method to generate nonlinear waves and the SPH method to solve strong nonlinear free surface problems. The accuracy of the coupling method is verified by comparing the numerical simulation and experimental results of regular and irregular waves. The results show that the coupling method can effectively improve the calculation efficiency and greatly reduce the numerical dissipation.

Lu et al. (2022a) developed a fully nonlinear near-far-field coupling solver for the wave-body interaction problem. The GPU-based HOS solver is used to simulate the wide range of far-field wave propagation and its interaction with the flow field, while the incompressible flow field solver based on OpenFOAM are used in the near-field to solve the nonlinear wave load and motion response of the hull. The calculation accuracy and reliability of the solver are verified by the simulation of ship seakeeping problem.

Saincher and Sriram (2022) propose a new one-way coupling solver by combining a three-dimensional fully nonlinear potential flow solver with a viscous flow CFD solver, and apply it to solving the interaction between a focused wave and a fixed and moving cylinder. Based on the one-way coupling method, Dempwolff et al. (2024) developed a new potential-viscous flow coupling solver. The shallow-water-equation (SWE) solver REEF3D::SFLOW was coupled with the RANS viscous flow CFD solver REEF3D::CFD, and its calculation accuracy was verified.

Zhao et al. (2022) proposed a new velocity decomposition method (VDM) where the potential flow velocity is calculated by solving the Laplace equation without considering the influence of the free surface, while the remaining non-potential flow velocity is determined by OpenFOAM for the complementary Navier-Stokes equation. Zhong et al. (2022) developed a potential-viscos flow two-way coupling algorithm solver based on the open-source software package OceanWave 3D through the region decomposition method. By simulating different types of wave propagation, the validity of the coupling process in bidirectional data transmission is proved, and the accuracy and computational efficiency of the model are verified.

2.4 Rarely Occurring Events

Rarely occurring events for ships can generally be divided into three categories: (1) slamming, with the hull (bow, bottom or stern) of the vessel impacting onto the wave surface, (2) green water events, where a mass of water flows onto the deck, possibly impacting on the superstructure or cargo and (3) emergence events of propellers or other equipment, sometimes associated with ventilation. Other rarely occurring events, related to dynamic stability are the topic of the Stability in Waves Committee and not included here.

2.4.1 Water entry

Water impact problems of wedge type shapes are often considered as a basic model for bow and stern slamming or flat plates for bottom slamming or green water impact problems. Studies can be experimental, looking into two- or three-dimensional impacts at model scale, or numerical, with methods ranging from semi-empirical and analytical, incompressible (potential flow and Euler methods) to fully compressible and two-phase CFD approaches.

2.4.1.1 Experimental

Subramaniam et al. (2021) investigated trapped deck water and its effect on the roll dynamics of an offshore supply vessel by free-running model experiments. They measured the water pressure and observed the water motions on deck by camera. The presence of roll damping is evaluated by determining the phase difference between the ship roll and the deck water motion. The analysis of the ship roll and deck water motion points to damping within the operational speed range in regular as well as in

irregular waves. Furthermore, the investigations show that at higher Froud numbers the positive damping effect is reduced. For astern wave conditions a positive damping effect of deck water motion was observed.

Hasheminasab et al. (2022) investigated the effect of adding a spray rail on a catamaran section model with a centre bow on the slamming pressures recorded during water entry, Figure 10. Pressure transducers were placed at three locations on the model and three water entry speeds were considered. The results show that the addition of the spray rail provides a 60% reduction in peak acceleration and 70% reduction in peak pressure. The effects of air entrapment are also discussed.

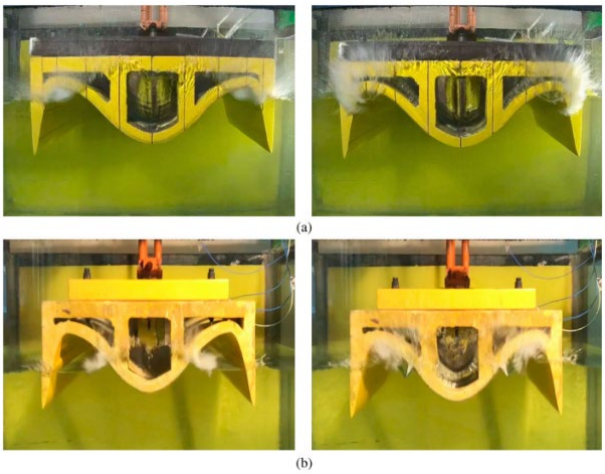

Figure 10: Effect of a spray rail on the water entry of a catamaran section model with a centre bow from Hasheminasab et al. (2022).

Liu et al. (2023b), Figure 11, developed a novel fluid–structure interaction (FSI) scheme based on the immersed boundary method to numerically investigate the high—speed water entry of different projectiles. This method allows to suppress the non-physical force oscillation and also uses a quaternion-based six degrees of freedom motion system to describe rigid body motions. Using analytical solutions, experimental data and literature data, the accuracy and robustness of the FSI scheme were validated. Different nose shapes were investigated, and the tail slamming phenomenon was extensively discussed.

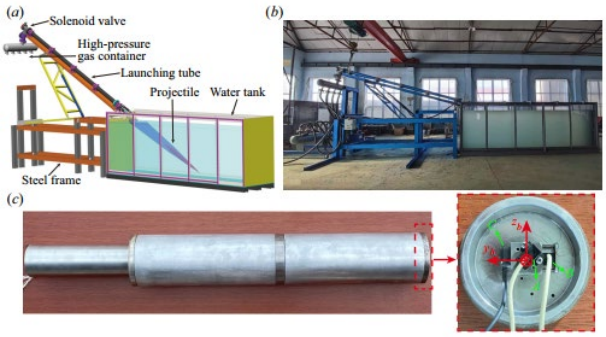

Figure 11: Experimental setup (Liu et al. 2023b).

An experimental study performed by Jain et al. (2022), Figure 12, investigated wedge and cone impacts into water across a wide range of velocities, precisely controlled using a linear motor. Pressure transducers placed on the impactors recorded pressure data, revealing under-pressure prior to peak pressure upon impact, likely due to hydrodynamic factors. Comparisons with various theoretical models showed that the Zhao & Faltinsen model aligns closest with measured pressure peaks. Theoretical treatments assumed 2-D flows for wedges and axisymmetric flows for cones, a method validated by comparing predicted pressure ratios to experimental results. Air cushioning prior to impact, causing water surface deflection, was examined, with results indicating the entrapment of air layers depends on the gradient of the deformed liquid surface compared to the impactor. In these slamming impacts, surface deformation due to inertial effects precedes viscous effects, which may lead to air bubble entrapment.

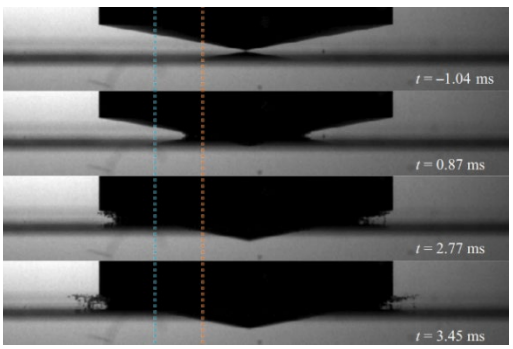

Figure 12: Early stages of a cone entering water (Jain et al. 2022).

Wang et al. (2022a) led an experimental study of the impact of three aluminium plates with different thicknesses and a pitch angle of 10° on a quiescent water surface, Figure 13. The impacts occurred with a combination of constant horizontal and vertical velocity. By varying the Froude number, the velocity normal to the free surface, the plate stiffness ratio (R_D) and the plate submergence time and by measuring the force normal to the plate surface, the moment of the plate's surface, the moment arm about the plate's trailing edge, the spray root position and shape and the plate's out-of-plane deflection along the centreline, they created a wide range of impact conditions. These impacts ranged from cases at small R_D in which the plate's deflection was less than a millimetre to impacts at large R_D in which the plate deflection was as large as 50 mm.

The authors analysed the results of 24 impact conditions for each of the three plates to identify the dynamic effect of the various dimensionless ratios on the results, namely Froude number, plate stiffness ratio and plate submergence time ratio.

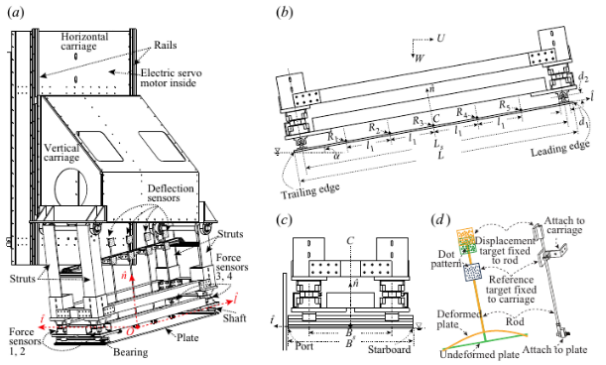

Figure 13: Experimental setup (Wang et al. 2022a).

2.4.1.2 Numerical

Liu et al. (2022a) numerically investigated green water and slamming loads of a ship advancing in freak waves. The authors separated their investigations in two steps: first the modelling of the wave and second the numerical simulation of green water on an FPSO and the motion of KCS were conducted. The representative stages of waves on deck are shown in Figure 14. The observation of the motion showed that the dominant factors of first and second green water events were different. The initial green water event was primarily driven by wave motion, while the second was predominantly influenced by the motion of the ship. The relation between heave and pitch motion and the largest ship position of the freaking waves were analysed, which showed that the maximum movement appeared in the second green water. Regarding the slamming pressures, the authors found that the wave slamming area was mainly located in the connection area between the deck and the superstructure midship.

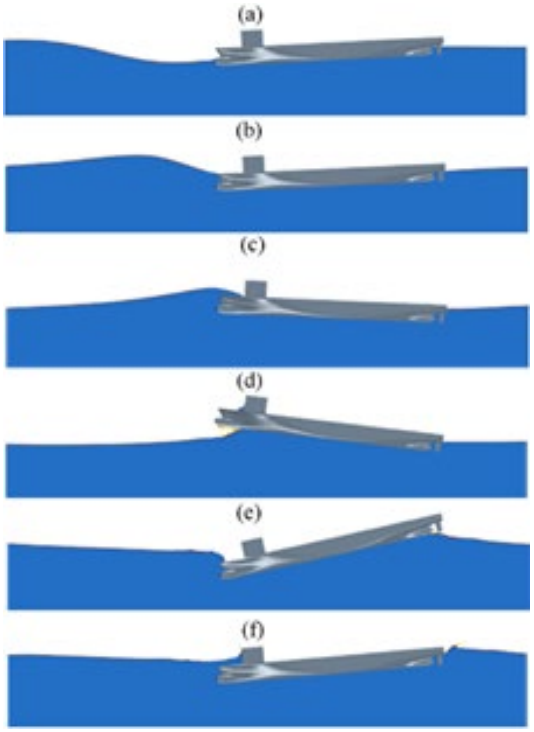

Figure 14: Representative stages of waves on deck presented by Liu et al. (2022a).

Molaemi et al. (2023) investigated the generic two-dimensional impacts on vertical cylinders on a non-flat water surface, Figure 15. This was done through physical experiments with impact on a stranding wave for both crest and trough impact. They found the wave load relative to the flat impact to be smaller for crests and larger for troughs. On a trough impact noticeable air entrapment takes place which

results in a slamming coefficient up to Cs = 30. For crest impacts it can be as low as 2.5. A second finding is that the crest slamming coefficient increases with the relative wavelength λ/D and decreases with the relative amplitude A/D. The authors explain this relationship by the ratio between the local instantaneous water surface curvature at the point and moment of impact and the cylinder curvature, which becomes closer to one for shorter wavelengths and higher amplitudes. Consequently, the wetted length grows at a faster rate at the initial impact time.

The authors successfully reproduced their findings in numerical simulations and analytical extensions of the von Kármán and Wagner methods. These numerical results were used to demonstrate how entrapment of air pockets can lead to oscillatory slamming loads with sub-atmospheric pressures. The numerical simulations enabled the extension of the results from the physical experiment to short wavelengths. In these conditions, impact on subsequent crests during the entry can lead to multiple slamming peaks and formation of multiple air pockets.

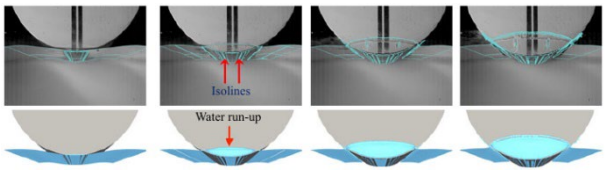

Figure 15: Comparison between experimental and numerical results (Molaemi et al. 2023).

2.4.2 Slamming

Slamming assessments are focused on quantifying the occurrence rates of bow slamming and stern slamming, as well as quantifying the magnitude of the impact loads.

Silva et al. (2023) investigated the slamming effects of FPSO platforms. They analysed standard mooring balcony structures numerically as well as experimentally. Furthermore, an analysis of the modification by various wedge type and fender type protection configurations of the aft mooring balconies as well as a perforated balcony were investigated, too. Using a diffraction model for identification of the most critical waves and a simplified CFD model the maximum expected vertical slamming loads were identified. With these specifications the model tests were performed and analysed. Figure 16 shows the experimentally evaluated absolute maximum loads for different balcony configurations for one test setup. The authors lined out that the results indicate that wedge type and cylindrical (fender type) structures beneath the balcony may reduce the extreme loads up to 50% and the perforated balcony structure may reduce the magnitude of slamming forces up to 80%.

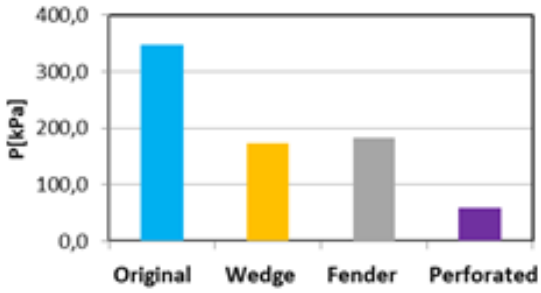

Figure 16: Results of Silva et al. (2023) for the investigation of absolute maximum loads for different balcony configurations for test setup H_s = 4.11m, T_p = 9s, Balcony airgap 3.03m.

A “double slamming” phenomenon at trimaran connecting bridge was studied by Tang et al. (2021a) at falling body experiments at seven heights. The "first slamming" is caused by the jet of the main hull into the water and the "second slamming" is generated when the cross structure enters the water. The relationship between the distribution of the slamming pressures and the velocity was analysed by the authors. Their intention was to provide the theoretical basis for the load prediction and structural design of the cross bridge of trimarans. With a falling frame experimental setup and 10 installed pressure sensors on the trimaran cross section in a scale of 1:100 the authors investigate the pressure pulses. Additionally, they observed the tests by video with a framerate of 1000 fps. Therefore, the authors were able to uncover a general understanding of the trimaran

slamming events e.g. a rising jet caused by the first slamming event and its water entry speed coupled behaviour.

Chen and Wu (2021) carried out model experiments of wave load and slamming pressure for an example ship with a bottom sonar opening. Experiments with multiple speeds, wave heights and wave directions were carried out to measure the motion of the ship model, vertical and horizontal bending moments of the hull beam, torque, bow slamming pressure and bottom pressure at the large opening area. The test ship model was designed under the premise that the model is similar to the real ship in terms of geometrical shape, motion and power. Figure 17 shows the model with bow opening used in the tests. Among other things, they figured out that due to the hull slamming phenomenon, high frequency flutter signals in the vertical bending moment resulted in obvious nonlinear characteristics of the vertical bending moment. Slamming pressure increased with navigation speed. The authors also pointed out that the sonar opening had some effect on the bow vertical acceleration. The bow vertical acceleration decreased when the sonar opening was closed.

Figure 17: Model and bow opening used in the investigations of Chen and Wu (2021).

Wang et al. (2022b) numerically investigated slamming events by simplifying the ship as a wedge. With the wedge-shaped body they analysed the law and mechanism of the slamming pressures for different entering speeds as well as inclining angles of the wedge. The authors show that the slamming load changes first with the increase of the inclination angle, and that the peak value of slamming load increases with the increase of the inclination angle of the wedges, while the decreasing speed of slamming load slows down with the decrease of the inclination angle of the wedges. Furthermore, they figured out that with increasing initial speed, the peak value of the torque increases, too, and the time until the peak value is reached becomes shorter. The higher the initial velocity, the faster the slamming load reaches the peak value, and the higher the peak value. Something similar was carried out both numerically and experimentally by Liu et al. (2021a) with a steel wedge with stiffened panels and a deadrise angle of 45°. Their focus was on the comparison of the peak pressure, duration time and stress responses on the wedge structure. The authors found a good agreement between simulations and experiments.

Antolik et al. (2023) provided experimental and theoretical treatment of a simplified hydroelastic problem involving the water entry of a 2 DoF (one axial elastic mode) impactor with a hemispherical nose, Figure 18. The impactor nose and body are coupled with a set of compliant flexure springs in order to achieve a system that closely approximates a simple harmonic oscillator. Comparisons between the experimental results and reduced-order models are presented and show that the latter can be used for early-stage design work.

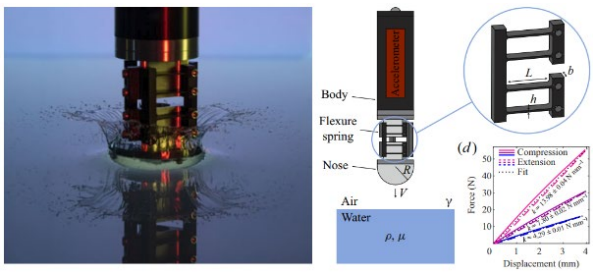

Figure 18: View of the flexible impactor used by Antolik et al. (2023).

Acharya et al. (2023) investigated bottom slamming with one-way and two-way coupled methods to estimate peak pressure at any point in the longitudinal axis. The results showed the trends are similar for both coupling methods with steady differences. One-way coupling can be helpful to estimate peak pressure although it does not capture the detail of spatial distribution of pressure at high forward speed (Fn > 0.2). The authors also developed an empirical formulation at forward speed to estimate peak pressure for the S175 hull. This formulation fails to predict peak pressure correctly for Fn < 0.2 but performs as well as the DNV's for Fn = 0.275.

Wu et al. (2021) conducted a numerical and experimental study of the slamming problem for a trimaran hull to validate the modified MPS (Moving Particle Semi-implicit) method developed by one of the authors, Figure 19. This numerical method is for a 2D fluid structure with free surface, thus the model used in the 20 drop-tests is an extrusion of the trimaran hull cross section. The authors achieved a convergence of the MPS method and a good agreement with the experimental results in time history, where the difference of peak magnitude and its occurrence time is within the allowable error range. The MPS method also simulates correctly the change of free surface during entry, the overturning and breaking of free surface and splash at different stages. These results show that the modified MPS method can simulate these complex fluid dynamics, but it does not take into account the impact of air whose effect is obvious when it becomes trapped at the inner side of the root of the exterior hulls.

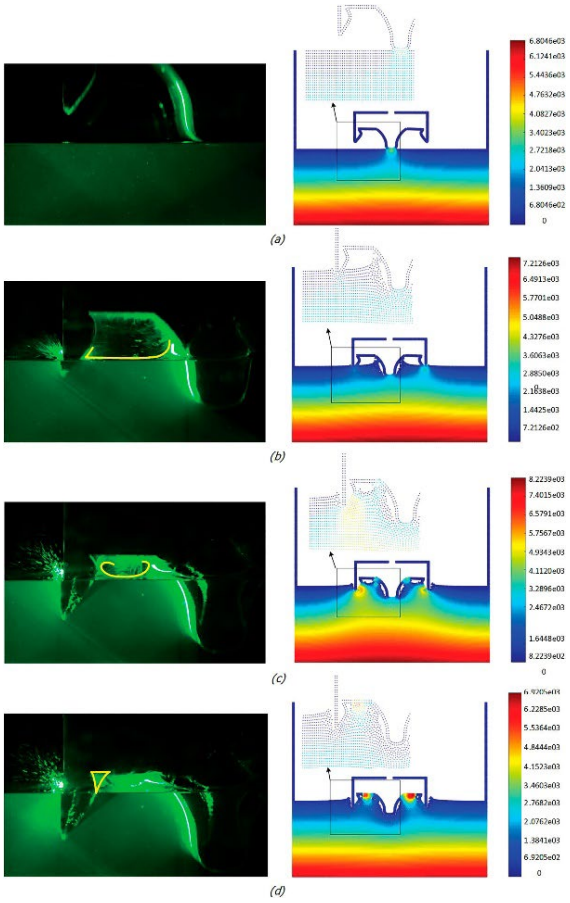

Figure 19: Comparison between pressure contours from numerical simulation and free surface profiles (Wu et al. 2021).

2.4.3 Green water

Park and Nam (2023) analysed green water events numerically by using an artificial neural network (ANN). They predicted the peak values of relative wave motion and the occurrence of green water events. The authors applied two ANN models for their investigations. The so-called T-ANN model is based on the time series of the incident wave and linear relative wave motion (RWM) calculation as input, and the F-ANN model which uses local parameters from the incident wave and linear RWM calculation rather than directly using the time series. For the input data model, test data of the KFPSO were used. Both models predicted the peak values of RWM with good accuracy, shown in Figure 20 for a location close to the bow. The authors found that the ANN models significantly improved the prediction performance for

relative wave motions compared to the linear calculations. Furthermore, it is shown that the ANN model based on the time series was more accurate than the feature-based ANN model.

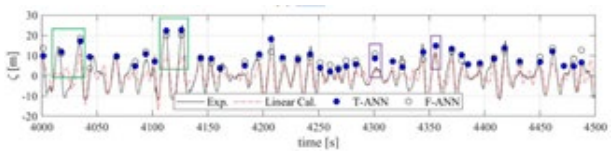

Figure 20: ANN predicted results at a location close to the bow for test time series by Park and Nam (2023).

Van Essen et al. (2021) compare different numerical screening indicators for green water loads on a containership with experiments. Their idea of 'screening' is to use lower-fidelity numerical methods to identify the occurrence of extreme load events such as slamming or green water at the basis of indicators. A good indicator has a significant correlation with the design load but is easier to calculate. Based on this first analysis, a high-fidelity tool is then used to determine the loads during these events. Their study with this technique in comparison with experiments shows that the peaks and steepness of the relative wave elevation around the bow serve as effective indicators of green water loads, alongside the undisturbed wave crests at the bow. Fine mesh CFD simulations were conducted for the identified events using a selected indicator as a reference. The outcome yielded a green water load distribution remarkably similar to that observed in the experimental data. Furthermore, the authors show that this screening method could massively reduce the required high-fidelity modelling time.

Liao et al. (2021) developed a 3D hybrid Eulerian–Lagrangian method for simulating green water on the deck. Two benchmark cases, green water on a fixed simplified FPSO model and green water on a ship model, were used to perform comparisons and validate the proposed method. It was found that the green water behaviour on deck, Figure 21, is well captured by the new method. Pressure values are mostly in good agreement with the experimental results (although underestimated) for most pressure gauges, but the impact pressure peak value differs considerably. Further work will focus on improving the peak pressure value prediction and CPU time optimisation.

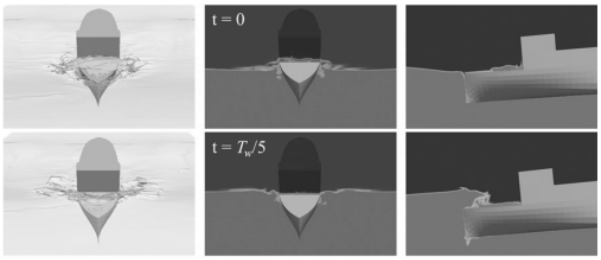

Figure 21: Green water behaviour captured by the method proposed by Liao et al. (2021).

Zhang et al. (2021a) numerically investigated the pressure induced by green water events from freak waves on the deck and superstructure of a typical simplified ship, Figure 22. They used a 3D numerical wave tank and the Peregrin breather solution model to generate freak waves. They found this model, previously validated under regular wave conditions, able to give reasonable results to investigate qualitatively the process and characteristics of green water events from freak waves. The authors characterised six different stages of said events and inferred the most dangerous areas on deck and on superstructure.

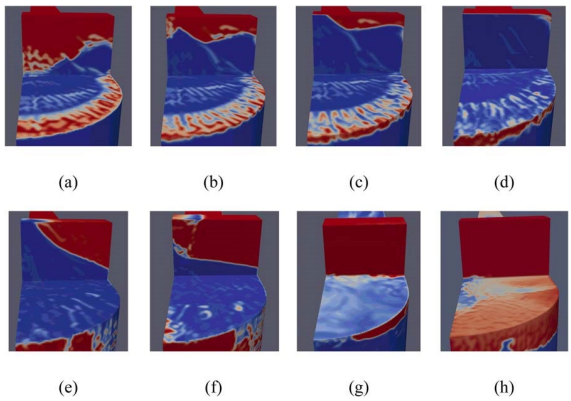

Figure 22: Stages of green water motion after arriving at superstructure, Zhang et al. (2021a).

2.5 Sloshing

Sloshing in ship tanks with liquid cargo is still a problem to which significant research has

been dedicated in this last ITTC term. This can be attributed to an increased interest for the ship transportation of liquified natural gas LNG, in turn connected to supply constraints due to the Russian invasion of Ukraine and to the use of natural gas as a transitional fuel towards the path of reduced emissions. More recently, additional interest can be a consequence of the growth in research on transportation of liquid hydrogen LH2 in cryogenic conditions; using hydrogen as an energy vector has emerged as an alternative to reduce greenhouse emissions.

In this context, studies have been carried out using experimental and numerical simulations, but also, in recent times, machine learning based models. The studies refer, among other things, to the prediction of sloshing impact loads and boil-off rates, to a better understanding of free-surface dynamics, to assessing the influence of sloshing on the coupled dynamics of ships when transporting liquid cargo, to the investigation of sloshing reduction devices, and to modelling fluid-structure interaction (FSI) in sloshing related problems. A short but interesting review paper in the period was written by Zheng et al. (2021a).

As for sloshing impact loads, Ahn et al. (2023) conducted a large series of joint industrial experiments using six-degree-of-freedom irregular sloshing tests. The case study was a tank from a real 174K LNG Carrier, scaled 1/50. They focused on impacts on the upper part of the tank (Figure 23, Figure 24). In this paper they provided an assessment of sloshing loads based on a comparison of short- and long-term approaches distinguished by the guidelines of various classification societies. Their key findings indicated that the different analysis procedures of the international classification societies lead to different sloshing loads for the same cargo hold design of the LNGC. Another of their key findings is that using the long-term approach was more than twice as conservative as the short-term one.

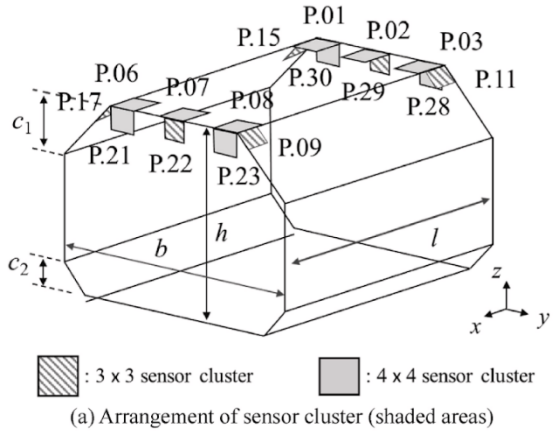

(a) Arrangement of sensor cluster (shaded areas)

Figure 23: Arrangement of sensor clusters (Ahn et al. 2023).

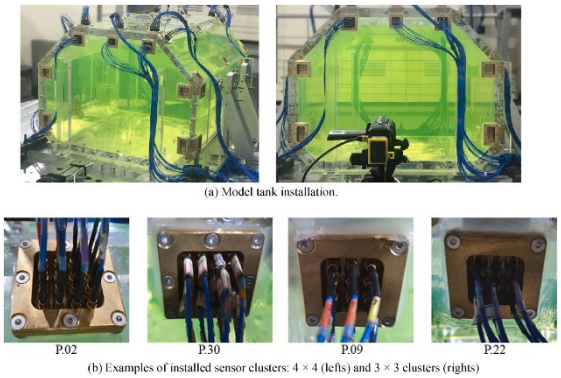

(a) Model tank installation.

(b) Examples of installed sensor clusters: 4 × 4 (lefts) and 3 × 3 clusters (rights)

Figure 24: Model tank installation and cluster of sensors (Ahn et al. 2023).

Also, Ahn et al. (2021) developed a neural network to predict extreme sloshing loads, with good agreement for validation cases. Later, Ahn (2023) used genetic programming (GP) to predict sloshing impact loads. Although the scope of the research was limited, promising results were obtained, suggesting this technique can be used in the future to save experimental work.

As for free-surface dynamics, the interesting topic of turbulence modelling when conducting sloshing flow simulations with RANS solvers was investigated by Mahfoze et al. (2022). They arrived at the conclusion that excessive dissipation was induced by such types of models. Damping through sloshing has been the target of investigations in this period, with a focus on that induced in vertical motions (Martinez-Carrascal and Gonzalez-Gutierrez, 2021). Remmerswaal

and Veldman (2022) tried to provide evidence linking the variability of sloshing loads to free-surface physics. To this aim, they looked into how the physics can be simulated, discussing the influence of capillarity, the onset of instabilities and a number of numerical details in their VOF based scheme.

Regarding the transportation of cryogenic hydrogen, Liu et al. (2022c) investigated sloshing in these cases. They report that heat transfer is enhanced when the first sloshing mode is excited, finding in these conditions the largest forces and moments but also the largest fluid pressure drops due to these heat transfer effects. Also in this context, Smith et al. (2022) presented an approach for estimating fuel boil-off behaviour in cryogenic energy carrier ships, such as future liquid hydrogen (LH2) carriers. Their results indicate that an LH2 ship with the same tank volume and glass wool insulation thickness as a conventional LNG carrier stores 40% of the fuel energy and is characterized by a boil-off rate nine times higher and twice as sensitive to sloshing. Their results indicate that LH2 carriers will necessitate significant redesigns if LNG carrier standards are desired.

As for coupled dynamics, Koo et al. (2021) carried out time-domain simulations, including coupled sloshing loads, of the offloading of an FLNG on an LNGC. They used their own time-domain solver and were able to document the influence of the tank filling level on the roll response (Figure 25) Along this line, Lyu et al. (2022) modelled ship motion-sloshing interaction with forward speed in oblique waves. They did this study considering a 138000 m^3 LNG carrier. They paid particular attention to beam seas, for which, the derivation of a roll damping model was of particular relevance.

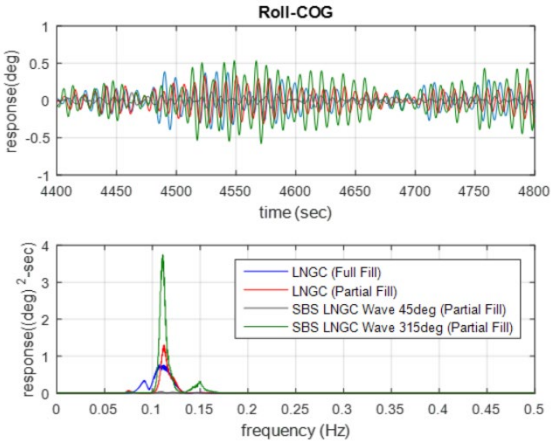

Figure 25: Comparisons of LNGC Roll Responses for offloading Operational Sea State (Koo et al.2021).

The influence of sloshing on the onset of parametric roll was studied numerically by Liu et al. (2022b). They used an in-house CFD solver (Figure 26). They showed sloshing could significantly decrease the natural roll frequency of the ship model, which led to a lower speed range where the parametric roll occurred compared with the model without sloshing.

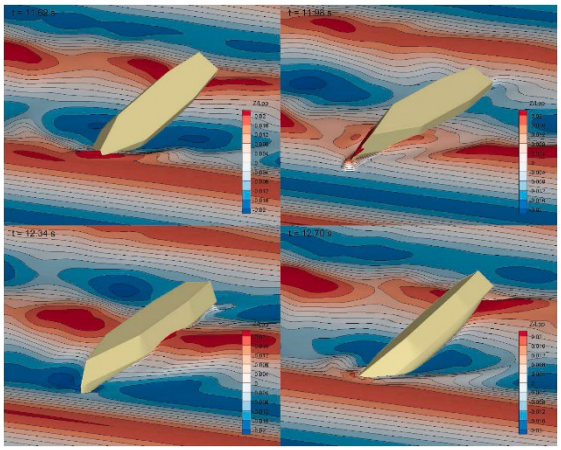

Figure 26: Snapshots of CFD simulation of coupled sloshing motions and parametric roll (Liu et al., 2022b).

Also, regarding coupled dynamics, Igbadumhe et al. (2023) carried out experiments with an FPSO comparing the inclusion of a tank partially filled with liquid to using an equivalent "frozen" mass (Figure 27). They studied beam sea conditions and found that in some frequencies the influence of the sloshing loads could significantly change the roll angle (Figure 28).

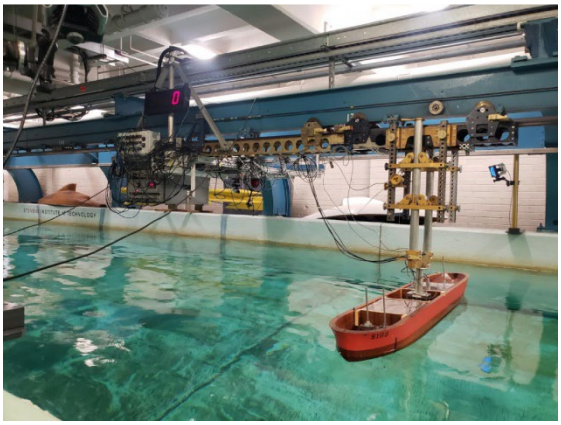

Figure 27: Coupled sloshing experiments (Igbadumhe et al. 2023).

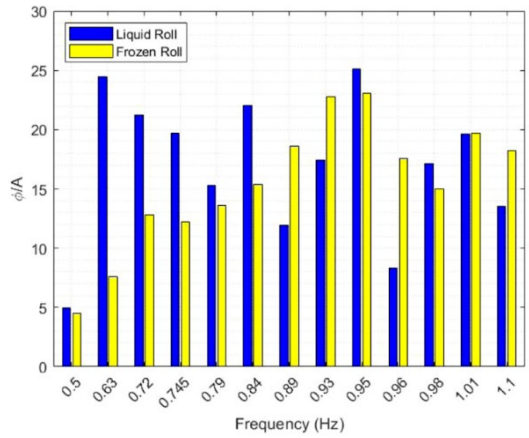

(a) Loading condition 2 FPSO roll response amplitude for each excitation frequency for both liquid and frozen condition

Figure 28: Roll response in coupled sloshing experiment (Igbadumhe et al. 2023).

Finally, Faltinsen and Timokha (2021) adapted their multimodal theory to model the coupling between resonant sloshing and the lateral motions in a 2D rectangular tank.

Related to coupled dynamics but with a different angle, Zheng et al. (2021b) conducted an experimental investigation on the effect of sloshing on ship added resistance in head waves. They used a scale model of a relatively small (23603 m^3) LNG carrier. They found (see Figure 29) that sloshing could help reducing added resistance due to its favourable influence in reducing ship motions. A combined numerical-experimental study dealing with this same topic was carried out by Zhu et al. (2021).

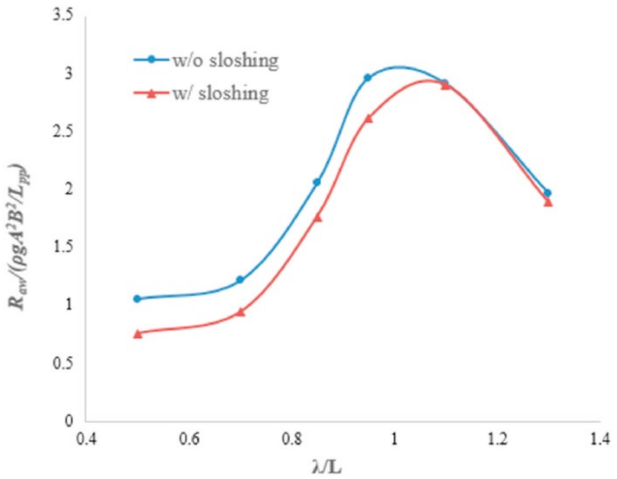

Figure 29: Comparisons of added resistance in waves with and without sloshing, (Zheng et al, 2021b).

A last relevant reference in this period for couple dynamics is an experimental and numerical investigation of the hydrodynamic response of an aquaculture vessel by Tao et al. (2023). Their case study consists of a 258 m long vessel with 83000 m^3 aquaculture tanks (Figure 30). They showed that the double-row tank arrangement scheme adopted by their vessel could reduce the coupling effect of sloshing and hull motion effectively.

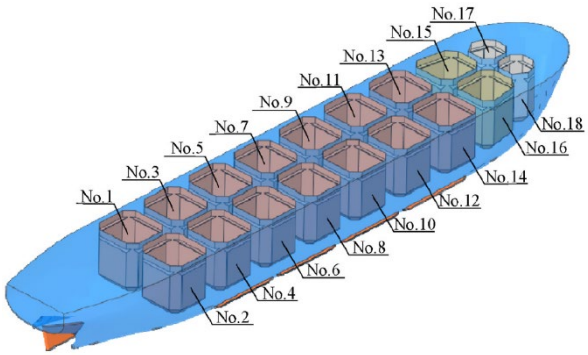

Figure 30: Layout of the aquaculture vessel by Tao et al. (2023).

As for FSI problems Wang et al. (2021b) modelled the influence of hydroelastic effects in a tank transporting LNG. Adina CFD, Adina Structures and coupled FSI ADINA solver were used for modelling. They found the average pressure in the elastic tank to be smaller than for the rigid tank.

As for sloshing reduction devices Barabadi et al. (2023) proposed to use floating foams to reduce the intensity of sloshing inside tanks. They demonstrate the sloshing reduction by using a combined experimental and numerical approach. Also to reduce sloshing, Ma et al. (2021) used vertical baffles. They modelled the flow with a Lattice-Boltzman scheme (Figure 31) and assessed the efficiency of the baffle arrangement by linking the pressure field with the viscous dissipation.

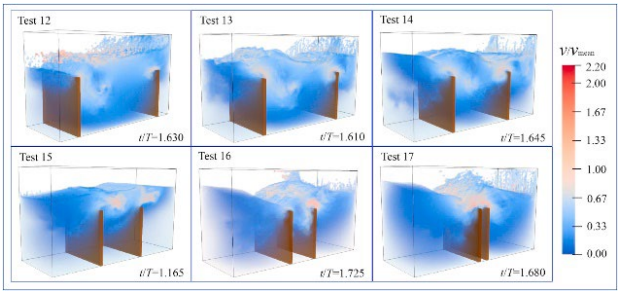

Figure 31: 3D snapshots of sloshing modelling with baffles by Ma et al. (2021).

2.6 Hydroelasticity

2.6.1 Experimental study on container ships using a backbone model

A segmented model with a backbone is extremely useful for experimentally investigating the hydroelastic response of ships. Tian et al. (2022) produced two different scaled backbone models to collect benchmark model test data for a 20000 TEU container ship of about 400 m in length and summarized their findings for producing accurate backbone models by comparing them with modal analysis of 3D FEM models. Zhang et al. (2022) conducted experiments on wave loads and hydrodynamic response to head-on and oblique waves using a model with a variable cross-section backbone (10000 TEU container ship). The results indicate that hull stiffness has little effect on the frequency of slamming, but that wave loads due to slamming become more severe as stiffness decreases. Tang et al. (2022) similarly used a model with a variable cross-section backbone to systematically analyse nonlinear bending moments from experimental data, Figure 32. The effects of Froude number, wave direction, and wave height, asymmetry of the hogging and sagging moments, and phase differences between wave frequency and higher harmonics in extreme waves were investigated.

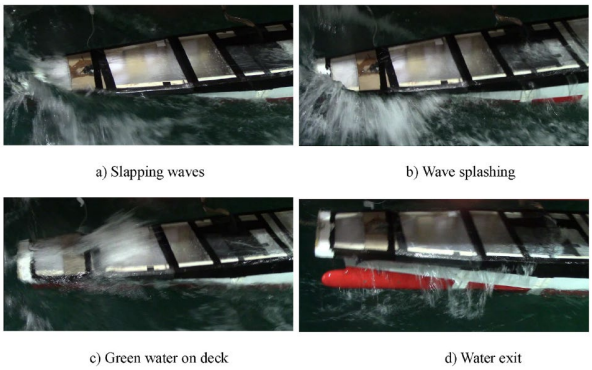

Figure 32: Image records of the model in extreme waves by Tang et al. (2022).

Ahn and Jung (2022) made comparisons by design wave conditions and by towing tests and numerical calculations for the final strength evaluation, including the increase in elastic response level due to whipping of the very large ore carrier (VLOC). The design wave conditions are equivalent design wave (EDW) and equivalent design sea state (EDS), where EDW is determined from the long-term analysis results and EDS is determined by the maximum contribution to the 10^{-8} exceedance probability of the vertical bending moment (VBM) in each sea state of the actual sea route. The towing tests were conducted on a segmented model with backbone support, and numerical calculations were performed under the same conditions using the nonlinear time-domain hydroelastic analysis program WISH-FLEX. As a result, the load effect from EDW was evaluated to be greater than that from EDS in both experimental and numerical calculations, and the load effect from experiments was evaluated to be greater than that from numerical calculations. Kim et al. (2023b) experimentally investigated the wave motion and loading of a container ship model without forward speed in oblique regular waves to determine the nonlinear effects of wave steepness on the vertical bending moment (VBM) and horizontal bending moment (HBM) near the centre of the hull, as well as on the 6-

DoF motion, Figure 33. The results show that as the wave steepness increases, the higher harmonic components including slamming phenomena increase. It was also qualitatively confirmed that the restoring moment of the mooring system correlates with the asymmetric HBM and the change in mean yaw motion.

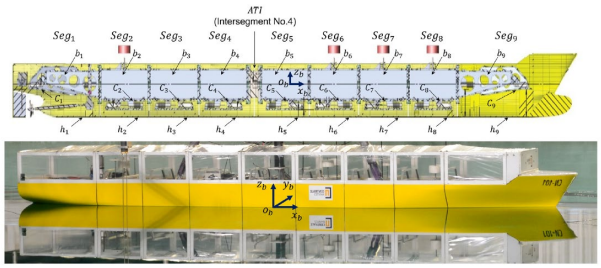

Figure 33: 9-segmented 6750-TEU containership model and load sensor location by Kim et al. (2023b).

2.6.2 Experimental and numerical analysis of sloshing

Sloshing loads in LNG tanks are complex phenomena that depend on the density ratio of gas and liquid, the phase transition of the fluid, and the elastic response of the tank wall. Lee et al. (2022a) studied the effects of the density ratio of gas and liquid in the tank and the phase transition of the fluid on the sloshing phenomenon. They measured the sloshing impact pressure on the wall and characterized it in terms of maximum impact pressure, pressure rise time, and pressure impulse area. These data may be useful for LNG tank design. Using the experimental sloshing loads, Park et al. (2022) performed direct dynamic structural analysis under different sloshing impact loading patterns to investigate the hydroelastic effects and dynamic response of a membrane-type cargo containment system (CCS). The results, Figure 34, show that the level and frequency of the dynamic structural response may be lower than previously estimated due to the additional mass and damping effects of the LNG considering the fluid domain.

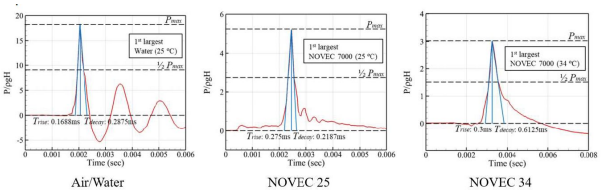

Figure 34: Pressure signal for the air/water and NOVEC 7000 (20%H Filling, ω/ω_0 = 1.27 by Park et al. (2022).

2.6.3 Numerical study of hydroelasticity

The recent trend toward larger hulls has the potential to make hulls relatively elastic. For such problems, Wei and Tezdogan (2022) proposed a fluid-structure interaction coupling scheme using the preCICE library communicating with the fluid solver OpenFOAM and the structural solver calculiX. Its effectiveness was demonstrated by comparing the hydroelastic behaviour of a container ship moving forward in regular waves. Tavakoli et al. (2023b) analysed the water surface impact of a 2D object using the fluid-structure interaction of finite volume method (FVM) incorporated in OpenFOAM and showed that the impact load is reduced by elastic motion. Kim et al. (2023a) extended the modal method to time-domain hydrodynamic analysis of floating bodies, Figure 35. Three numerical schemes were considered for wave force calculations: the case of deflection force only, the case of 6-DoF radiation force + deflection force, and the case of elastic degree of freedom radiation + deflection force, and their accuracy and efficiency were systematically compared.

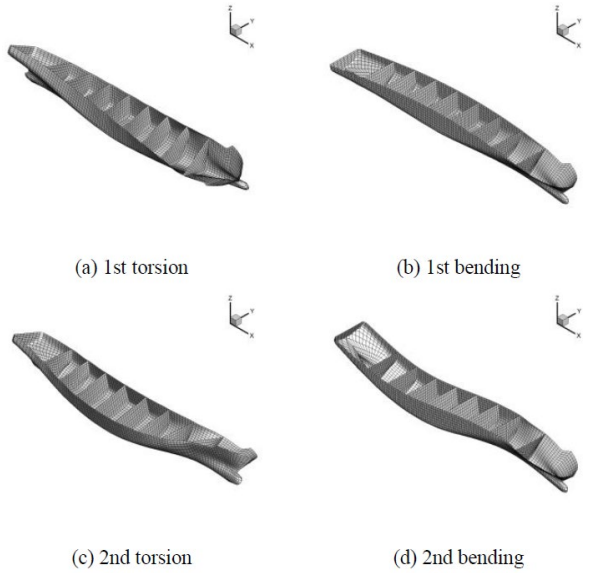

Figure 35: Elastic mode shapes of sample ship by Kim et al. (2023a).

Park and Lee (2022, 2023) proposed a method to perform hydroelastic analysis under various conditions on a single mesh model by non-matching meshing between finite element and boundary element methods. Wang et al. (2022c, 2023a) used Taylor Expansion Boundary Element Method (TEBEM) generalized to elastic modes to calculate the vertical motion, heaving motion, and vertical bending moment of a container ship moving forward in head waves. Nonlinear effects become more pronounced as the forward speed increases. Vertical hydroelastic response is currently focused, and horizontal, torsional, and coupled bending and torsion are neglected in this study. On the other hand, Riesner et al. (2021) proposed a time-domain numerical method to predict higher-order springing by coupling horizontal, torsional, and bending and twisting to account for forward velocity. The structural dynamics adopted a beam element approach, and the hydrodynamic solver considered nonlinearities induced by wetting surface changes due to incident waves. The vertical bending, horizontal bending, and torsional moments at the centre of the hull induced by sprigging were shown to compare favourably with experimental measurements. Pal et al. (2022) developed a semi-empirical reduced order model (ROM) based on coupled CFD-FEM analysis and experimental results. It accounts for the effects of springing and whipping at different probability levels when calculating the extreme value distribution of the VBM, as well as the effects of continuous bow and stern slamming. This method provides real-time ship loading prediction without the expensive computational cost of coupled CFD-FEM. Lu et al. (2023a) proposed a 3-D nonlinear time-domain hydrodynamic analysis method for ship wave loads considering asymmetric slamming and solved the seakeeping problem by combining modal analysis and 3-D Rankine panel method for 3-D finite element models. The results show that asymmetric slamming has a significant effect on the horizontal torsional whipping response of the hull when the wave encounter frequency coincides with the natural frequency. Vijith and Rajendran (2023) proposed a nonlinear time-domain numerical solution method by combining a seakeeping solver based on potential flow theory and a structural solver based on Timoshenko beam theory. The solver captures the effects of higher-order springing and whipping in vertical bending and identifies whipping effects due to slamming. In most cases, the numerical results are shown to be in good agreement with experimental results, Figure 36.

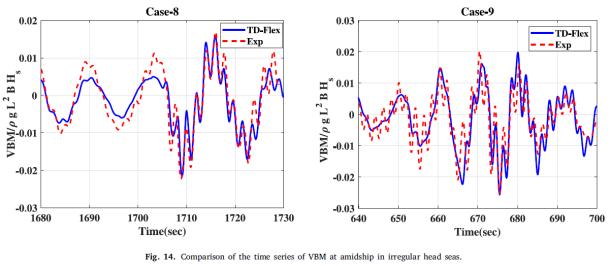

Figure 36: Comparison of the time series of VBM at amidship in irregular head seas by Vijith and Rajendran (2023).

In this study, Wei et al. (2023) applied a fluid-structure coupled interaction framework to model the interaction between flooding and the wave field in the damaged tank of a moving forward ship in OpenFOAM and analyse the structural deformation in MBDyn. The results are useful for assessing the safety of damaged vessels and determining whether they suffer

secondary damage due to hydrodynamic elastic response.

2.6.4 Numerical analysis of water surface impact

Hosseinzadeh et al. (2021) numerically investigated the water surface impact of a two-dimensional symmetric elastic wedge due to free-fall motion using a two-way coupling approach between finite volume and finite element methods. Coupling methods for two-dimensional symmetric elastic wedge sections under various conditions are presented. It is observed that the importance of hydroelasticity increases with decreasing slope angle and increasing impact velocity. Feng et al. (2021) proposed an efficient fluid-structure interaction (FSI) coupling between the boundary element method (fluid part) and the mode superposition method (structural part) to study the hydroelastic slamming of wedge cross sections, Figure 37. Results showed that the maximum response of the structure was underestimated, and a time difference effect was found between the results of the separated and coupled solutions.

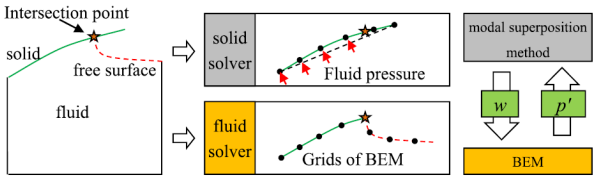

Figure 37: Partitioned solution of solid solver (modal superposition method) and fluid solver (BEM) by Feng et al. (2021).

2.6.5 Theoretical analysis of hydroelasticity

The theoretical-analytical approach clarifies and develops the physical principles and mechanisms of hydrodynamic elasticity. Hong et al. (2021) used Legendre polynomials and Chebyshev polynomials, which are mathematically orthogonal but do not satisfy the free end boundary conditions, to represent the mode function of a uniform Timoshenko beam, Figure 38. The mode superpositions represent the hydroelastic forces on the ship and the resulting bending deflection of the ship in waves. In combination with the Rankine panel method, the hydrodynamic forces for the modes were calculated. Since the Eulerian beam model tends to overestimate the natural frequencies of elastic motion in the high elastic modes, there is an advantage in using Timoshenko beams that account for deformation due to shear forces. As the number of modes increases, the total deflection of the ship is found to converge, and the results obtained using the Legendre polynomials and Chebyshev polynomials are in almost perfect agreement with those obtained using the dry eigen modes of the Timoshenko beam over a wide wave frequency range. The Legendre polynomials were shown to be concise, common, and can be used with the weighted residual method, indicating that they are expected to be versatile enough to be applied to a wide range of engineering problems.

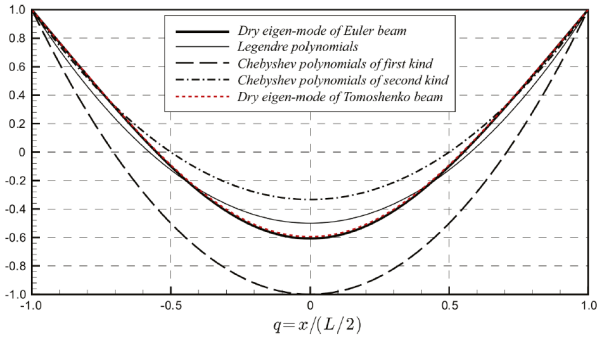

Figure 38: The first elastic mode shapes (j = 7) of mode functions used by Hong et al. (2021).

Jagite et al. (2021) analysed the hydroelastic response of a number of container ships. The dynamic ultimate strength of reinforced panels was investigated, and realistic loading scenarios were derived. They also developed a new strain rate sensitivity model. Korobkin and Khabakhpasheva (2022) addressed a three-dimensional unsteady problem of a rigid body impacting a floating plate with a viscoelastic layer on its surface. The reaction forces of the viscoelastic layer are determined by a nonlinear, one-dimensional Winkler-Kelvin-Voigt model. The plate deflections are described using the normal modes method, and the added mass

matrix of the plate is calculated analytically. Plate deflections are calculated for various positions of the impact. Spinosa and Iafrati (2022) treated a water surface impact on a rectangular flat plate. A simplified quasi-static model based on modal expansion for the structural response and a self-similar solution for the hydrodynamic problem was used. The inertial contribution was found to be small, justifying the use of a quasi-static approach. Tavakoli et al. (2023b) theoretically proved that the pressure acting on an elastic body can be predicted using a simple equation that uses momentum exchange. They presented a new methodology for analysing the hydroelastic response of a flat plate to water immersion using the momentum transferred to the solid immediately after impact, Figure 39. Although the paper is limited to flat plates, it could lead to practical methods for FSI problems in ships and offshore structures.

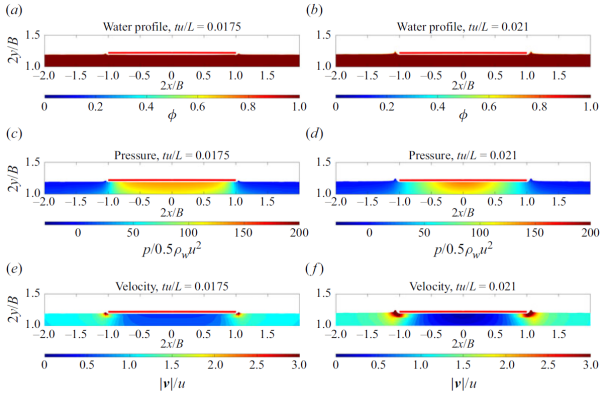

Figure 39: Snapshots showing the fluid motion around an elastic plate entering water. The plate thickness is not to scale by Tavakoli et al. (2023b).

2.7 Added Resistance in Waves and Power Requirements

2.7.1.1 Semi-empirical Formula for Added Resistance in Waves

In the ship design stage, it is necessary to consider the added resistance in the operational environment to accurately estimate the ship's performance. While model test or direct 3-D numerical computations ensure accurate and reliable results, they obviously require high costs with extensive times, as well as detailed information of ship hull design. With the accumulation of more model test data, new semi-empirical formulae have been developed for the rapid estimation of added resistance in the early design stage, applicable not only to head sea but also to various wave headings. Moreover, to address the limitation of applicability to novel hull shapes or unconventional vessels with extreme dimensions, revised empirical formula have also been proposed recently.

Mittendorf et al. (2022) proposed a data-driven methodology for the parameter calibration of a semi-empirical approach for estimating added resistance in arbitrary wave headings, taking into account uncertainty quantification. They endeavoured to refine the semi-empirical formulation by Liu and Papanikolaou (2020), optimizing the parameter vector with respect to two datasets for both full and slender ships, comprising 25 different ships and approximately 1100 data points obtained from publicly available model tests. The validity of the proposed method was confirmed through comparison with experimental data and established prediction methods, indicating satisfactory accuracy of the mean estimate and reliability of the adapted semi-empirical formulation, Figure 40. They noted that calibrating the semi-empirical definition resulted in a performance increase of around 9%, significantly reducing parameter uncertainty.

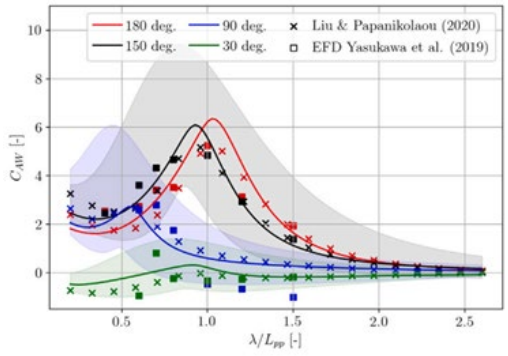

Figure 40: Comparison of added resistances between experimental data and semi-empirical formulae with uncertainty estimates (Mittendorf et al., 2022).

Liu and Papanikolaou (2023) enhanced the semi-empirical SNNM (SHOPERA-NTUA-NTU-MARIC) method by combining numerical experiments for the consideration of ships with extreme dimensional ratios, where experimental data are limited. They introduced the parameter L/B into the SNNM method based on large-scale numerical calculations using a potential-flow-theory-based 3D panel code NEWDRIFT+. The improved SNNM formula was validated against an experimental database comprising 131 data points from 11 ships with extreme dimensional ratios of various types. The validation study demonstrated a higher correlation coefficient and smaller mean percentage error compared to the original formula, indicating a significant enhancement in the prediction of added resistance in waves for various types of ships with extreme dimensional ratios

Mittendorf et al. (2023) provide statistical analyses of mean added resistance estimations in actual wave conditions based on in-service data from a fleet comprising more than 200 container vessels. The prediction data resulting from an indirect calculation of added resistance, utilizing shaft power measurements and empirical estimates of the remaining resistance components, were presented alongside comparisons with theoretical estimates. In this study, the calculation of the theoretical added resistance has been carried out by using a semi-empirical formula proposed by Mittendorf et al. (2022) for the added resistance transfer function and then applying the spectral method for long- and short-crested irregular waves. The comparison reveals a bias in bow oblique waves and higher sea states of the spectral estimates, as well as a large variance of the empirically derived predictions, particularly evident in beam-to-following waves. The authors addressed that added resistance is generally difficult to predict in actual conditions due to the substantial associated uncertainties, particularly in short and oblique waves.

Kim et al. (2022) proposed a new estimation method by combining two existing semi-empirical methods, CTH and L&P methods, which have high accuracy and availability against arbitrary wave headings. The new combined method was validated by full-scale measurements of a general cargo ship and a containership. They reported that the combined method showed good overall performance in estimating added resistance in the range of high wave height, resonance frequency, arbitrary wave headings, and low ship speed.

Lee and Kim (2023) developed an empirical-asymptotic approach (SNNM-SNU formula) for the added resistance of ships at arbitrary speed and headings by combining the SNU formula for short waves and the SNNM formula for long waves. They validated the developed method through a series of comparative studies, demonstrating that the proposed method shows a good agreement with experiments and exhibits strong capabilities in estimating added-resistance in the high-frequency region for oblique waves.

2.7.2 Data-driven Model for Estimation of Added Resistance in Waves

The feasibility of a data-driven model utilizing deep learning techniques to estimate added resistance in waves has recently been studied with the aim of improving accuracy compared to existing semi-empirical formula. The data-driven model has typically been constructed based on deep neural networks using extensive experimental data. Additionally, attempts to integrate data-driven and physics-based models have been observed, showing some corrective effects on the physics-based model.

Duan et al. (2022b) introduced a method based on deep feedforward neural networks (DFNs) for predicting the added resistance of ships in head waves. They utilized a dataset comprising 25 different ships, including 10 vessels with experimental data from published studies and 15 ships with calculation data obtained through a potential flow solver. They reported that the DFN model with multiple

hidden layers exhibited higher prediction accuracy for added resistance compared to single hidden layer models. Furthermore, they observed significant improvements in prediction accuracy when additional information such as pitch radius of gyration and bow entrance angle was included in the DFN model input. The study demonstrated that the prediction accuracy of the developed DFN model is better than that of the semi-empirical formula, suggesting the feasibility of its practical application for predicting added resistance in head waves.

Yang et al. (2022) proposed a data-driven and physics-based symbiotic model (DPSM) for predicting the added resistance of ships in head waves, Figure 41. The 2D strip method was employed to construct a physics-based model, providing physics-based information and constraints, while the data-driven module was developed based on a fully connected neural network structure and radial basis function. The authors demonstrated that the DPSM results closely align with experimental data, exhibiting a noticeable adaptive correction effect on the outcomes of its embedded physics-based model. Furthermore, they showed that the DPSM achieves superior generalization ability compared to fully data-driven models by leveraging the strengths of both the physics-based and data-driven approaches.

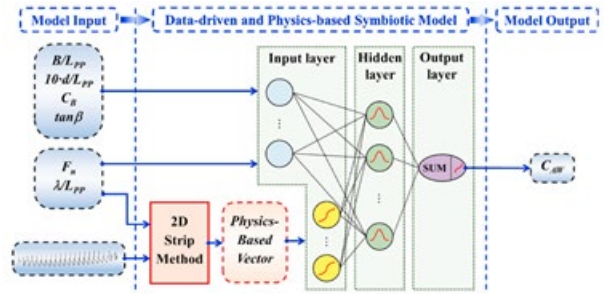

Figure 41: Combined method with data-driven and physics-based models for predicting the added resistance of ships in waves (Yang et al. 2022).

Cepowski et al. (2023) developed artificial neural network (ANN) models to predict added resistance using basic design parameters of ships. The experimental data, measured from 19 ship models representing a wide range of diverse vessels, was used to train the ANNs. The added resistance was predicted by calculating the algebraic mean of the results obtained from five ANNs using different segregated data. The authors asserted that this ensemble of artificial neural networks ensure more reliable and accurate estimates than using an individual ANN.

2.7.3 Experimental Studies on Added Resistance in Waves

Model tests have been used as high-fidelity methods to predict or validate the added resistance of ships in waves, especially focusing on irregular waves or quartering waves. Additionally, some experimental studies have been carried out to understand more about the physics related to added resistance in waves, such as the sloshing effects on added resistance.

Kim et al. (2021) estimated the motions and added resistance of an LNG carrier with twin skegs through experimental investigations under various wave heading angles. They reported that the added resistance due to waves is significant in bow quartering seas and not negligible even in following and stern-quartering seas. Additionally, they discussed the uncertainty in the model test, indicating that the error level is larger in shorter wave lengths. For validation, a series of numerical computations were carried out using the potential-flow-based Rankine panel method (WISH) and RANS-based CFD method (STAR-CCM+). They found that the added resistance estimated by numerical methods followed the trends observed in the experiment but could be scatted at a wide range of wave lengths and heading angles, Figure 42.

Zhu et al. (2021) conducted an experimental and numerical investigation on the sloshing effects on the added resistance of ships in waves, Figure 43. They utilized a modified Wigley hull equipped with two inner tanks in the model test to observe the hydrodynamic responses under head wave conditions. Numerical computations were performed based on the three-dimensional Rankine panel method for both seakeeping and

internal sloshing flow using linear potential flow theory. They found good agreement between experimental data and numerical results, both with and without sloshing effects. Additionally, they reported that when the wave encounter frequency approaches the tank's natural frequency, a strong coupling effect at medium filling tanks can restrain ship motion responses as well as added resistance. Zheng et al. (2021b) also carried out a model test for an LNG carrier with a single prismatic tank to study the effect of sloshing on ship motion and added resistance in waves. They found that sloshing inside the tank alters the ship's motion, particularly reducing surge the most, and it modifies the added resistance under the specific conditions.

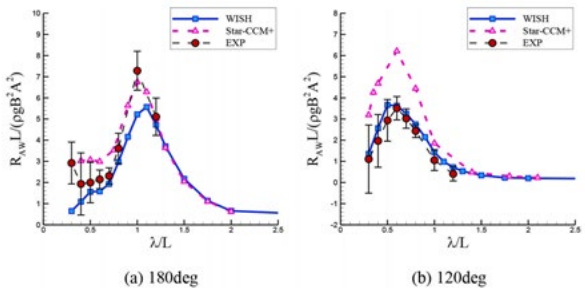

Figure 42: Comparison of added resistances from experiment and numerical computations (Kim et al. 2021).

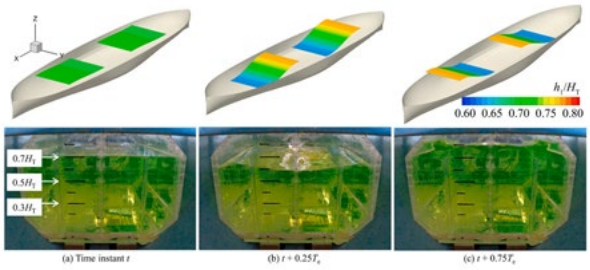

Figure 43: Snapshots of inner sloshing development (Zhu et al. 2021).

Yasukawa and Enui (2021) studied the effect of the pitch moment of inertia on the added resistance in waves using model tests and strip-method-based calculations for an S175 container ship. Their findings indicate a reduction of approximately 30% in added resistance when the pitch radius of gyration is decreased from 0.27L to 0.23L. Furthermore, they observed that this effect is notably pronounced in bow waves but insignificant in beam and following waves.

Yu et al. (2022) assessed ship resistance and propulsion performance for an 1800 TEU container ship through model tests in regular head waves and spectral method in irregular waves. They demonstrated that the added propeller revolution, thrust, and torque in waves exhibit a linear increase as the added resistance does to balance an overloaded propeller. They observed that the added delivered power in waves originates not only from added resistance but also from decreased propulsive efficiency.

Park et al. (2023) conducted a design optimization of the hull form and appendage of a 6500 DWT tanker to reduce added resistance, considering in-service navigation condition. In this study, the added resistance was firstly evaluated based on regular-wave CFD simulations, followed by the use of the spectral method to calculate the added resistance in irregular waves. A series of model tests was also performed to validate the improvements of the optimal hull form over the original design. The optimized hull featured a bow hull form with a sharper entrance and increased length between perpendiculars, along with a stern hull form with a V-shaped section to reduce viscous pressure resistance. The results show that the daily fuel oil consumption and CO_2 emissions for the optimal hull form under in-service conditions can be reduced by 14.8%.

2.7.4 Numerical Studies on Added Resistance in Waves

Various levels of numerical methods can be applied to directly evaluate the added resistance acting on ships in waves. Recently, CFD methods have been widely used to predict the added resistance in regular waves, with considering various wave heading effects or nonlinear effects, but they still require significant computational times, especially in the case of irregular waves. Time-domain numerical methods based on potential flow models have also been used to predict the added

resistance in both regular and irregular waves with relatively short computational times.

Jawa and Minoura (2023) proposed a novel probabilistic method to address the nonlinearities of added resistance concerning wave height in short-term sea conditions. Their approach incorporates a correction function, Figure 44, for the nonlinearity of added resistance, where the relative ratio of nonlinearity is derived from CFD calculation results. The proposed nonlinear PDF method enables the prediction of added resistance in irregular waves while accounting for the nonlinearity with respect to wave height.

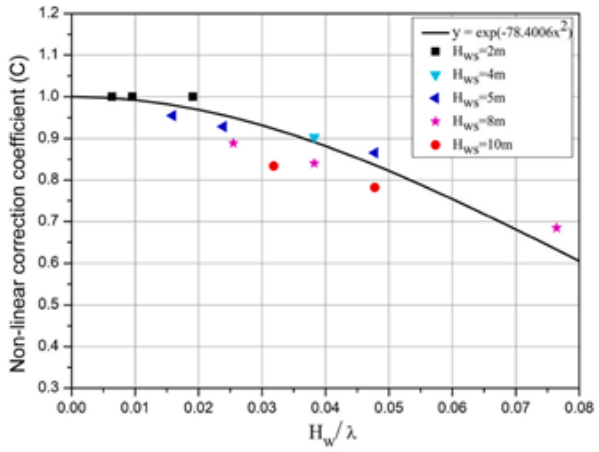

Figure 44: Non-linear effect correction function with respect to wave steepness (Jawa and Minoura 2023).

Yu et al. (2023b) predicted the motion responses and added resistance for the surge-free KCS model in head and oblique regular waves using a hybrid approach of potential and viscous flows based on the functional decomposition model SWENSE (Spectral Wave Explicit Navier-Stokes Equations). In the SWENSE method, the total physical field is decomposed into the incident wave field, where the linear wave model with the Wheeler stretching method is used, and the complementary field. They presented that surge motion has a significant impact on the seakeeping performance of the ship in astern seas, especially regarding added resistance. They also explained that the nonlinear added resistance is mainly caused by the nonlinear features of the incident, radiation and diffraction wave systems.

Dogrul et al. (2021) conducted a numerical investigation on the motions and added resistance of the Delft catamaran 372 in regular head waves using unsteady RANS CFD simulations. They showed that the interference factor varies with wave frequency, where the interference factor of total resistance in head waves oscillates around that of the calm water due to the pitch motion.

Lee et al. (2021a) carried out a series of CFD analyses for ship performance in regular waves. They employed the body-force propeller method of the virtual disk model to represent the effect of the propeller and reduce the computational time. The self-propulsion factors and power predicted by CFD were compared with results obtained using the load variation method.

Coslovich et al. (2021) developed an unsteady fully nonlinear boundary element method to calculate the ship motion and added resistance for the KVLCC2 hull in regular head waves at design speed. This study utilized an adaptive grid refinement scheme and a Mixed Eulerian-Lagrangian (MEL) approach based on potential flow model. They introduced the nonlinear decomposition for the free surface elevation and the velocity potential. It was found that generally good agreements can be observed for heave and pitch motion and added resistance compared to experimental data, especially for long waves.

Li et al. (2022b) conducted optimizing the dynamic trim of a 300000 DWT VLCC, considering both wind and wave loads. They introduced the Taylor Expansion Boundary Element Method (TEBEM) for calculating added resistance in both regular and irregular waves. They demonstrated that dynamic trim optimization was performed, resulting in a recorded fuel saving potential of approximately 0.04%.

2.8 CFD Applications

CFD applications are wide, and this section cannot be exhaustive. The degree of maturity of CFD is very high in some topics. As an example, Park et al. (2023) extended the scope of the design process to the performance of a ship in the in-service condition, with an emphasis on the added resistance due to waves. In their study, hull and fins are optimized thanks to Star-CCM+ simulations.

Added resistance and added power is indeed a very hot topic for CFD applications. Complex incoming waves are considered as oblique or cross waves. Other topics with nonlinear physics are also commonly tackled with CFD, such as roll damping, sloshing, high-speed vessels, and impacts.

A large portion of the studies is conducted with finite-volume implicit RANSE solvers, in particular with solvers built from the open-source platform OpenFOAM, and with the commercial Simcenter STAR-CCM+. There are still in-house solvers that are state of the art and very competitive on complex problems.

CFD is largely used for impact flow computation as slamming or other rarely occurring events, and the reader can refer to the specific sections.

2.8.1 Added resistance

Kobayashi et al. (2021) present a detailed guideline to compute motions and added resistance with an application on the Duisburg Test Case and the Japan Bulk Carrier. The results are obtained with an in-house solver with overset capabilities.

Lee et al. (2022b) compute the motion and added resistance on the KVLCC2 under various regular and irregular waves conditions with STAR-CCM+. The effect of the wave steepness is shown.

The consideration of the wave steepness in evaluating the added resistance is also the subject of Jawa and Minoura (2023). They compare several Fine Marine computations in regular and irregular waves to experiments.

Li et al. (2022c) also conduct simulations in irregular sea on the DTMB 5512 destroyer model with an in-house viscous overset code.

Islam and Soares (2022) using OpenFOAM also simulate the KCS in head regular waves.

Zhang et al. (2021d) use a functional SWENSE decomposition to simulate the KVLCC2 in waves with a finite difference in-house code. A similar work on the KCS is performed with another finite difference in-house code in Yu et al. (2023b).

Cho et al. (2023) study the added resistance and motion of a SVLCC in bow quartering waves using a soft spring system. They present the differences in results obtained when removing the mooring lines and restricting three DoF's. The solver is STAR-CCM+.

CFD is also used for smaller size ships, Zheng et al. (2023b) study with STAR-CCM+ the performance of a tugboat in waves.

Sun et al. (2023) study with an OpenFOAM solver the impact of the moonpool configuration on motions and added resistance.

2.8.2 Added power

Lee et al. (2021b) provide some methodology to use a virtual disk in a self-propelled simulation done with STAR-CCM+.

Yu et al. (2023a) compare the results obtained using several body-forces propeller models, and a discretized propeller for a KCS advancing in waves. The simulations are performed with an in-house RANS solver. They discuss the applicability conditions of the propeller models.

Wang et al. (2023b) also compared the results of a KCS in waves by doing OpenFOAM simulations with an actual discretized propeller and with a body force model. The solver is an in-house OpenFOAM package with overset capabilities, Figure 45.

Figure 45: Vortical structures around ship hull. Above: actual propeller. Below: body force propeller, (Wang et al. 2023b).

Htay et al. (2021) also used a body-force model in CFD Ship-IOWA to assess the effectiveness of a Rudder Bulb Fins System.

Bi-directional waves are simulated with STAR-CCM+ to study the seakeeping behaviour of an S175 by Huang et al. (2021a). Green water and slamming are discussed.

A similar work is presented by Lu et al. (2022b), where the influence of cross waves in DTMB5415 motions is proposed.

A body-force propeller model developed in an in-house OpenFOAM package is tested in bow quartering seas in Wang et al. (2022d). The results are shown to be reasonable, and the difficulty associated with the oblique seas are discussed. Other wave directions are tested with the same solver in Wang et al. (2023c). Motions and added resistance are presented.

Sanada et al. (2022) assess the accuracy of CFD in estimating the added power in head and oblique seas for the KCS. An uncertainty analysis is conducted on both numerical and experimental results. They concluded that both EFD and CFD are fit for ship design use.

2.8.3 Sloshing and coupled motions with liquid tanks

Liu et al. (2022b) conduct a complex simulation, reproducing a parametric roll condition on the ONR Tumblehome carrying a liquid tank. They use an in-house overset RANSE solver.

Huang et al. (2021b) also investigate coupled motions with an in-house finite difference RANSE code and in Tao et al. (2023) for the vessel carrying aquaculture tanks. STAR-CCM+ is used with overset.

2.8.4 Roll motion

Duan et al. (2023) used Star-CCM+ to predict the roll damping and the excessive acceleration of a ship with moonpool.

Li et al. (2023c) simulate with an in-house URANS solver the extreme roll motion of the ONR Tumblehome in beam sea.

Still on the same ONR Tumblehome, Wu et al. (2022) reproduce the parametric roll happening in head waves, with an in-house overset RANSE code, Figure 46.

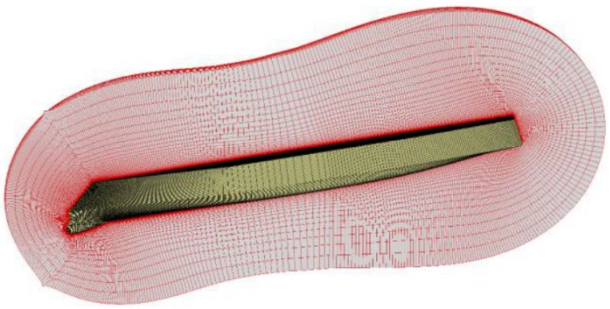

Figure 46: Body-fitted mesh used in the overset solver, Wu et al. (2022).

Koop et al. (2021) present modelling practices dedicated to decay calculations. The practices were verified during the Reproducible CFD JIP.

Decay calculations are also the object of Spyrou and Papadakis (2021), with an in-house URANSE solver.

Zhang et al. (2021e) reproduce Ikeda's forced roll experiment with a high-order fractional step finite volume solver. They compute the 2D coefficients and discuss the flow pattern and the effect of separation.

2.9 Seakeeping of High Speed Marine Vehicles

High-speed craft operating in waves are subject to significant and frequent slamming impacts. These do not only affect structural integrity but also human performance and safety. Consequently, research on the seakeeping of High-Speed Marine Vehicles (HSMV) seems to focus on three main areas:

1. Experimental and numerical predictions of motions and loads

2. Novel predictive methods for motions and loads (e.g. by machine learning)

3. Ride Control Systems (RCS) to improve passenger comfort and to actively reduce slamming and the resulting structural loads.

Over the past three years the most investigated types of HSMV were wave-piercing catamarans and trimarans.

2.9.1 Experimental and numerical investigations

A number of experimental and numerical studies on seakeeping of HSMV has been published over the last three years. Research focused on numerical solutions clearly dominates and experimental investigations were mainly conducted to validate the numerical studies. Numerical methods applied for the seakeeping of high-speed craft need to cope with highly nonlinear behaviour due to the large variations in wetted surface and impacts. This results in the adoption of nonlinear time domain methods. Besides the more traditional inviscid methods, CFD methods are becoming more and more popular.

Mai et al. (2023) experimentally studied the wave induced motions and loads on a 1.5 m long catamaran model that was towed with a spring-setup. Tests in both, regular and irregular waves were conducted in the wave basin of Changwon National University, Korea. The results obtained in regular waves consist of 6-DoF motions (response amplitude operator), wave-induced forces, and vertical acceleration. Results are compared with other catamarans and numerical methods to verify the accuracy of the experimental method. Results from tests in irregular waves, corresponding to sea states 2, 3, and 4, were used to directly obtain statistics of the motion responses of the catamaran. The motion responses in irregular waves are analysed by statistical analysis methods, based on motion times series and spectral analysis which employed the motion RAOs in regular waves and wave spectrum density. The motion response showed a good agreement between the spectral and statistical analysis methods.

Tavakoli et al. (2023a) presented a strongly coupled FSI numerical investigation of the water entry process of elastic hard-chine sections. A finite volume method (FVM) based flexible fluid-structure interaction (FFSI) based on the OpenFOAM CFD code was used to solve the multi-physics problem, Figure 47. Quantitative comparisons between experimental and computational results are also provided. Results show that the structural responses can attenuate the pressure acting on the hard-chine section for deadrise angles of 10, 20 and 30 degrees. For a section with a deadrise angle of 45 degrees, however, the pressure peaks at the keel, and is insensitive to elastic motions. It is concluded that the numerical results, presented in a non-dimensional format, may be useful for preliminary design purposes.

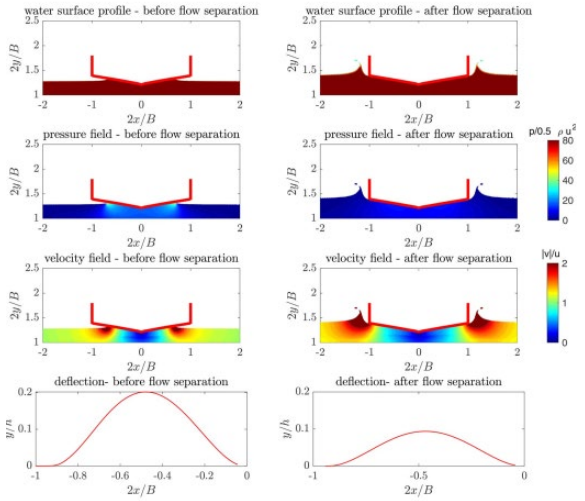

Figure 47: Fluid flow around a hard-chine section entering water at two different stages (Tavakoli et al. 2023).

Fu et al. (2021a, 2021b) studied the coupled roll-pitch motions of a trimaran in oblique stern wave conditions with the open source CFD code OpenFOAM. The numerical method is first validated against experimental data obtained in the towing tank of Harbin Engineering University and then used to study the motions of the vessel in waves. Results show i.e. that the rolling motion exhibits nonlinear characteristics.

Katayama et al. (2022) used the commercial CFD code STAR-CCM+ to calculate the flow field around different size prismatic planing surfaces and to investigate scale effects on their hydrodynamic forces. Their study highlights that, even in calm water, the accuracy of calculated frictional force is poor by appearance of Numerical Ventilation. In order to obtain more accurate results, the resolution of a partial mesh around the stagnation line needed to be increased and a surface tension model was considered.

Almallah et al. (2021) used the commercial CFD code STAR-CCM+ to study the global loads acting on the 98 m Wave Piercing Catamaran shown in Figure 50. A comparison to sea trial results indicated that full-scale CFD simulations combined with a rigid body dynamics formulation can be a reliable method to study motions and loads associated with high-speed vessels, Figure 48. The analysis was extended to oblique seas to investigate the torsional loads acting on the catamaran hull using CFD simulations by Almallah et al. (2022), Figure 49.

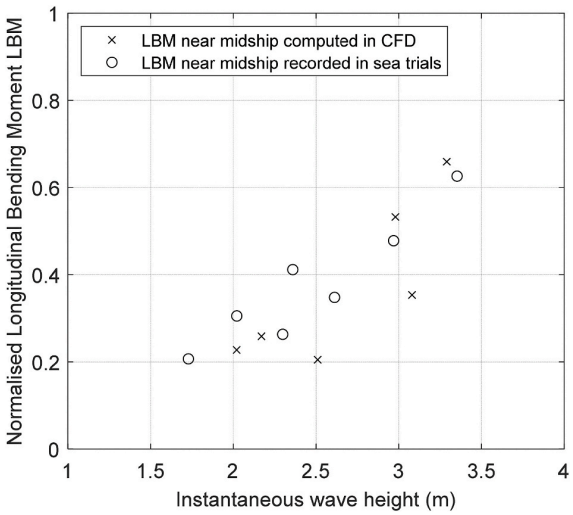

Figure 48: Slam longitudinal bending moment load as a function of instantaneous wave height prior to slam event (Almallah et al. 2021).

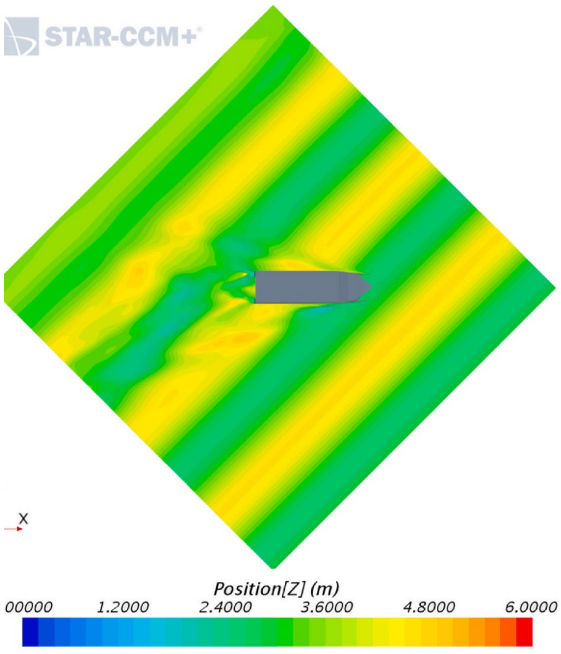

Figure 49: Water surface scene for verification of domain size in regular wave CFD in bow quartering seas at a speed of 20knots (Almallah et al. 2022).

Himabindu and Groper (2023), report on a Motion Assessment of Planing Craft in a Seaway (MAPCS) tool based on a nonlinear

time-domain approach. The tool is compared against several other approaches based on experimental, empirical and classification societies' formulae and it is found that the MAPCS approach provides more realistic estimations compared to the other methods that were studied.

2.9.2 Statistical analysis and machine learning

A number of researchers have applied signal processing concepts and machine learning techniques to the seakeeping of HSMV.

Diez et al. (2022), for example, used a k-means data clustering approach to study what type of wave sequences cause different types of severe slamming. Using CFD results for the test case of an 8 ft generic prismatic planning hull (GPPH) the authors identify the number of clusters present in the data, and thereby the slamming types. For this they use two metrics, the within cluster sum of squares and the silhouette. In addition, the t-distributed stochastic neighbour embedding (t-SNE) is used to visualize data clusters in a reduced dimensionality space. The paper discusses how the proposed approach allows to investigate what type of wave sequences causes severe acceleration, pressure and strain peaks.

Marlantes and Maki (2022) applied a Long Short-Term Memory (LSTM) recurrent neural network (RNN) approach to the seakeeping problem of a planing craft. The method can make predictions of nonlinear ship motions in a range of wave conditions when trained on response data from only a single seaway. The method is formulated around the equations of motion in the time domain, but the equations are augmented with data-driven terms from the LSTM-RNN. The resulting hybrid governing equations are solved numerically. Predictions from the method are compared to nonlinear test data of 2-DoF motion of a GPPH at forward speed in head seas, with time histories given for both regular and irregular waves. The training data requirements to classify a specific seaway are investigated and quantified. Predictions over a range of significant wave heights and peak periods are performed using training data from only a single seaway to show the effectiveness of the method in generalizing across different environmental conditions.

Sebhatleb et al. (2023) used classical, response reconstruction by transmissibility functions to predict slamming and wave load responses of the wave-piercing catamaran in Figure 50. The transmissibility functions and matrix are first derived from a small portion of the available sea trial data and then tested under the same operating condition they were derived. Then a single transmissibility matrix is used to reconstruct responses for various sea states, vessel headings and speeds. The transmissibility matrix is also tested under sea states that were not included in its derivation ("unseen data"). Good agreement is achieved, particularly for larger loading events that would be of interest to structural designers.

Zheng et al. (2023a) analysed heave and pitch motions of a trimaran, both with a "direct" CFD calculation method and with an "indirect" method based on particle swarm optimization (PSO) and polynomial fitting methods, to identify transfer function parameters. To compare the direct and indirect methods, tank tests of the trimaran were performed. Results show that the direct and indirect methods are all effective for calculating the heave and pitch motions of a trimaran.

2.9.3 Ride Control Systems (RCS)

Controlling vessel motions using Ride Control Systems (RCS) to ensure smoother journeys is a widely adopted practice and continues to be of interest to the industry. Such systems regulate vessel motions, enhance passenger comfort, and reduce structural loads.

Zhang et al. (2021b) report on developing a robust anti-pitching controller for a high-speed multihull. They propose a decoupled anti-pitching controller composed of a proportional–

differential (PD) control term and an extended state observer (ESO)-based uncertainty compensation term. The stability of the closed-loop control system is first proven theoretically. The effectiveness of the algorithm is then verified by simulations and experiments in which the heave and pitch are reduced by 20–35 % and 40–50 %, respectively.

Lau et al. (2022) analysed the influence of an active T-foil on motions and passenger comfort for a large high-speed wave-piercing catamaran (WPC, Figure 50).

Figure 50: 98 m Incat Tasmania Hull 061 WPC and swift ride-control surface locations (Lau et al. 2022).

More specifically, the influence of a ride-control system on the heave and pitch response amplitude operator (RAO) of the full-scale high-speed catamaran was investigated using extensive sea trial data from the US Navy. The reduction in motion sickness incidence (MSI) was estimated to examine the effectiveness of the RCS in improving passenger comfort. With the existing control algorithm, the vertical accelerations were found to be best controlled by the active T-foil working together with the active stern tabs, while the pitch RAO was mainly mitigated by deploying only the stern tabs. About a 23% reduction was observed in the peak heave RAO with deployment of an active T-foil. The MSI can be reduced by up to 23% with respect to the cases with stern tabs only. The analysis was later extended to oblique wave directions (Lau et al. 2023b) and, in terms of MSI percentage reduction, the ability of T-foil in vessel motion control in oblique seas was found to be limited compared to the results in head seas.

Lau et al. (2023a) developed the Forcing Function Method (FFM), a CFD-based approach to efficiently evaluate the effectiveness of different Ride-Control System geometries. Their work encompasses two main components: a standalone T-foil analysis and an assessment of the influence of various RCS geometries on a Wave-Piercing Catamaran, Figure 51 by FFM. In the standalone T-foil study, the lift and drag forces were investigated with respect to the angle of attack and immersed depth. The results indicated that the T-foil lift coefficient diminished logarithmically by decreasing the immersed depth smaller than 1 chord length. They utilised the FFM to examine different RCS geometries on a 2.5 m WPC model operating at a speed of 2.89 m/s (Fr∼0.6). The effectiveness of motion control is evaluated by measuring the changes in sinkage and trim over time after deflecting the FFM T-foil by ±15° in calm water. Through these CFD simulations, the impact of total planform area, number of T-foils, and longitudinal location of the T-foil were analysed. It was found that controllability of motion was a function of total planform area, regardless of the number of foils, and although moving the T-foil away from the bow reduces motion control in trim, it does not affect sinkage significantly.

Figure 51: Incat Tasmania 112 m wave piercing catamaran ‘Express 1’ and 2.5 m model in towing tank (Lau et al. 2023a).

Javanmard et al. (2023) report on a set of towing tank model tests in irregular waves to study the effectiveness of different control algorithms, including linear and nonlinear versions of the heave control, pitch control, and local control. The model was again a 2.5 m scaled model of a 112 m INCAT Tasmania high-speed catamaran. The RCS included a centre bow-fitted T-foil and two transom-mounted stern tabs, Figure 52.

Figure 52: 2.5 m model of Incat Tasmania 112 m WPC in the towing tank at Australian Maritime College. Location of the fitted T-foil (left) and stern tabs (right) operating as active RCS. Javanmard et al. (2023).

Ma and Zuh (2022) proposed an enhanced active disturbance rejection controller (ADRC) which compensates for the wave-induced heave and pitch motions of a fast trimaran. Controller parameters are optimized via a novel Levy flight-based ant colony algorithm (LACA). Numerical simulations and experiments under different sea conditions were conducted to validate the proposed method. Results showed the effectiveness of the proposed motion controller in improving the seakeeping performance of the trimaran.

Using the same trimaran ship model, Xu et al. (2023a) proposed a sliding mode predictive anti-pitching control considering appendages constraints. The control method combines the advantages of model predictive control and sliding mode control to both improve the strong robustness of the system and to ensure the optimization and the ability to handle constraints explicitly. The vertical motion model is established for multihulls with two types of appendages, T-foils and flaps, to achieve anti-pitching. According to the characteristics of the first-order autoregressive wave disturbance model, a low complexity disturbance observer is devised to estimate the wave disturbance force and moment online and combine the estimates with the prediction model to enhance the accuracy of the prediction. On this basis, a prediction model and an objective function are established with the sliding mode states as variables, and the sliding mode terminal stability constraint set is adopted to improve the stability of the closed-loop system. The effectiveness of the designed controller is verified by simulation and experiment, in which the multihull heave displacement is reduced by 52 % and the pitch angle is reduced by 58 %.

Li et al. (2023a) investigated the roll-pitch coupling of a trimaran in oblique head waves and how this can be attenuated by a T-foil RCS. They used fully nonlinear unsteady RANS simulations based on the finite volume method to study the motions of the vessel with and without RCS. Results show that lower forward speed and large wave steepness will lead to roughly coupled motion in oblique head waves and that nonlinear characteristics of ship motions were present during coupled motions. A T-foil RCS can significantly reduce the motion responses and have a positive effect on the coupled motion of the trimaran.

2.9.4 Design aspects

Marin-Lopez et al. (2021) and Paredes at al. (2022) describe the conceptual design of a small high-speed craft providing inter-island transportation in the Galápagos. An optimization procedure at conceptual design level was developed. First, time histories of vertical accelerations on an existing ferry were measured and analysed. Weighted acceleration signals are compared with those from well-known experimental tests and are also used to evaluate the index of motion sickness with ISO 2631 standard to determine the number of persons affected by craft motion. Then, an optimization procedure using feasible directions is implemented with a combination of resistance and CG acceleration of the vessel to be minimized. Both functions were evaluated using well-known empirical formulations. The results show that by increasing length and deadrise angle, and moving LCG forward, it is possible to reduce the acceleration by 20 % while obtaining a 4 % reduction in resistance.

3. PROCEDURES

As part of ToR 2 the committee was tasked to review the existing ITTC Recommended Procedures relevant to seakeeping and identify any requirements for changes in the light of current practice. After discussions with the Advisory Council the updates summarised in the next sections were made.

The Committee also added a list of suggested keywords and an abstract for DOI registration to each procedure.

Additionally abstracts and keywords for DOI registration were written for all procedures and submitted to the ITTC Secretary.

3.1 Seakeeping tests HSMV (7.5-02-05-04)

The procedure was updated with some minor editorial revisions. Furthermore, a reference that was not cited in the text was removed from the reference list.

3.2 Seasickness HSMV (7.5-02-05-04.1)

The procedure was updated by correcting erroneous references and pointing out that the underlying ISO standards are superseded. Nevertheless, the ITTC procedure (and the superseded ISO standard explained in it) are still valuable because it directly shows discomfort boundaries, whereas the newer standard uses the concept of "motion sickness dose value", MSDV.

3.3 Structural loads HSMV (7.5-02-05-06)

The following changes have been done to procedure 7.5-02-05-06:

- Minor changes to the text in Section 1.
- Section 2 is renamed from "Test techniques and procedures" to "Model design and test techniques for HSMV"
- Section 2 has been restructured and now includes these subsections:
    - 2.1 Relevant HSMV procedures
    - 2.2 Loads and load effects
    - 2.3 Design of models for measurement of global load effects
    - 2.4 Local loads and load effects
- The order of the sections "Parameters" and "Validation" has been interchanged.
- The layout of the "Parameters" section has been changed from numbered to bulleted points.
- The list of parameters to be taken into account has been updated.

3.4 Seakeeping experiments (7.5-02-07-02.1)

Minor editing changes proposed.

3.5 Power prediction in irregular waves (7.5-02-07-02.2)

The following minor editorial revisions were applied:

- Some display errors in Table 1 - Summary of prediction methods - has been fixed.
- Uncited references have been removed.

3.6 Rarely occurring events (7.5-02-07-02.3)

Some minor editorial revisions were applied. In addition, the following changes were applied:

- Chp1: The reference to ITTC procedure 7.5-02-05-07 has been deleted as the - procedure was withdrawn
- Introduction of Section 2.4: The text was extended by recommendations to references for determination of statistical quantities. Respectively the reference list was extended.
- Section 2.5: An example with reference was added to study the severity of extreme conditions. Furthermore, a short paragraph about too high or too low events was deleted.
- Section 4.1: The parameter list was adapted to the ITTC standard

3.7 Validation of seakeeping computer codes (7.5-02-07-02.4)

This procedure has been deleted.

3.8 V&V of linear/weakly nonlinear computer codes (7.5-02-07-02.5)

The following changes have been done to procedure 7.5-02-07-02.5:

- Last line in Section 2.3, a dot is added to ITTC procedure 7.5-02-07-02.1.
- Last line in Section 2.4, Harmonic motions and loads. Is deleted. Because for time domain linear seakeeping simulations the assumption of Is not necessarily right.
- In Table 1 linear method, Impulse-Response-Function, is added.
- In Section 3.1 Geometry formula is corrected from KM+BM to KB+BM is equal to KG+GM
- In Section 5.7 Check cargo modelling is corrected.
- In reference, Ikeda Y, Himeno Y, Tanaka N.，1978，Prediction method for ship roll damping，Report No.00405 of Department of Naval Architecture, University of Osaka.is added

3.9 Global loads seakeeping (7.5-02-07-02.6)

Besides editorial revisions the following changes were applied:

- Section 2.1: The text was made more to the point and a paragraph about comparison of complexity in model construction was deleted. Another paragraph was rewritten to increase readability
- Section 2.2: A figure of different model types for global load tests was added.
- Section 2.4: The section was partly rewritten to condense the important information and increase the readability
- Section 2.8: The headline and content were supplemented with respect to towed model tests. Additionally, the first paragraph about the powering of the model was rewritten from the perspective of the current state of science.
- Section 2.9: Two paragraphs were rearranged with the images within this section and sensor recommendations were added.
- Section 2.10: The first section was supplemented by statements on the importance of decay tests and how to perform those tests.
- Section 3.1: In this section as well as at the reference list a reference was added.
- Section 4.1: The parameter list was completed and adapted to the ITTC standard.

3.10 Sloshing (7.5-02-07-02.7)

Minor editing changes proposed.

3.11 Calculation of weather factor - fw (7.5-02-07-02.8)

Procedure 7.5-02-07-02.8 was slightly modified with the following changes:

- The reference section has been updated.
- List of symbols and parameters has been updated and aligned with ITTC notation.
- A secondary axis has been added to Figure 2 to underline the issue of fw-waves and small vessels.
- Editorial changes have been made, including compliance with ITTC standard format of procedures (e.g., placing the “Parameters and Symbols” section at the end, not at the beginning)
- Section 4 has been re-named from “Recommended Practical Method” to “Example Practical Method” to underscore that the combinations shown in Table 3 are not mandatory.
- Table 3 has been modified to make it more practice oriented.

4. NEW GUIDELINE ON CFD FOR SEAKEEPING (TOR3)

Under ToR 3 the committee was asked to create a new guideline on verification and validation of the CFD methods for seakeeping analysis.

The task was approached through the following five steps:

1. Review of literature and existing procedures that could be relevant for this topic.
2. Identify key areas within the general topic of CFD methods for seakeeping analysis.
3. Contact Specialist Committee on Combined CFD/EFD and discuss what is their view on seakeeping and CFD.
4. Contact a number of prominent researchers in the field asking concrete questions regarding the need for ITTC guidelines on Seekeeping and CFD ("How to use" guidelines and V&V).
5. Elaborate recommendations regarding this topic.

Each step with details and discussions are presented in the next subsections.

4.1 Review of literature

Seakeeping analysis with CFD includes a number of diverse physical problems that are covered by the other procedures of the SKC, e.g:

- Rarely occurring events
- Global loads
- Motions
- Added resistance
- Sloshing
- Damage stability in waves
  Hydroelasticity in waves

The requirements for the CFD simulations would depend on the particular problem.

Literature on how to use and V&V for these topics is generally scarce, though several papers were published in the recent years.

For subjects such as maneuvering or resistance or self-propulsion, ITTC CFD "how to use" guidelines exist separated from V&V procedures. They indicate the requirements of the numerical models (turbulence, scheme order) and provide information on parametrization (domain size, time stepping, grid discretization).

The ToR mentions several types of CFD solvers, but the V&V approach is mostly used with mesh-based CFD solvers (except sloshing, where particle methods can be competitive).

4.2 Identify key areas

Wave generation and propagation are fundamental parts of seakeeping CFD simulations except uncoupled sloshing. CFD is much more dissipative than an actual test and the quality of the wave is by itself a problem that could require guidelines and V&V. This also introduces the question whether waves should be calibrated beforehand for a procedure on how to conduct a CFD seakeeping test. If the answer is positive, how should this calibration be carried out (on which mesh, …).

Other aspects that might need attention:

- How to obtain calm water resistance?
- How to introduce the waves in the domain?
- How to deal with velocity ramping?
- How to avoid residual transients, etc. ?
- Towing points, springs need to be specified.

About V&V, the generic V&V guidelines deal with a set of constant scalar outputs (calm water resistance, sinkage, trim, etc.). For seakeeping problems the outputs can be much more complex. What are the quantities that should be targeted by the V&V? Is it something like the 1st harmonic of a series of quantities, or mean values as in added resistance problem, the

maximum load during an impact, or even a transient time trace?

4.3 Contact Specialist Committee on Combined CFD/EFD

A dialogue was opened with the SC on Combined CFD/EFD Methods. However, not much momentum was gained with such dialogue.

4.4 Contact prominent researchers

A number of prominent researchers in the field were contacted following this interchange asking concrete questions regarding the need for ITTC guidelines on Seakeeping and CFD ("How to use" guidelines and V&V). Diverse answers were received from Prof. El Moctar, Prof. Maki, Dr. Koop and Dr. Vaz. Such answers have been useful to confirm that:

- the matter is relevant,
- there is no clear consensus on how to proceed, with many open questions along the aforementioned lines.
- therefore, it could be too early for a full V+V guideline
- a V&V procedure is important to be able to justify potential "How to use" guidelines (time stepping, mesh size).

4.5 Elaborate recommendations

Considering all what has been mentioned, our recommendation for the next term reduces to propose that ITTC should create a Specialist Committee on Seakeeping and CFD, with the following tentative ToRs:

- Follow the new literature on the topic.
- Assess whether the same structure as in manoeuvrability should be followed ("How to use" guidelines and V&V separated guidelines).
- Assess how to adapt such guidelines to the seakeeping particularities, e.g. whether to focus explicitly on particular matters such as average value of added resistance in waves, or whether to have a holistic approach, looking into the unsteady variables such as short-term statistics of resistance, motions, etc., or any other given events.
- Define the role of the quality of the input wave, and how to handle it in the V&V procedure. Should waves be calibrated first?
- Define how to obtain calm water resistance, necessary for the computation of the added resistance in waves.
- Define how to introduce the waves in the domain.
- Define how to deal with velocity ramping and how to avoid residual transients etc.
- Specify how towing points, springs should be defined.
- Decide whether to focus on conducting a wide comparison study by several groups to settle the matter before writing guidelines.
- Decide whether some use can be given to the experimental ITTC seakeeping benchmark carried out during the 2021-2024 term.
- Decide whether a practical approach should be developed as well to be able to get confidence in the results without having to go through a likely expensive V&V study.
- Define how to conduct V&V when coupling CFD solvers with structural solvers in springing or whipping problems.

5. FUNCTIONALITY OF FW-PROCEDURE FOR SMALL SHIPS (TOR4)

5.1 Background

As part of ToR 4 the committee was tasked to investigate the "functionality" of the fw-procedure (7.5-02-07-02.8) when applied to ships smaller than 150 m in length.

As a first step the history of this task has been tracked, and it became apparent that the issue is not about the prediction methods listed in procedure 7.5-02-07-02.8 but about in how far the wind and wave conditions defined by IMO are appropriate for small ships.

In the fw-context IMO currently specifies only one single “representative” sea condition, regardless of ship size, see Table 1 below.

Table 1: Representative sea conditions based on IMO (2012).

Significant wave height $H_{1/3W}$	3.0 m
Mean wind speed 10m above sea surface U_{10}:	12.6 m/s
Zero-up crossing period T_2	6.16 s

The corresponding long-crested wave energy spectrum from IMO (2012) is plotted in Figure 53. As illustrated by the secondary abscissa in the figure this spectrum contains a lot of energy in the wavelength region of around 100 metres. It can therefore be expected that ships of around 100 m length and below will severely pitch when encountering such waves. These motions, and the related accelerations might require a voluntary speed reduction by the ship’s master to avoid excessive motions and loads.

Consequently, the wave conditions are not “representative”/typical any longer.

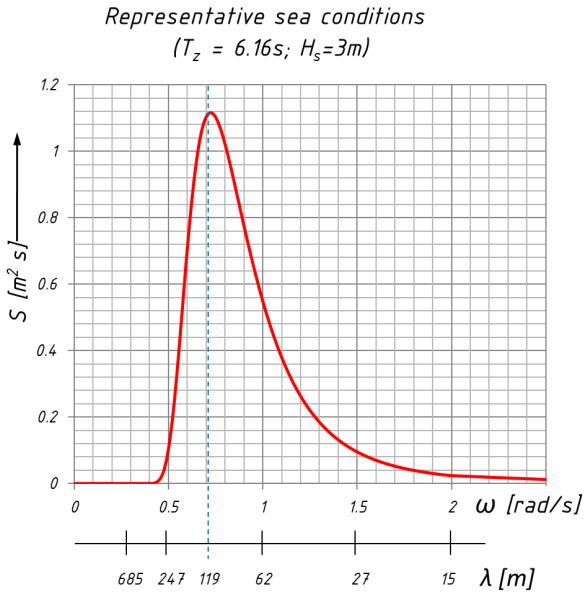

Figure 53: Wave energy spectrum *S(ω)*. Secondary x-axis shows length of regular deep-water wave with same frequency.

5.2 Available data for small ships in fw-waves

A literature search resulted in only one published value of the weather factor fw for a small ship. Gerhardt and Kjellberg (2017) conducted experiments for a 96-metre vessel in fw-wave conditions according to IMO (2012) (Table 2). For this ship we get fw=0.67. The corresponding ship speed at 75% MCR is about 9knots.

As part of their work the committee has located the original experimental dataset behind the Gerhardt and Kjellberg (2017) publication, re-evaluated the results, and compared motions and accelerations to criteria for voluntary speed reduction from the literature, Nordforsk (1987). Results are summarised in Figure 54.

Table 2: Main parameters of ship tested in fw-waves by Gerhardt and Kjellberg (2017).

Parameter	Value
Length, Lpp	96 m
Breadth, moulded	18 m
Draft forward (FP)	4.7 m

Parameter	Value
Draft aft (AP)	4.7 m
Block coeff.	0.74
Displacement	5900 m^3
GM	0.76 m
Radii of gyration, roll	0.33 B
pitch & yaw	0.23 Lpp

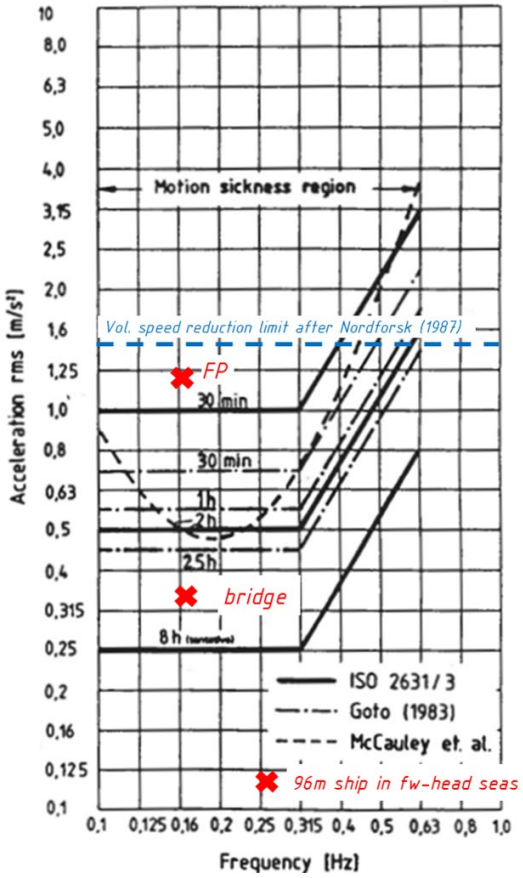

Figure 54: Severe discomfort boundaries with regard to vertical acceleration as a function of frequency for different exposure times (Nordforsk 1987). Also shown are seakeeping model test results for a 96 m ship (Gerhardt and Kjellberg 2017).

As Figure 54 shows, motion induced vertical accelerations will create some discomfort, particularly near the forward perpendicular but values are below, albeit close to, the limit for voluntary speed reductions from Nordforsk (1987), illustrated by the blue line in the figure.

The probability of green water on deck was also evaluated by the committee and found to be 0.06, slightly above the limiting value of 0.05 (events per 100 wave encounters) from Nordforsk (1987).

In summary it can be said that a voluntary speed reduction for small vessels appears to be relevant and should be investigated further. Future investigations should focus on ships smaller than 100 m, but still within the applicability of the EEDI.

5.3 Suggested changes to fw-procedure

As a result of the above investigation ITTC procedure 7.5-02-07-02.8 was slightly modified to further highlight the issue of voluntary speed reduction for small ships, see Section 3.11 above.

5.4 Suggested next steps

Since experimental data for small ships in fw-conditions is rare, it is recommended that the next Seakeeping Committee uses simulations to investigate the topic of 'voluntary' speed reduction for vessels smaller than 100 m in length, but still within the applicability of the EEDI. If required, such simulations can also be used to develop alternative, milder sea states for small ships.

6. NEW GUIDELINE ON MINIMUM POWER REQUIREMENT (TOR5)

Under ToR 5 the committee was asked to "investigate if there is any practical problem in the application of MEPC.1/Circ.850/ Rev.2 for minimum power requirement, and develop a new ITTC guideline, if needed."

6.1 Background

The introduction of the EEDI more than a decade ago, slow steaming, and the wish to reduce bunkering costs have resulted in a trend to install less powerful engines in ships. To avoid vessels becoming underpowered and thus unsafe, the International Maritime Organization

(IMO) has published a guideline regarding the "Minimum Propulsion Power to Maintain the Manoeuvrability of Ships in Adverse Conditions". IMO "Interim Guideline" MEPC.1/Circ.850/Rev.2 outlined the details of how to determine this "Minimum power".

Since July 2021 there is a Rev. 3 of this IMO circular. The most significant change from Rev.2 to Rev.3 is dropping the required speed for safe manoeuvring from in between 4 and 9 knots (depending on relative size of the rudder) to just 2 knots, while simultaneously prescribing slightly harsher weather conditions.

The work of the 30th ITTC Seakeeping Committee has focused on Rev. 3 as the latest version of the IMO circular.

6.2 New ITTC guideline

After discussions with the ITTC Advisory Council a new ITTC "Guideline on determining Minimum Propulsion Power to Maintain the Manoeuvrability of Ships in Adverse Conditions" has been drafted. This draft has been shared and discussed with the Manoeuvring and Full-Scale Ship Performance committees and their feedback has been incorporated.

The draft is mainly based on MEPC.1/Circ.850/Rev.3 but it gives additional explanations and fills in gaps where required. Additionally, the draft guideline contains an example that follows the calculation process step by step and works out minimum power for the KVLCC2 tanker. It is hoped that this case study helps with understanding the calculation process and provides useful benchmarking data. A shortened summary of this case study is reproduced in Section 6.4 below.

For space reasons the 19-page draft guideline is not reproduced here, but it is available from the ITTC Secretary.

6.3 Problems found in IMO Circ.850/Rev.3

The main issues that the committee found in IMO MEPC.1/Circ.850/Rev.3 are:

1. The IMO circular appears to be contradictory in the choice of peak wave periods.
2. The IMO circular gives "default conservative" estimates for thrust deduction factor and wake fraction. These values appear to be questionable.
3. It is unclear whether the IMO-suggested 3 % thrust increase to account for rudder action in waves is realistic.

The following subsections briefly explain the above three issues. More details can be found in the draft guideline available from the ITTC Secretary.

6.3.1 Peak wave periods

The IMO circular appears to be contradictory on what range of peak wave periods T_P should be used in the minimum power assessment (step 16 of the IMO assessment contradicts the T_P values listed under the spectrum definitions by IMO).

6.3.2 Choice of propulsive factors

The IMO circular states that: "calm-water resistance, self-propulsion factors and propeller open-water characteristics, are defined by the methods approved for EEDI verification" and also gives "default conservative" estimates for thrust deduction factor and wake fraction; t=0.1 and w=0.15 respectively.

These values for t and w are based on IMO submission MEPC 72/5/9 by China (Figure 55) and reflect results from one single set of self-propulsion model tests in the speed range of 2-7 knots. It is unclear how the challenges in conducting low speed model tests were addressed and what type of ship (full block or low block coefficient) the results represent.

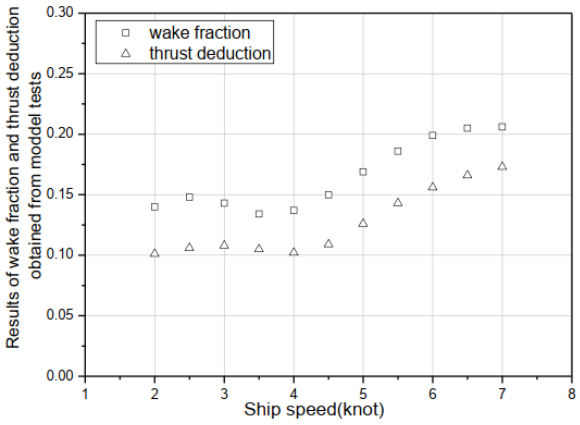

Figure 55: Wake fraction and thrust deduction factors at low speeds, from IMO submission MEPC 72/5/9.

As illustrated by the KVLCC2 case study in the next section, power predictions based on t=0.1 and w=0.15 are not necessarily conservative for a full-block ship. Particularly the choice of t=0.1 appears to be optimistic, compare top part of Figure 59.

More research on the behaviour of thrust deduction factor and wake fraction for different ships at low speeds is clearly needed before general recommendations about default values for t and w can be made. In addition to looking at w and t separately, such research should also evaluate the resulting hull efficiency η_h.

In the absence of more reliable data, the ITTC draft procedure now recommends relying on other methods approved for EEDI verification, i.e. ship specific model tests. In most cases, such model test results should already be available from the mandatory EEDI tests at standard speeds (i.e. 75 % MCR). Extrapolating wake, thrust deduction factor and relative rotative efficiency from these tests down to a speed of 2 knots appears to be preferable over the use of the generic IMO default values.

6.3.3 Rudder drag in waves

At this stage it is unclear whether the above 3 % value for added thrust due to rudder action is realistic. Further research in this area is required.

6.4 KVLCC2 case study

To investigate if there is "any practical problem in the application" of the IMO procedure this section contains a summary of a case study that follows MEPC.1/Circ.850/Rev.3 and the ITTC draft guideline step by step.

6.4.1 Benchmark case KVLCC2

Due to the availability of data and the usefulness as a benchmark case it was decided to use the KVLCC2 for such a case study.

Figure 56 shows a photograph of the 4.7 m long model used for the seakeeping tests related to the case study. A second, larger model was used to assess calm water performance in a towing tank.

Figure 56: KVLCC2 model used for study.

6.4.2 Adverse conditions

The environmental conditions in the IMO guideline are not defined by one single wave condition but by spectra with modal (peak) periods varying from 7 s to 15 s. As a result, not one but several predictions of minimum power need to be carried out. The highest power value calculated during this process determines the required engine MCR. For a large ship like the KVLCC2 (L_{pp}=320 m) three example spectra according to Table 1 are plotted in Figure 57.

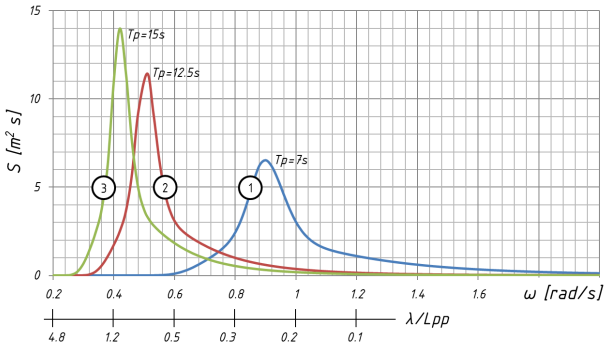

Figure 57: Example JONSWAP spectra. *Hs*=6 m and 3 different modal periods Tp. Secondary x-axis shows length of regular deep-water wave with same frequency, relative *Lpp*.

6.4.3 Resistance components

Figure 58 illustrates resistance components for the KVLCC2 sailing at 2 knots. As can be seen the calm water resistance is negligible compared to added wind and wave resistance. The total resistance for the three example spectra becomes:

R①=1060.2 kN

R②=1286.9 kN

R③=1089.8 kN

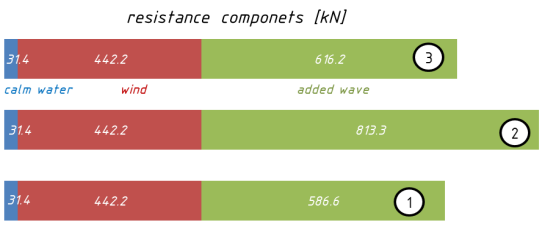

Figure 58: Comparison of resistance components for KVLCC2 at 2 knots.

The individual resistance components behind these numbers were determined as follows:

- Calm water resistance: Towing tank tests with a 7 m model
- Added wind resistance: Based on X'_w = 1.1
- Added wave resistance: Regular wave tests with the model from Figure 56.

6.4.4 Choice of propulsive factors

Based on the data presented in Figure 59 the following values for the propulsive factors were used in the case study: t=0.18 and w= 0.3 (blue lines in Figure 59). The figure also shows the IMO default values in red. A representative value for the relative rotative efficiency was also chosen based on tank tests results: η_R = 1.052.

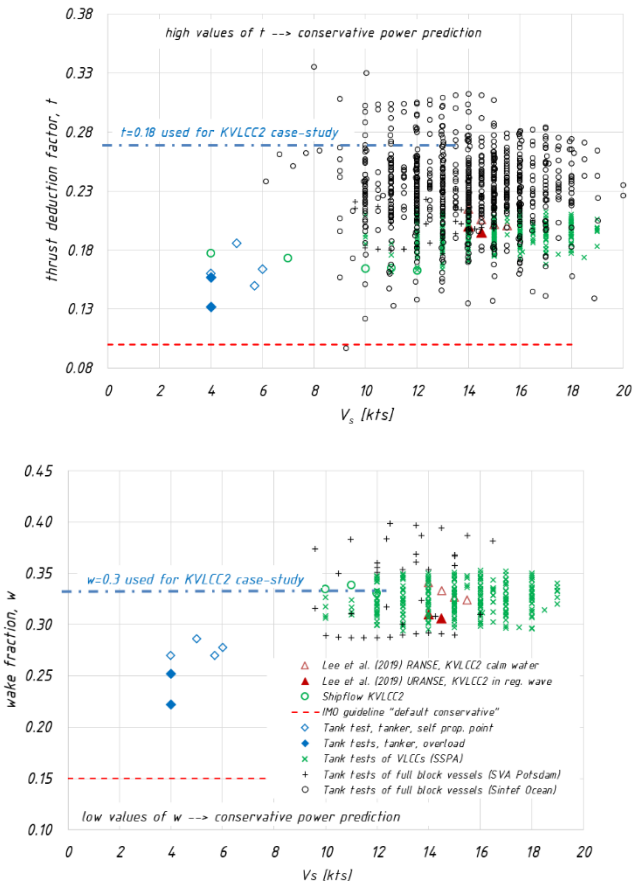

Figure 59: Wake and thrust deduction factors for tankers.

6.4.5 Calculation of required break power

Figure 60 shows results from the calculation of required power to maintain a speed of 2 knots in wind and waves.

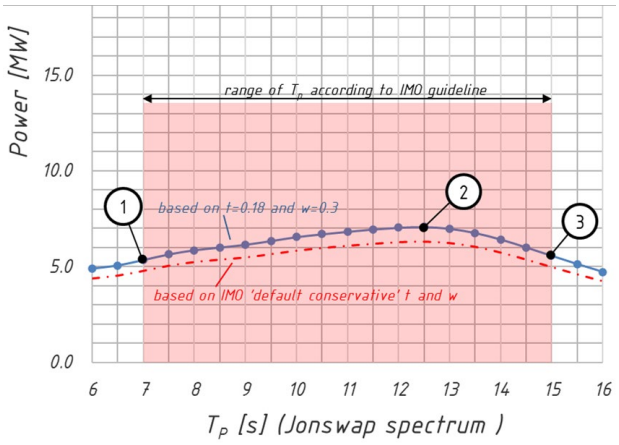

Figure 60: Required power to maintain a speed of 2 knots as function of modal period *Tp*.

The maximum required power and the corresponding *rpm* for the KVLCC2 correspond to point ② on the blue line in Figure 60:

$$P_B^{req} = 7.1\ MW \quad @\ 45.2rpm$$

The red line in Figure 60 represents power values based on the "default conservative" estimates of thrust deduction *t* and wake fraction *w*. As can be seen the IMO "default conservative" estimates produce power values that are not conservative.

6.4.6 Available break power

The above value of 7.1 MW is only the required shaft power to propel the ship at 2 knots. For combustion engines, torque and other limitations must be considered.

To determine the available brake power P_B^{av} of the installed engine, Figure 61 finally plots the operational points 1-3 (i.e. power/rpm combinations corresponding to wave spectra 1-3) into load diagrams for two engines.

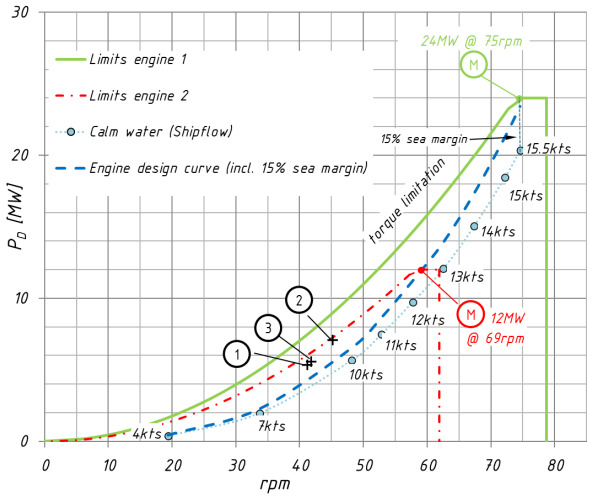

Figure 61: Engine load diagram.

Engine 1, with an MCR of 24 MW at an *rpm* of 75, is a typical VLCC-engine (green solid line). It can bring the KVLCC2 up to a design speed of 15.5 knots in calm water with a sea margin of 15 %. Engine 2 (red dash-dotted line) is much smaller (12 MW @ 69 *rpm*) and can be considered a "slow steaming" option. It will propel the ship at about 12.2 knots in calm water with the same sea margin as the larger engine.

It can be seen from the figure, that the larger engine will deal effortlessly with all the situations the KVLCC2 might encounter under the "IMO adverse conditions". This is because the operational points (①②③) end up below the torque limit line (solid, green curved line).

Engine 2 on the other hand will just be able to provide the required power for *Vs* = 2 knots. As illustrated in the figure at Point ② the available engine power equals the required power:

$$P_B^{av} = P_B^{req} = 7.1\ MW \quad (@\ 45.2rpm)$$

For the KVLCC2 such an engine with an MCR of 12 MW is the minimum that can be installed while still complying with IMO minimum power requirements.

6.5 Suggested next steps

The ITTC "Guideline on determining Minimum Propulsion Power to Maintain the Manoeuvrability of Ships in Adverse Conditions" that was drafted by the 30th Seakeeping Committee is a technical interpretation of IMO MEPC.1/Circ.850/Rev.3. During the preparation of the guideline three issues became apparent, see Section 6.3 above. The next ITTC Seakeeping Committee should investigate these in detail and update/improve the draft guideline prepared by the 30th committee accordingly. For more details see Section 11.3 at the end of this report.

7. NEW GUIDELINE ON WIND LOADS FOR SHIPS (TOR6)

Under ToR 6 the SKC was asked to develop a guideline on wind loads for ships, collaborating with the committees related to this issue.

After review of the first progress report (dated August 2022), the SKC was asked by the Advisory Council (AC) to list and summarise the methods for estimating wind loads in ITTC procedures; see Table 3 and Table 4.

Table 3: Wind load prediction methods as recommended in various ITTC procedures.

ID #	Procedure	Generic Values	Dedicated WT	Dedicated CFD	Direct modelling (wind during experiment)	Datasets for typical ships	Generic regression method	Refers to ITTC 7.5-04-01-01.1
①	ITTC 7.5-02-03-01.4	✓	✓					
②	ITTC 7.5-02-03-01.5							✓
③	ITTC 7.5-02-07-02.8		✓	✓		✓	✓	✓
④	ITTC 7.5-02-07-03.6		✓					
⑤	ITTC 7.5-02-07-04.1		✓		✓			
⑥	ITTC 7.5-02-07-04.2				✓			
⑦	ITTC 7.5-02-07-04.4		✓	✓		✓	✓	
⑧	ITTC 7.5-03-02-05	Not applicable (guideline on how to do CFD)						
⑨	ITTC 7.5-04-01-01.1		✓	✓		✓	✓	
⑩	ISO 15016:2015		✓			✓	✓	

Table 4: Summary of wind related content.

ID #	Procedure	Summary of wind part
①	ITTC 7.5-02-03-01.4 78 Performance Prediction Method	Guideline mentions air drag coefficient of ship above waterline. Can be determined from wind tunnel tests. Value of 0.8 can be used as default value
②	ITTC 7.5-02-03-01.5 Predicting Powering Margins	Refers to ITTC 7.5-04-01-01.1: (and ISO 15016 which is very similar)
③	ITTC 7.5-02-07-02.8 Calculation of the Weather Factor fw for Decrease of Ship Speed in Wind and Waves	Section 3.5.2 says: *"This resistance component is calculated in accordance with ITTC Procedure 7.5-04-01-01.1: Preparation, Conduct and Analysis of Speed/Power Trials"* Wind force coefficient best found from WT tests. Alternatively: WT tests of similar ship, WT results from Blendermann, viscous flow CFD or Fujiwara
④	ITTC 7.5-02-07-03.6 Dynamic Positioning System Model Test Experiments	Text: "In general, the following model test program should be carried out for floating structures equipped with DP systems: Wind tunnel tests to determine wind resistance coefficients"
⑤	ITTC 7.5-02-07-04.1 Model tests on intact stability	Direct modelling of wind forces via fan-arrays or force coeff. From separate WT tests.
⑥	ITTC 7.5-02-07-04.2 Model tests on damaged stability in waves	"Model must be allowed to drift freely under influence of waves and wind" Direct modelling of wind forces via fan-arrays as one possible method, no other methods specified
⑦	ITTC 7.5-02-07-04.4 Simulation of Capsize Behaviour in Irregular Beam Seas	"Wind load coefficients in six degrees of freedom can be obtained from wind tunnel experiments and CFD, or from empirical methods based on non-dimensional wind tunnel data. Examples are Isherwood (1972), Blendermann, (1994) and Fujiwara (1998)
⑧	ITTC 7.5-03-02-05 Use of CFD methods to calculate wind resistance coefficient	Guideline on how to use CFD for prediction forces acting on above water parts of ships
⑨	ITTC 7.5-04-01-01.1: Preparation, Conduct and Analysis of Speed/Power Trials	For calculating the resistance increase due to wind one of the following methods are to be used. F.1. Wind resistance coefficients by wind tunnel test If wind resistance tests for the specific, or similar, vessel have been performed in a qualified wind tunnel, the wind resistance coefficients derived by these measurements shall be used to compute the wind resistance of the vessel in the trial condition. F.2. Wind resistance coefficients by CFD F.3. Data sets of wind resistance coefficients Guideline gives dataset for common ship types F.4. Regression formula by Fujiwara et al.
⑩	ISO 15016:2015: Guidelines for the assessment of speed and power performance by analysis of speed trial data	Annex C: Resistance increase due to wind C.2.1 Wind tunnel test C.2.2 Data set on the wind resistance coefficient C.2.3 Regression formula by Fujiwara et al.

It was found that many different methods are recommended in various procedures. It was found that the best and most recent recommendation on how to determine wind resistance was in Annex F of ITTC procedure 7.5-04-01-01.1 - Preparation, Conduct and Analysis of Speed/Power Trials.

The SKC made the following recommendations at the start of 2023 and in the second progress report (dated August 2023):

- Extend Appendix F of ITTC 7.5-04-01-01.1 so that it covers aerodynamic forces and moments in more degrees of freedom (minimum surge, sway, pitch and roll);
- Lift the hereby revised Appendix into a standalone procedure;

- Modify all procedures listed above: remove all recommendations about wind loads and refer to new procedure.

In October 2023, feedback from AC was received and the SKC was asked to develop a standalone wind load guideline based on Appendix F of 7.5-04-01-01.1

This was done at the start of 2024 and at the end of February, the draft document was circulated to other relevant committees for comments and when relevant, modified accordingly. A table of the modifications needed in other ITTC procedures was also produced and circulated for comments. The final version of this table will be handed over to the next committee via the ITTC secretary.

The work of the current SKC and the discussions with other committees have shown that there is a need to address a significant number of wind-related issues. Tasks could include:

- Include wind load coefficients for side force, yawing moment and roll moment in the new guideline on "Wind Loads on Ships";
- Improve this guideline, make it more comprehensive and turn it into an ITTC procedure;
- Survey state of the art in describing atmospheric boundary layer profiles (ABL) and natural turbulence spectra of the wind over the sea. Unify equations to describe ABL profiles across all ITTC procedures;
- Make recommendations how to measure wind speed and direction in the disturbed flow around a moving ship;
- Develop ITTC guidelines on wind tunnel testing of ships;
- Investigate the question whether Wind Tunnel Facilities working with ships, marine structures and wind propulsion technologies should be invited to join ITTC.

8. EXPERIMENTAL BENCHMARK ON ADDED RESISTANCE (TOR7)

In the 30th term the Seakeeping Committee has organised a world-wide benchmarking study on measuring added resistance in waves.

8.1 Background

Under ToR 7 the Committee was asked to "Organize a benchmark experimental campaign, including the added resistance measurement in oblique seas and different loading conditions, and the characterization of the uncertainty in the measurement of added resistance." To this end all ITTC members were invited to join a benchmark study.

8.2 Organisation of study

The study was prepared and organised by a working group consisting of nine members from the Seakeeping Committee (F. Gerhardt; M. Minoura; B. Bouscasse, BW Nam, K. Domke, A. Souto-Iglesias, W. Duan, Y. Pan, B. Malas). A series of initial discussions and industry interviews resulted in the following structure of the study.

8.2.1 Call for participation

All ITTC membership organisations were invited to participate in a benchmark campaign with the following format:

- Seakeeping tests with scale models of a VLCC/tanker (KVLCC2, Table 5)
- Tests in regular and irregular waves. Head and following seas as well as oblique wave directions.
- Choice of two KVLCC2 models that can be borrowed free of charge (Table 6). Alternatively, model built by participant.
- All steps from model preparation over testing procedures to measurement-evaluation to be documented and shared with ITTC.

- All experimental costs to be paid for by participants.
- ITTC to summarise results and share with all participants.
- Option to withdraw results before final publication.

Table 5: Main parameters of KVLCC2 as used in this benchmarking study (target values).

Ship particulars	Value
L_{pp} [m]	320.0
Beam, B [m]	58.0
Design draft, T [m]	20.8
Gyradius roll [m]	0.40·B
Gyradius pitch [m]	0.25·L_{pp}
Gyradius yaw [m]	0.25·L_{pp}
GM [m]	5.7
Displacement [m^3]	312 784
VCG	18.6

Table 6: Main particulars of available KVLCC2 models.

Ship particulars	SSPA/RISE	CEHIPAR
Scale	68	80
LPP [m]	4.706	4
Beam [m]	0.853	0.725
Draft [m]	0.306	0.26
Displacement	995 kg	611 kg
Weight (empty model)	250 kg	120 kg

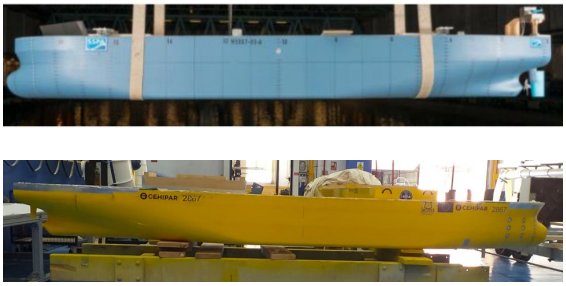

Figure 62: The two freely available models (SSPA/RISE top, CEHIPAR bottom).

The test program is summarised in Table 7 below. Participants could choose between three different levels of involvement:

- Towing tank: head and following seas only, time requirement about 5 days
- Seakeeping basin (light version): 3 wave directions, time requirement about 9 days
- Seakeeping basin (full version): 7 wave directions, time requirement about 22 days

8.2.2 Participating organisations

A total of sixteen ITTC member organisations answered the call and expressed general interest in the study. Of these, ten organisations were eventually able to conduct tests and submit results in time. In alphabetical order:

1. CSSRC
2. Gdansk University of Technology
3. Hanwha Ocean
4. IMABARI Ship Model Basin
5. KRISO
6. MARIN
7. Osaka University
8. RISE
9. Samsung model basin
10. SVA Potsdam

To preserve anonymity each of these organizations was assigned a random letter from A-J.

8.3 Test program and participation

The suggested test program from the call for participation is shown Table 7 below. Table 8 provides an overview of the facilities A-J and Table 9 finally summarises actual test programs as conducted in each of the ten facilities.

Table 7: Suggested test program from call for participation

Regular waves				Wave direction						
Design draft, 15.5 knots			180 (head)	150	120	90	60	30	0	
		H/λ	Nr. repeats							
λ/Lpp	0.2	4% 2%	4	4	4	4	4	4	4	
	0.3	4% 2%	4	4	4	4	4	4	4	
	0.4	4% 2%	3	3	3	3	3	3	3	
	0.5	4% 2%	3	3	3	3	3	3	3	
	0.6	2%	3	3	3	3	3	3	3	
	0.7	1%	3	3	3	3	3	3	3	
	0.8	1%	2	2	2	2	2	2	2	
	0.9	1%	2	2	2	2	2	2	2	
	1	1%	2	2	2	2	2	2	2	
	1.1	1%	2	2	2	2	2	2	2	
	1.2	1%	2	2	2	2	2	2	2	
	1.3	1%	2	2	2	2	2	2	2	
	1.4	1%	2	2	2	2	2	2	2	
	1.6	1%	2	2	2	2	2	2	2	
	2	1%	2	2	2	2	2	2	2	

Nr runs				
per dir.	52	SSPA-example calc		
Tank	104	Tank		
Basin (light)	156	Basin (light)	7.8	days
Basin (full)	364	Basin (full)	18.2	days

Irregular long-crested waves					
IMO min power (ToR #5)	Nr runs		SSPA-example calc		
MEPC.1/Circ.850/Rev.3	Tank	17	Tank		
Vs=2kts	Basin (light)	17	Basin (light)	1	days
Jonswap Hs=6m	Basin (full)	102	Basin (full)	6	days
Tp= [7s, 7.5s...15s] 17 waves					
short crested by spreading fct.					
or 1.3*head wave Raw					
minimum 17 runs in head waves					

Fw tests (ToR#4)	Nr runs				
ITTC 7.5.-02....-2.8	per dir.	0	SSPA-example calc		
Vs @ 75% MCR	Tank	2	Tank		
ITTC spectrum Hs 3m	Basin (light)	2	Basin (light)	0.1	days
Tz=6.16s	Basin (full)	12	Basin (full)	1	days
short crested by cos^2 spreading fct.					
or 1.0* head wave Raw					
12 runs (6 long-crested wdir, 2 speeds)					
min 2 runs (180deg, 1 speed above, 1 below 75% MCR)	we need more than 100 waves for this project				

Total, per draft					
	Nr runs				
	per dir.		SSPA-example calc		
	Tank	123	Tank	0	
	Basin (light)	175	Basin (light)	9	days
	Basin (full)	478	Basin (full)	25	days

Levels of involvement

Table 8: General information on facilities A-J and model data

	General info								
Participant	Facility type	Wavemaker	Setup	Scale	Rudder present	Propeller present	turbulence stim.	Method of of determining model inertia	GM / incliantion test
A	Tank	plunger type	towed with springs	68	yes	dummy hub	trip wire	same load plan as Participant G	yes
B	Basin	flap type	towed (free in roll heave pitch; springs in surge sway yaw)	58	yes	dummy hub when towed	2 trip wires	inertia measuring and adjustment platform	yes
C	Basin & Tank	segmented flap	1. free sailing surge retrained 2. soft mooring 3. Free sailing 4. towed (free in heave + pitch) 1-3 basin, 4. tank	68	yes	yes	trip wire	shaker table	yes
D	Basin	segmented flap	soft mooring with springs	58	no	no	studs	CAD modelling, swing testing	yes
E	Tank	segmented flap	Towed (2kts) & free sailing (15.5 kts)	68	yes	yes	studs	CAD modelling, inclining test, free decay test	yes
F	Basin	plunger type	towed with springs	98.6133	yes	no	studs	swinging in pitch	yes
G	Basin	flap type	soft mooring with springs	68	yes	dummy hub when towed	trip wire	swining in yaw and roll	yes
H	Tank	plunger type	soft mooring with springs	50	yes	dummy hub	studs	swing table	yes
I	Tank	flap type	towed	110	no	no	trip wire	swinging in pitch	yes
J	Tank								

Table 9: Test program in facilities A-J and information on data analysis

Participant	Test program					Min. Nr. of wave enc.		Data Analysis	
	wave calibrations prior to tests	regular waves, 15.5 knots	regular waves, 2 knots	minimum power 2 knots irreg. Waves	fw tests	Regular waves	Irregular waves	Regular waves	Irregular waves
A	yes	180 & 0 deg	x	180 deg, 17 periods	irregular waves, 180deg, 2 speeds	10	50		Statistical analysis, zero-up crossing from time histories, Significant values from counting zero-up
B	yes	180, 150,120, 90,60,30, 0 deg	180deg	180 deg, 11 periods	x	15	200	Fourier Analysis	
C	no	180, 150,120, deg	x	x	irregular waves, 180, 150, 120 deg, 1 speed	?	0.5h full scale time	Fourier Analysis	
D	yes	180, 150,120, deg	x	180 , 150deg, 12 periods	irregular waves, 180, 150, 120deg, 3 speeds	10	100	Fourier Analysis	Statistical analysis, zero-up crossing from time histories, Significant values from counting zero-up
E	yes	180deg	x	180,150,120 ,90,45,0 deg, up to 14 periods	irregular waves, 180deg, 3 speeds	10	150	Fourier Analysis	
F	yes	180, 150,120, 90,60,30, 0 deg	x	180 deg, 12 periods	irregular waves, 180, 150, 0deg, 2 speeds	10	100	Fourier Analysis	
G	yes	180, 150,120, 90,60,30, 0 deg	180, 150,120, 90,60, deg	x	x	10	100	Fourier Analysis	Statistical analysis, zero-up crossing from time histories, Significant values from counting zero-up
H	yes	180 & 0 deg	x	180 deg, 17 periods	irregular waves, 180deg, 3 speeds	10	200	Fourier Analysis	
I	yes	180deg	x	x	x	15	x	Fourier Analysis	
J									

8.4 Results

8.4.1 Achieved mass properties and metacentric heights

Achieved metacentric heights (GM-values) from the different participants are shown in Figure 63. As can be seen in most cases the deviation from the target value of 5.7 m is smaller than ±1.5% with many participants reporting values less than ±1%.

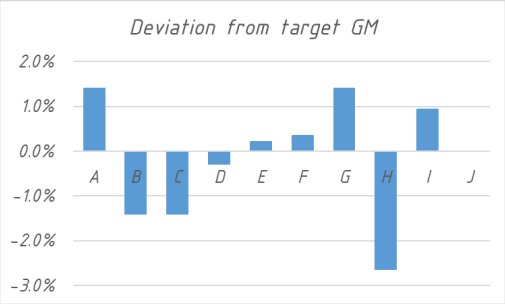

Figure 63: Deviation of achieved GM values from target value, participants A-J.

As Figure 64 and Figure 65 show, the deviations from the target volume displacement of 312784 m^3 and the target pitch gyradius of $0.25 \cdot L_{pp}$ and are even smaller.

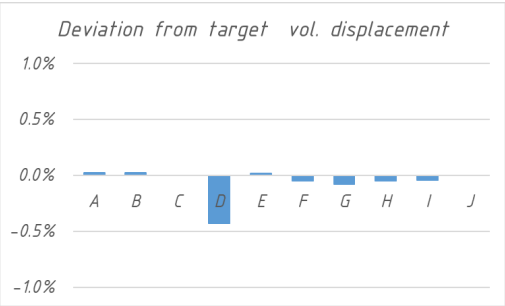

Figure 64: Deviation of achieved displacements from target value, participants A-J.

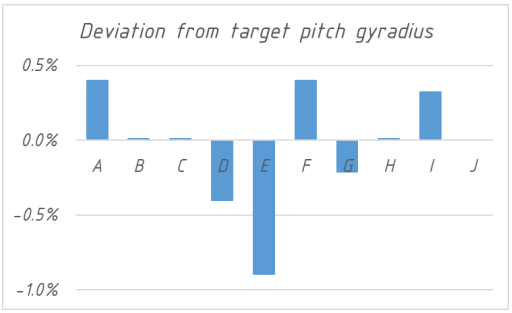

Figure 65: Deviation of achieved pitch gyradii from target value, participants A-J.

Figure 66 illustrates that most institutions do not put equally tight requirements on achieving the nominal yaw gyradius, deviations are up to 2%. As far as pure seakeeping tests are concerned this approach of focusing on the pitch inertia instead appears to be sensible.

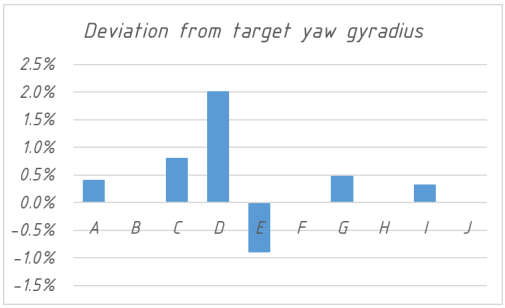

Figure 66: Deviation of achieved yaw gyradii from target value, participants A-J.

Only a few participants reported achieved values for roll gyradii. Values are summarised in Figure 67. Due to the model design and structural strength reasons, participant B chose 0.37 B as the roll inertia of the model This explains the large deviation of around 7%.

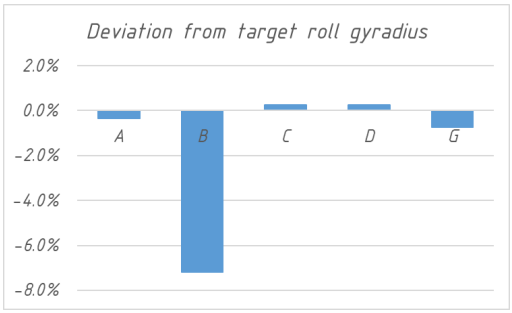

Figure 67: Deviation of achieved roll gyradii from target value, only relevant participants.

8.4.2 Repeatability of regular waves

Participants were asked to supply wave surface elevation measurements from repeatedly sending the same signal to the wavemaker and comparing measured results to the target values. Results for wavelength ratios of λ/L_{pp} = 0.3, 0.5, 1.1 and 2.0 are shown in Figure 68.

8.4.3 Regular wave tests at 15.5 knots

Figure 69 shows a comparison of the Quadratic Transfer Functions (QTF) in regular head seas as reported by the various participants.

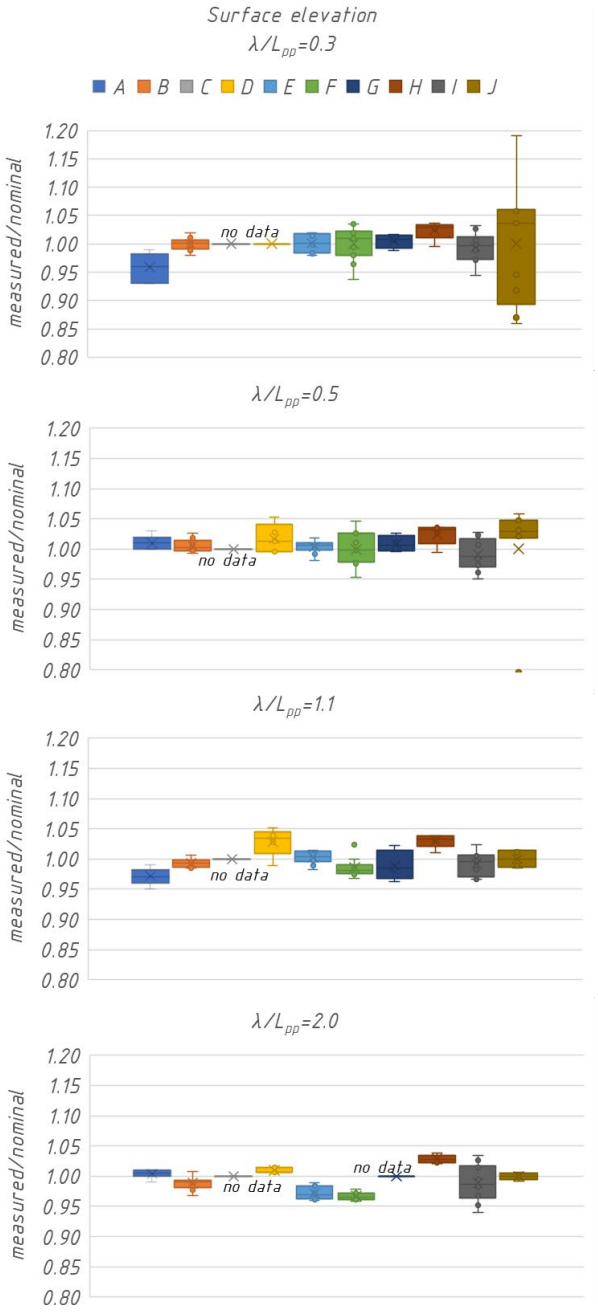

Figure 68: Comparison of measured and target surface elevations ("wave heights") for 4 wavelength ratios.

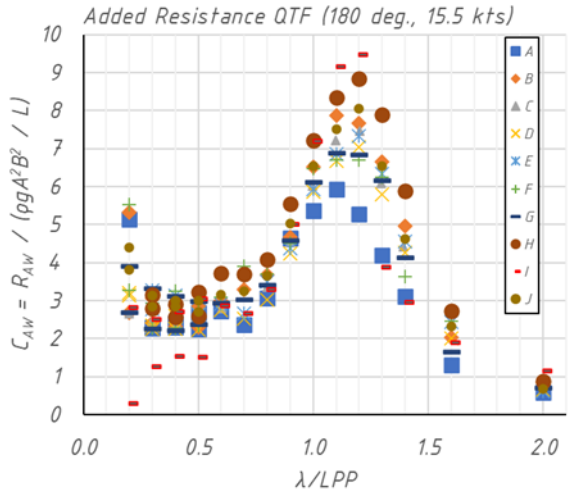

Figure 69: Added resistance coefficient QTF in head seas, comparison of results from all participants.

Figure 70 and Figure 71 show the corresponding Response Amplitude Operators (RAOs)

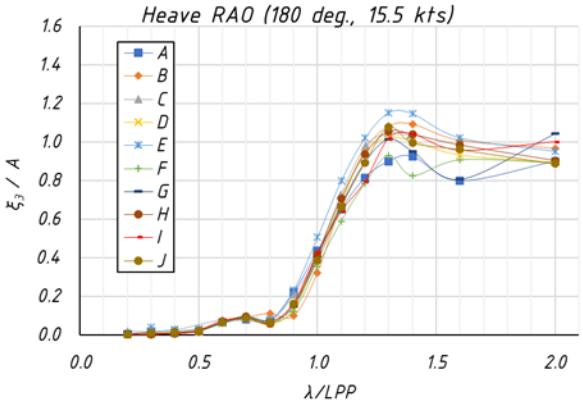

Figure 70: Heave RAO in head seas, comparison of results from all participants.

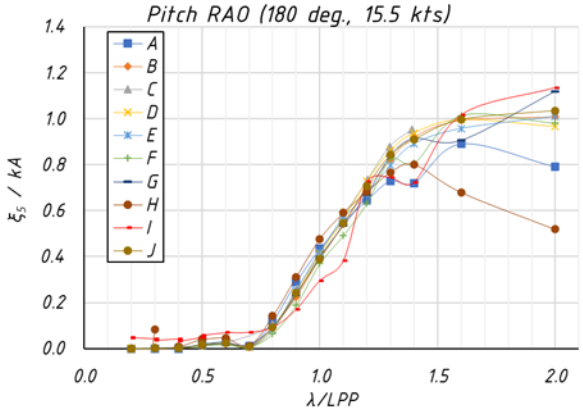

Figure 71: Pitch RAO in head seas, comparison of results from all participants.

Figure 72 to Figure 77 show comparisons of the added resistance coefficient QTFs for wave direction ranging from 150 degrees to following waves.

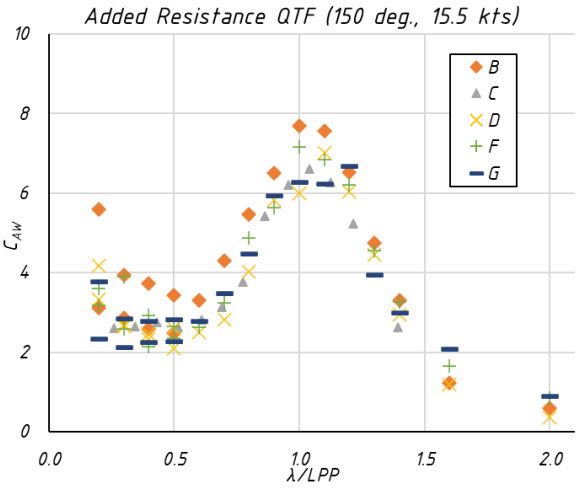

Figure 72: Added resistance QTF in 150 degree wave direction.

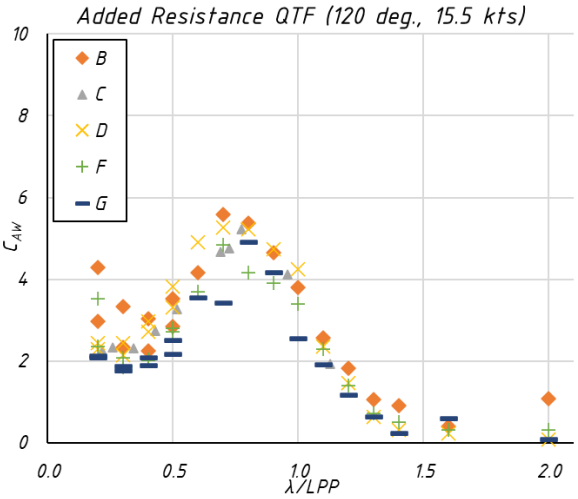

Figure 73: Added resistance QTF in 120 degree wave direction.

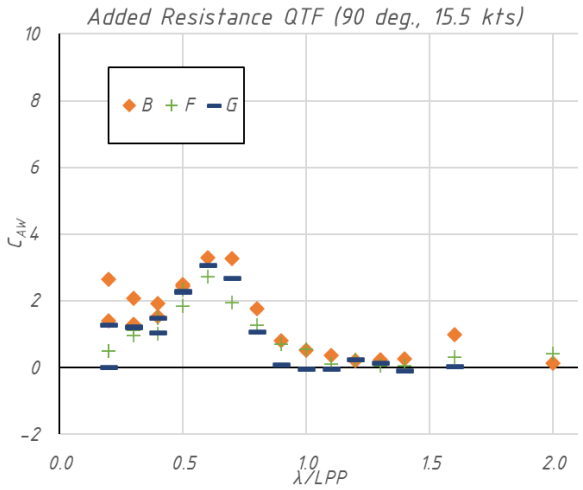

Figure 74: Added resistance QTF in beam waves.

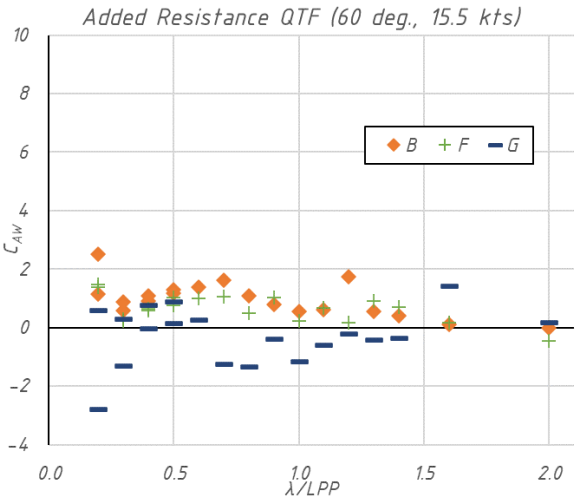

Figure 75: Added resistance QTF in 60 degree wave direction.

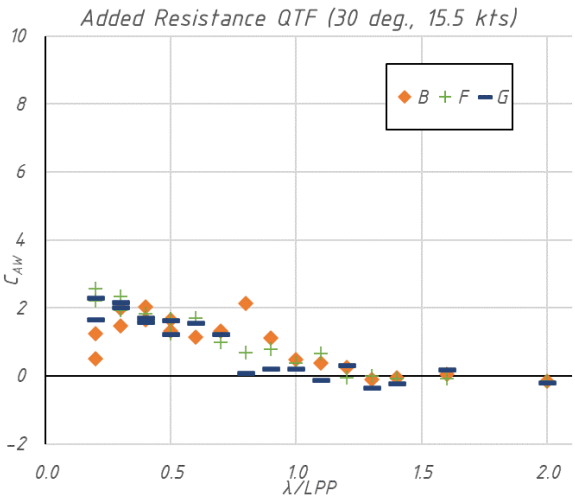

Figure 76: Added resistance QTF in 30 degree wave direction.

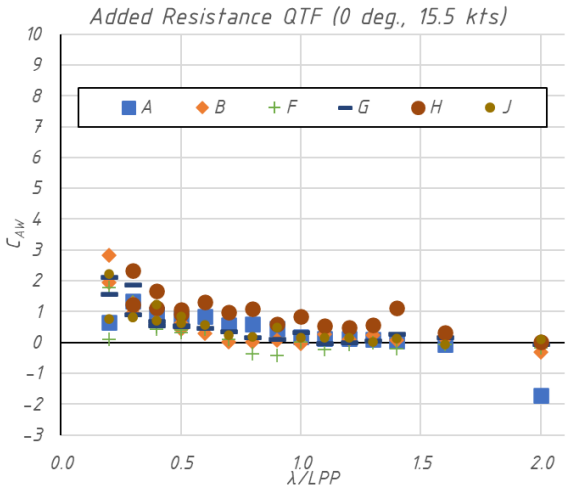

Figure 77: Added resistance QTF in following waves.

Participants B, F, and G conducted seakeeping tests in a basin and provided measured data for all wave directions. Their results are compared in the "radar plots" below, Figure 78 to Figure 81.

8.4.4 Irregular wave tests at 2 knots

In addition to the design speed tests in regular waves, tests in irregular waves were conducted at the very low speed prescribed in the IMO regulations on "minimum power".

IMO MEPC.1/Circ.850/ Rev.3 defines the "adverse conditions", under which the ship should be able to sustain the advance speed V_s by means of JONSWAP wave spectra with a range of peak (modal) periods varying from 7 s to 15 s. Before this background participants in the benchmarking study were asked to conduct irregular wave tests with the KVLCC2 sailing at 2 knots.

Participants A, D, E, F, H, and J submitted results for this part of benchmarking campaign, and these are compared in Figure 82. As illustrated in Table 8 all participants chose to use a towed model for these low-speeds tests.

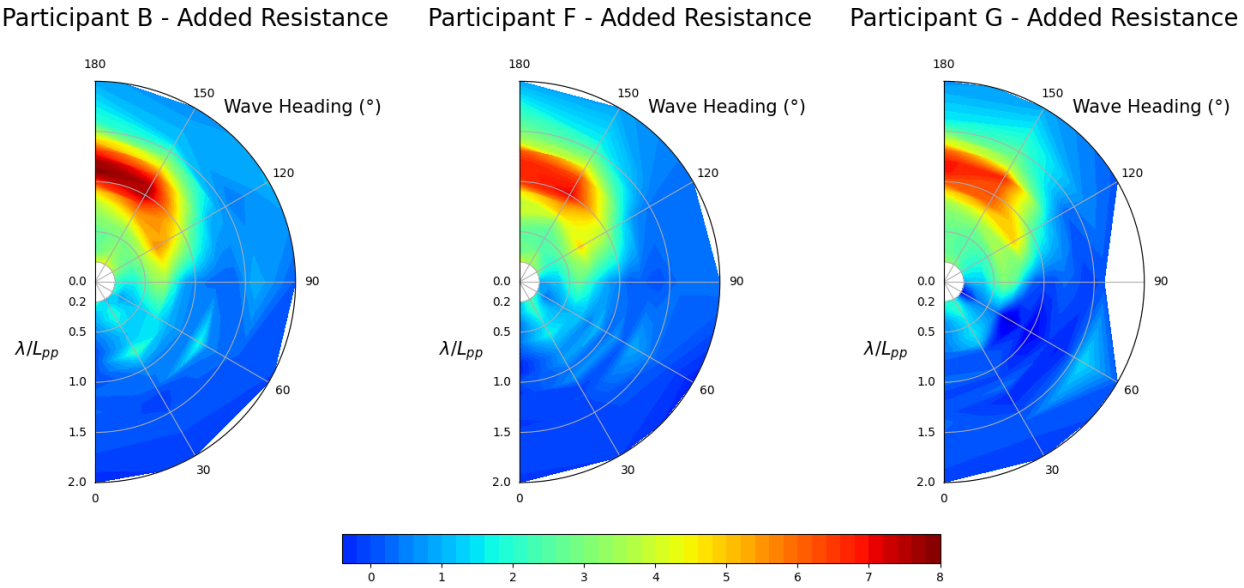

Figure 78: Added resistance coefficient QTF as function of wave direction, same non-dimensionalisation as Figure 69.

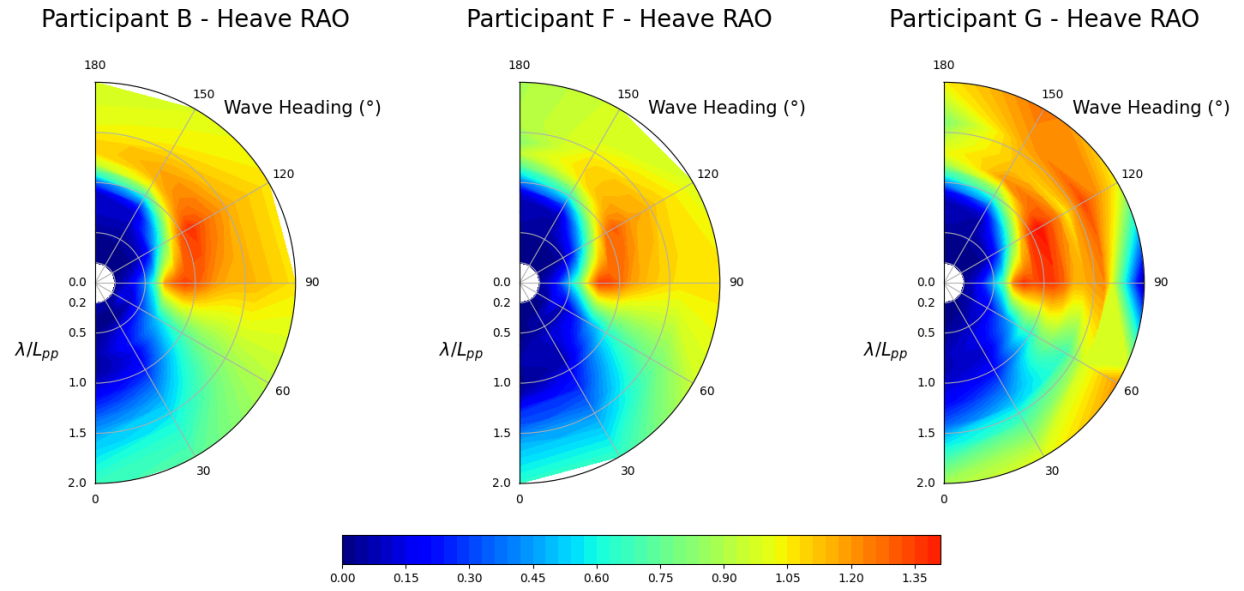

Figure 79: Heave RAO as function of wave direction, same non-dimensionalisation as Figure 70.

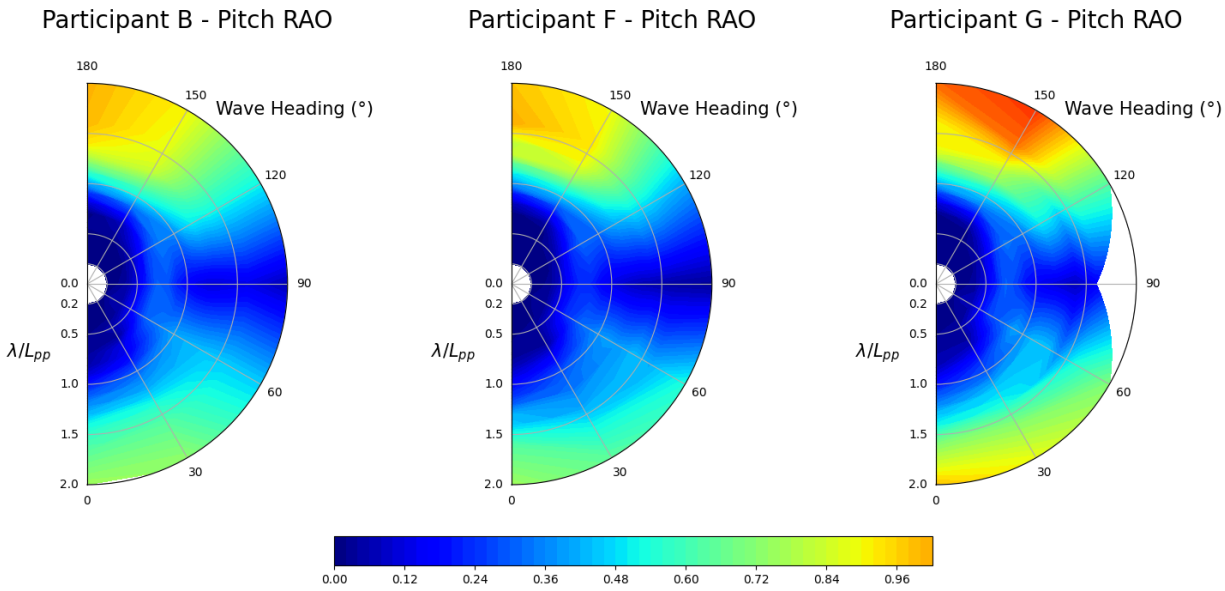

Figure 80: Pitch RAO as function of wave direction, same non-dimensionalisation as Figure 71.

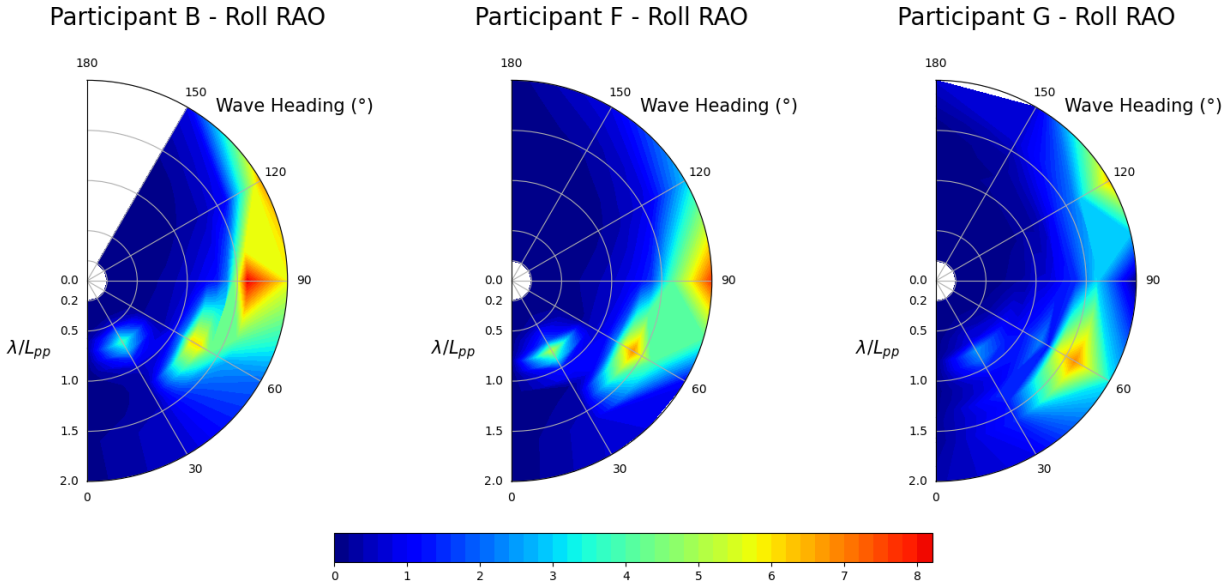

Figure 81: Roll RAO as function of wave direction, same non-dimensionalisation as Figure 71.

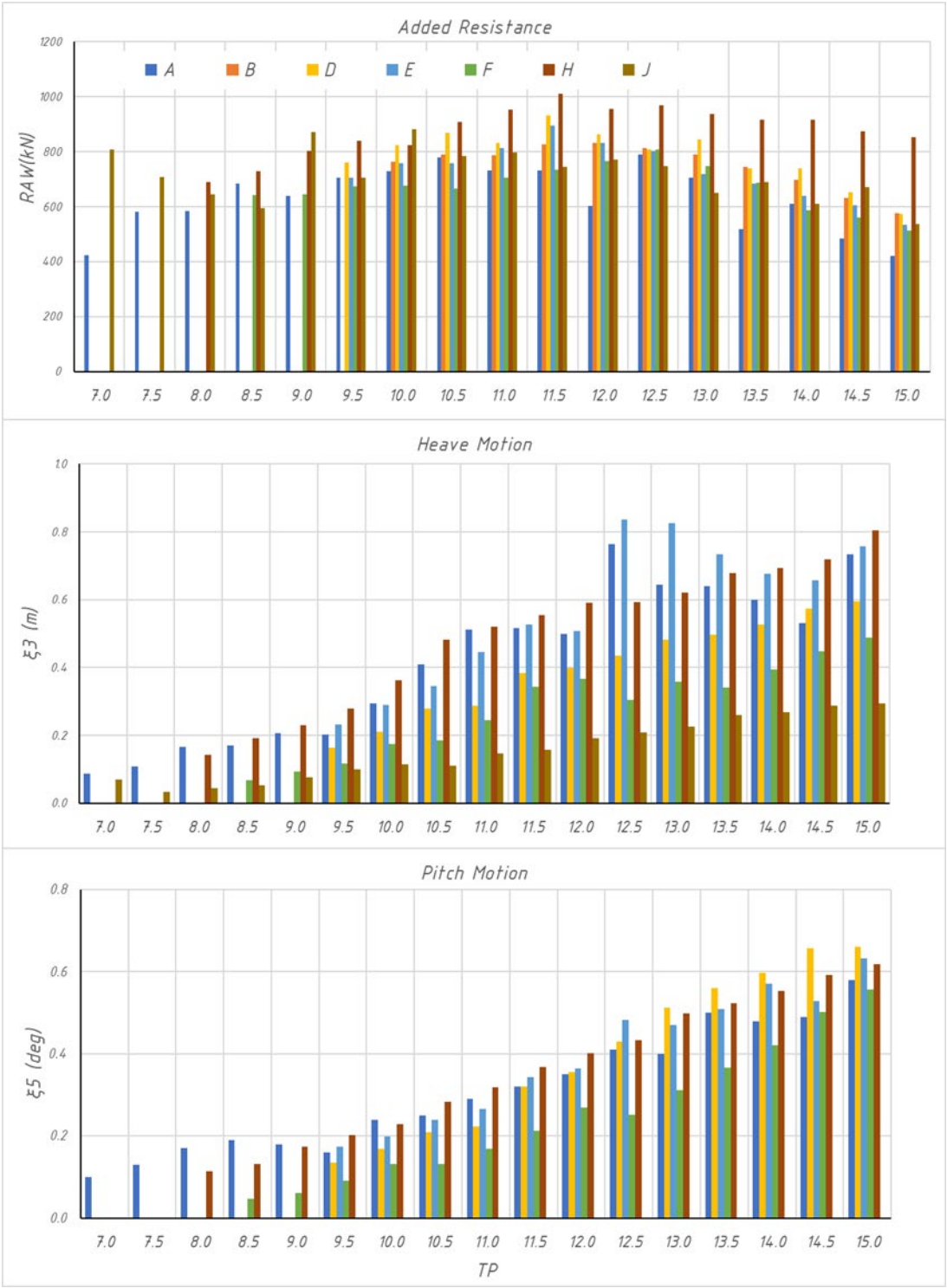

Figure 82: Tests in irregular head waves at 2 knots. Added resistance, heave and pitch motions (standard deviations) as function of peak period T_p. Values scaled to full-scale. Comparison of results from participants A, D, E, F, H and J.

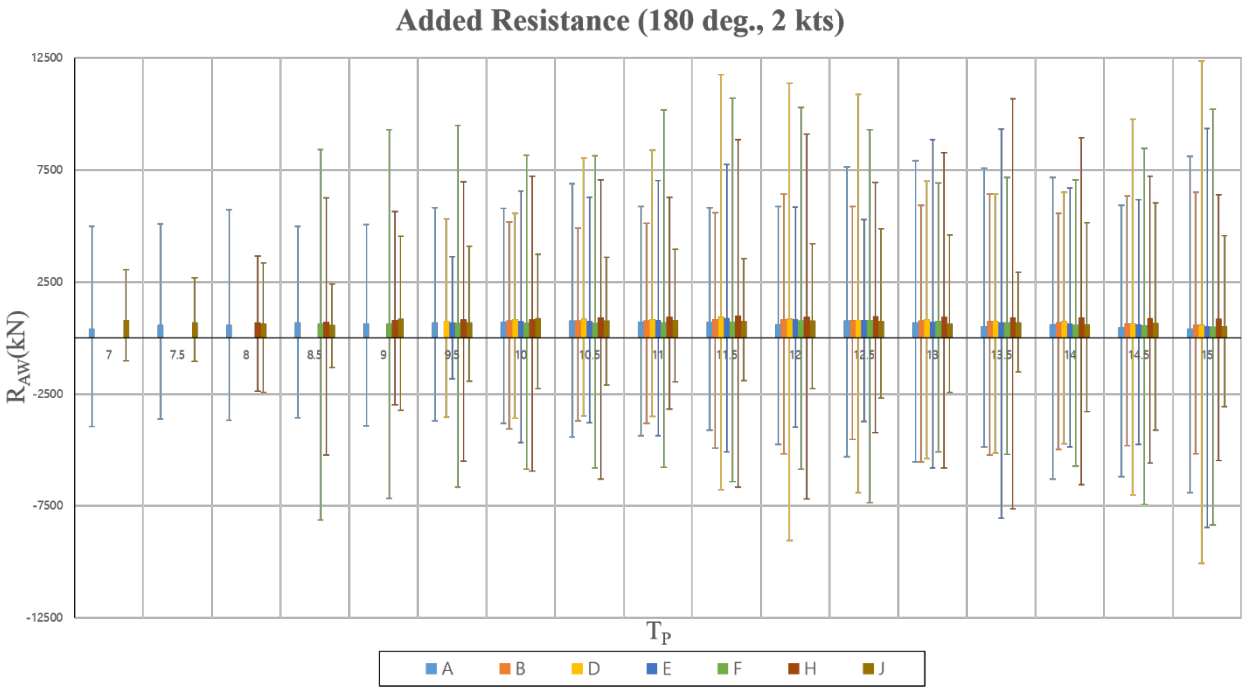

Figure 83: Comparison of mean, max and min values of added resistance recorded in irregular head waves at 2 knots. Mean values are these shown in top plot of Figure 82.

8.4.5 Tests in irregular fw-waves

Participants A, C, D, E, F, and H also submitted results from tests in irregular "f_w-waves" i.e. the sea state stipulated in IMO Circular MEPC.1/Circ.796 and explained in ITTC procedure 7.5-02-07-02.8.

Results are shown in Figure 84. Participant C (grey triangles) submitted results from tests with various towing and propulsion arrangements, these are labelled in the figure.

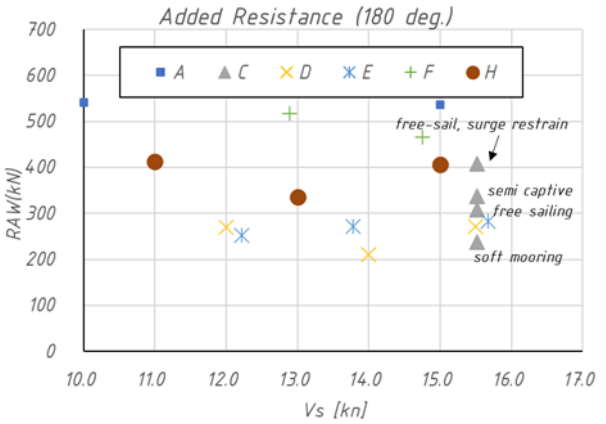

Figure 84: Tests in irregular head waves of *fw*-type i.e. significant wave height 3 m and zero-up crossing period 6.16 s.

8.5 Analysis of results

Below follows an attempt to analyse the submitted results and find some trends. For space reasons, the analysis focuses on the bulk of the submitted data i.e. the design speed tests in regular waves.

8.5.1 Regular wave tests at 15.5 kts

Figure 85 shows an idealised added resistance transfer function (QTF) and some main parameters describing it. Based on this the following parameters were analysed in more detail:

- Peak value
- Peak position
- "tail end" value

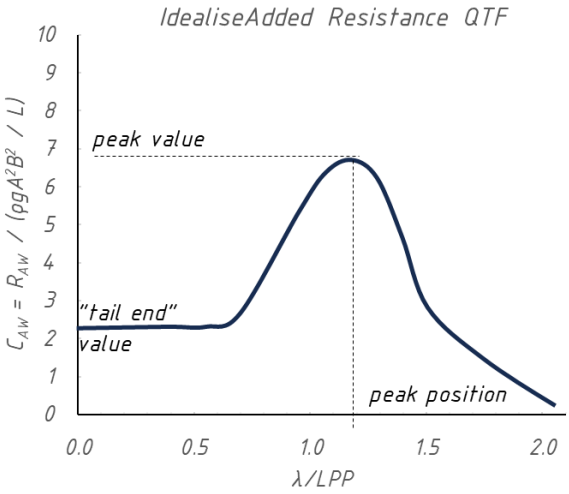

Figure 85: Idealised QTF and parameters describing it.

Figure 86 shows results from the analysis of the peak value. As can be seen, variation in head waves is larger than in oblique waves. This could partly be a result of the different sizes of the datasets, only 5 participants conducted tests in oblique waves.

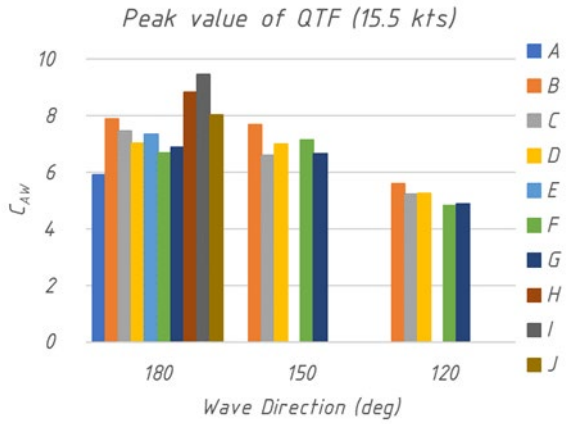

Figure 86: Analysis of QTF peak values reported by participants A to J.

As illustrated in Figure 87 the standard deviation of reported QTF peak values in head seas is about 13% (green corridor in Figure 87)

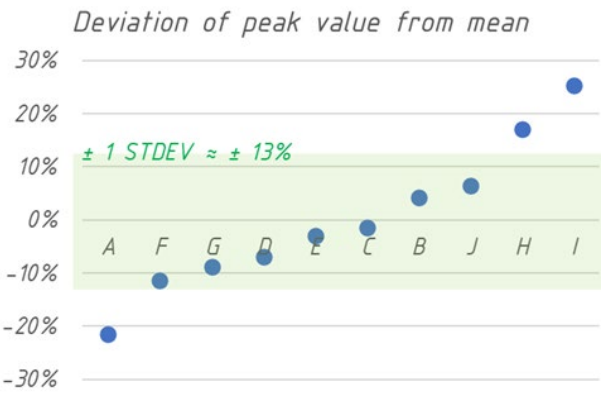

Figure 87: Deviation of head sea QTF peak values from mean.

The corresponding standard deviation for oblique waves becomes about 5% and 4% for wave directions of 150 and 120 degrees respectively.

Figure 88 looks at the variation in reported peak positions. As can be seen six of the ten participants predict the peak to occur at a wavelength ratio of λ/Lpp = 1.2 and four participants report peaks at 1.1. The situation is similar for oblique wave directions of 150 and 120 degrees.

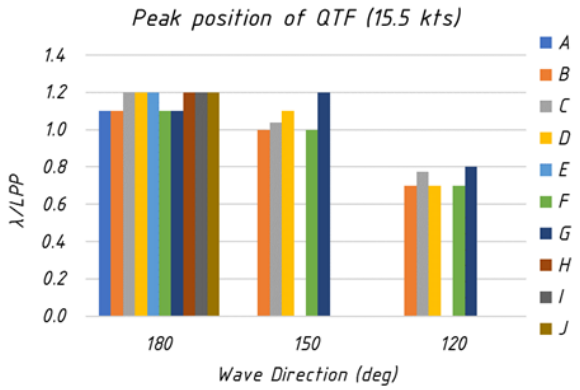

Figure 88: Analysis of QTF peak positions reported by participants A to J.

QTF behaviour at the short-wave "tail-end" is analysed in Figure 89 and Figure 90 for the two wavelength ratios of λ/L_{pp} = 0.5 and 0.2. As can be seen, the spreading increases with shorter wavelength.

The reason for this divergence is that such experiments are difficult to conduct. Added resistance, as the difference between time-averaged data from measurements in waves and calm water measurements, is very small and becomes sensitive to disturbances. The issue is illustrated further in Figure 91, where the individual repeat runs behind the data in Figure 89 and Figure 90 are plotted, and also analysed in terms of wave-steepness. As can be seen, the spreading from run to run increases significantly for λ/L_{pp} = 0.2.

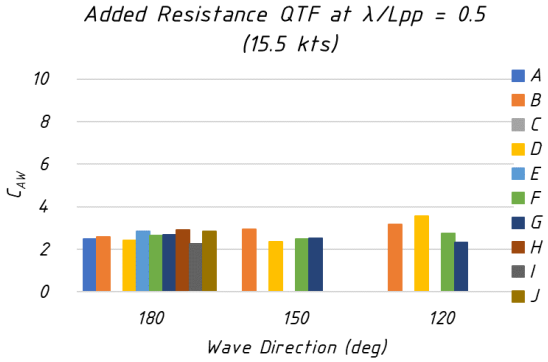

Figure 89: Analysis of QTF tail-end value in short waves (λ/L_{pp} = 0.5).

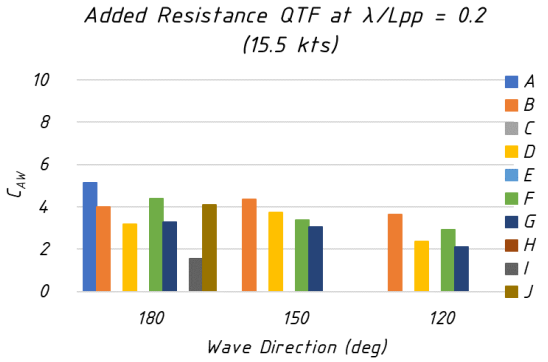

Figure 90: Analysis of QTF tail-end value in short waves (λ/L_{pp} = 0.2).

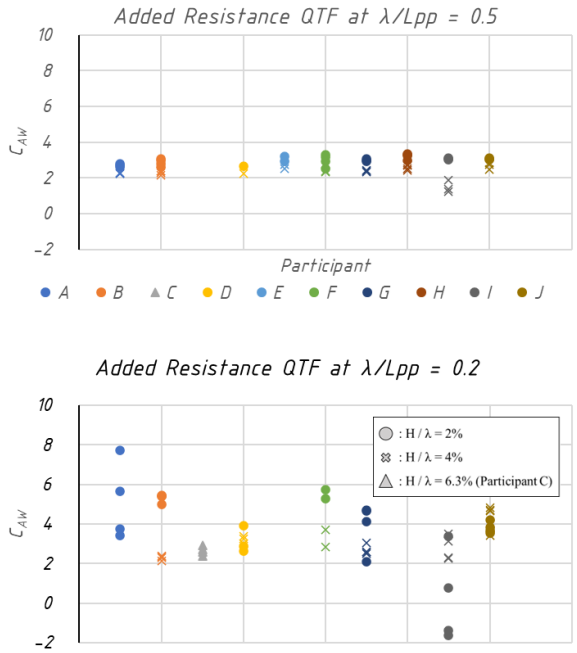

Figure 91: Analysis of QTF tail-end value in short waves. Variation with wave-steepness and in between repeat runs.

8.5.2 Irregular wave tests at 2 kts

Figure 83 provides an impression of how challenging "IMO-minimum power" added resistance tests at low speeds are. As can be seen, the extreme values recorded during such tests are by about a factor of 10-20 larger than the mean value that one needs to extract.

The maximum value of the added resistance occurs at around a spectral peak period of around 12 s, compare Figure 82, top plot.

Figure 92 shows a more detailed analysis of submitted results at this peak period. As can be seen, the mean value across all participants is about 800 kN with a standard deviation of 100 kN, corresponding to 12 %.

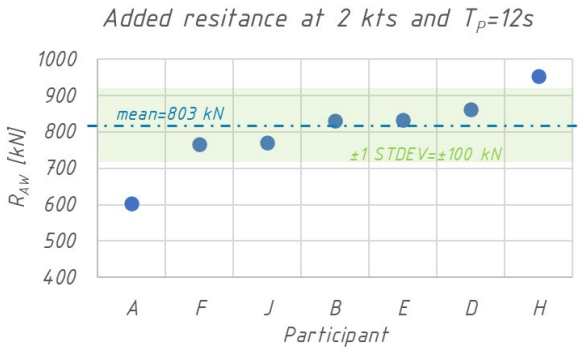

Figure 92: Analysis of added resistance spreading between participants. IMO minimum power conditions, ship speed 2 knots, T_P=12s.

8.5.3 Analysis by facility type, scale factor, and type of experimental setup

The Committee also attempted to analyse submissions in terms of the following parameters:

- Basin vs. tank tests
- Scale factor / model size
- Type of setup:

Results for the head sea added resistance QTF are illustrated in Figure 93 to Figure 95. These figures are identical to Figure 69 but highlight the above parameters.

Results obtained in basins seem to be more similar to each other than those measured in towing tanks, Figure 93.

No clear trends can be observed from the scale factor analysis in Figure 94. The two smallest models (scale 110 & 99.6) are at the extremes of the plot.

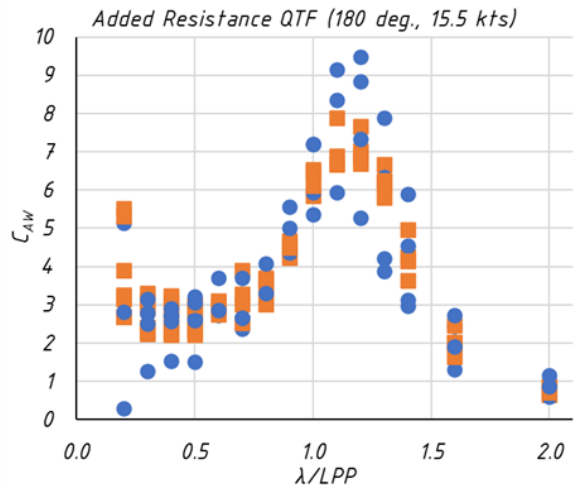

Figure 93: Head Sea QTF: Analysis by facility type.

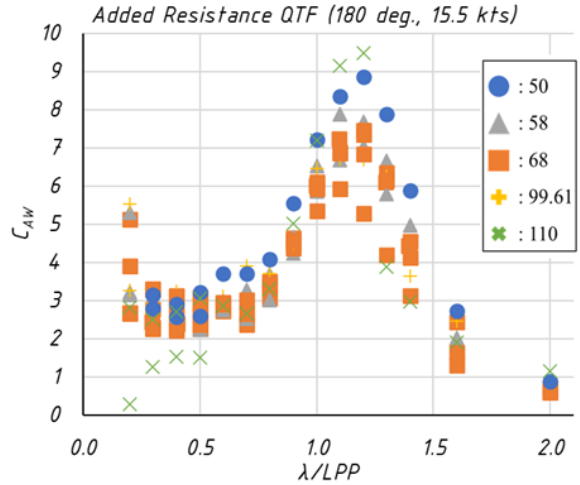

Figure 94: Head Sea QTF: Analysis by scale factor.

Figure 95, the analysis by type of setup, seems to show the trend that soft-mooring and free sailing tests are closer together than the group of results from towed tests.

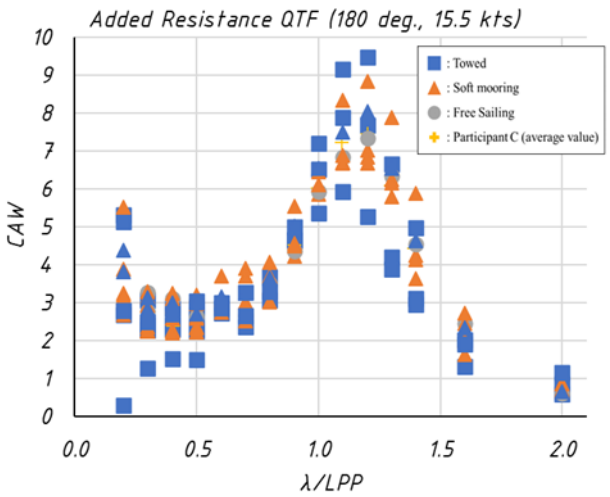

Figure 95: Head Sea QTF: Analysis by type of setup (participant C submitted data using a range of techniques, compare Table 8).

8.6 Conclusions

The following preliminary conclusions can be drawn from the above analysis:

<u>Added resistance Quadratic Transfer Function (QTF) at design speed and in regular waves:</u>

- Six of the ten participants predict the head sea QTF peak to occur at wavelength ratios of $\lambda/L_{pp} = 1.2$. The other four participants report the peak at λ /Lpp = 1.1.
- The mean value of the peak height in the head sea QTF becomes C_{AW}=7.6 with a standard deviation of around 13% around this value, depending on participant
- At about 5% and 4% the corresponding standard deviations for wave directions of 150 and 120 degrees are smaller.
- The short-wave “tail ends” of the QTFs are difficult to measure. For λ/L_{pp} <0.5 experimental spreading increases significantly.

Low speed testing under IMO minimum power conditions:

- These tests are challenging to conduct, and all participants used towed models for this, either with soft-mooring or spring arrangements.
- For the KVLCC2 the maximum value of the added resistance occurs at a spectral peak period of about 12 s.
- The mean value of all submitted results at this period is about 800 kN with a standard deviation of 12% across participants.

Other conclusions:

- There appears to be a (difficult to explain) trend that soft-mooring and free sailing tests are closer together than the group of results from towed tests.
- Results obtained in basins seem to be more similar to each other than those measured in towing tanks. This is also difficult to explain.
- There is quite a variation in wave repeatability between the participating organisations, particularly is short waves.

8.7 Suggested next steps/future work

The next ITTC Seakeeping Committee could extend/deepen the above analysis of the benchmarking results and make the collected data accessible online. Such an online "repository" should include the post-processed time-averaged data and possibly also the raw time histories of the measurements (some participating organisations have agreed to share the data).

9. ONBOARD/REALTIME SEAKEEPING DATA (TOR8)

Under ToR 8 the SKC was asked to survey the state of the art for the acquisition and analysis in on-board and/or real-time seakeeping data, and investigate the need of ITTC activities, including future issues related to autonomous vessels.

Literature on the topic has been reviewed and stakeholders considered relevant for this topic have been identified, and eventually meetings carried out (Signaled inside parentheses):

Classification Societies (CCSS)

- DNV (H.A. Tvete, Program Director, Maritime at DNV, Oslo. and Principal Researcher Bingjie Guo, 20220630)
- BV (J. Pancorbo - Principal Surveyor - Spain, 20220601)
- ABS (E. Alvarez - Principal Surveyor - Spain, 20220601)

Shipowners

- ElCano - Gas carriers (meeting with fleet-operations department, 20221013)
- Sicar - General Cargo (meeting with fleet-operations department, 20220910)

Weather routing code developers

- Ali - F. Cañavate - 20230405

Researchers on seakeeping codes and weather routing, ships as buoys, etc.

- Matt Collette, Assoc. Prof., University of Michigan NA&ME Dep. 20230404
- Munehiko Minoura (Osaka U.) 20230501
- Nielsen (DTU) 20230510

Other stakeholders

- Other ITTC committees
- Sea Trials group
- Wind assisted vessels owners/operators
- IMO ITTC representative.

Among the take-aways from these interviews are that the CCSS' rules on autonomous ships are function/goal oriented. They think having seakeeping data is important but at this stage it seems they do not think it is reasonable to set standards on how such data should be acquired. The focus of CCSS is on safety at the moment, not on performance. However, the quality of seakeeping data could have an impact on safety:

- Motions may affect maneuverability and hence increase the chance of collisions.
- If ship motions are large, maybe some sensors do not work.
- Capabilities to identify objects may be affected by the motions.
- Routing may be affected by seakeeping data. Since there are no people onboard, motion restrictions can be relaxed.

Further for CCSS, monitoring motions can be relevant to decide which systems to pay more attention to e.g. fatigue.

As for shipowners, having standards on how full-scale data is monitored, which weather routing providers can comply with, can be an added value for these stakeholders. Use of such weather routing applications is often requested by charterers.

As for weather routing code developers, it seems that measuring motions very accurately may not be very useful for weather routing unless the wave excitation is also accurately measured. The reason is that the motion estimation is obtained based on satellite data for the forecasting of the sea state. Since this is not very accurate, the expected accuracy of the motion estimations will not be very accurate either, and therefore, having very accurate actual motion measurements is not in principle necessary.

As for applications in which motion data are used for short term motion predictions (crane ships operations for wind turbines, maintenance ships for wind turbines, SpaceX autonomous ship for rocket landing, autonomous ships maneuverability in specific collision checks, etc.), the weather routing code developer we interviewed stated that having such a procedure can be interesting for these applications. In such a case, it could be interesting to have standards on location and precision of sensors.

As for researchers on seakeeping codes and weather routing, ships as buoy etc., they agreed that high-quality full-scale seakeeping data is important for the progress of their research and provided some ideas on minimum standards for e.g. sampling frequency, magnitudes to register, etc.

To summarize, it seems the topic is relevant, but it could be too early to elaborate procedures on "the acquisition and analysis in on-board and/or real-time seakeeping data, including future issues related to autonomous vessels".

If such a procedure were considered pertinent, its potential scope could include these items:

- Define precisely the load condition of the ship when data are taken.
- Minimum recording frequency.
- Register motions.
- Register vessel speed (GPS, relative to water).
- Register heading.
- Register sea state: directional spectrum.
- Register wind.
- Register current.
- Document how to deal with communication and integration of the dedicated sensors with other systems in the ship, including how to use the communication capabilities of the ship to transfer information to ground stations.
- Document onboard location of sensors.

10. GUIDELINES ON MANOEUVRING IN WAVES (TOR9)

The Seakeeping Committee (SKC) was tasked to collaborate with the Manoeuvring Committee regarding the development of guidelines related to manoeuvring in waves, ToR 8 of the Manoeuvring Committee (MC). As part of this work the MC has modified two procedures (7.5-02-06-02, "Captive Model tests" and 7.5-02-06-01, "Free Running Model tests") to also include guidance on manoeuvring in waves. During August 2023 the SKC thoroughly reviewed the changes and proposed some modifications.

11. CONCLUSIONS AND RECOMMENDATIONS

11.1 State of the art and research trends

The Committee has reviewed the State of the Art in the field of seakeeping by examining publications for the calendar years 2021-2023. Papers published in more than 35 of the most relevant journals and conferences were reviewed and summarised, resulting in the conclusions below.

A limited number of *new experimental facilities* have opened or became operational since 2021. These include a large ocean basin in Singapore, a towing tank in Southampton, United Kingdom and a shallow water towing tank and a coastal and ocean basin in Ostend, Belgium. In addition, a small towing tank was refurbished in Virginia, USA.

Special *experimental setups* are often used for investigations related to hydroelasticity with segmented models as well as for deck wetness. The focus here is on the use of sensitive, partly new developed sensors, but also on optical sensor technology. It has become standard practice to validate measurements and CFD results against each other to check the plausibility of revealed effects and minimise the uncertainties.

The application of Machine Learning (ML) and Artificial Intelligence (AI) techniques has recently become a contentious issue. Current publications show promising application possibilities and only hint at the extent to which their influence will increase in the upcoming years.

Research about numerical methods on seakeeping focus on the development of fully nonlinear potential flow algorithms and viscous flow methods on the treatment of free-surface wave breaking. Major progress on coupling different potential flow and viscous flow methods has been achieved. Looking for the coming research progress, the wave-body interaction in complex strong nonlinear ocean environments are major challenges for ship seakeeping numerical methods. The development of various coupling algorithms with different advantages may become a hot spot in numerical simulation research and development for ship seakeeping problems.

Green water, slamming and water entry have been extensively investigated by many institutions over the world, both numerically and experimentally. There has been a focus on the validation of CFD calculations as well as the development of more time efficient hybrid methods. The validation results are promising, but there is still work to be done to achieve high fidelity numerical predictions.

Regarding *sloshing*, significant research has focused three areas: comparing results from experiments with tanks of LNG carriers to the guidelines regarding sloshing loads proposed by classification societies. Such research indicates that different rules led to significant differences in such loads, signalling a future line of research. Also increased interest is being paid to sloshing while transporting liquid H2 in cryogenic conditions. This is motivated by perspectives on the use of hydrogen as an alternative fuel for the decarbonization of maritime and ground transportation. Such research indicates that sloshing leads to a substantial increase in the boil-off rates. Finally, substantial work has been carried out considering the coupled dynamics of

sloshing and ship motions, a topic computationally expensive on which further research will likely be carried out during the next ITTC term.

Efforts on *hydroelasticity* problems were classified into five categories: experimental study using backbone segmented models, hydroelasticity on tank sloshing, water surface impacts, numerical study, and advanced theoretical study. Experiments using backbone segmented models have focused on oblique wave conditions, and future accumulation of experimental techniques and expansion of data is expected. Since backbone models are difficult to fabricate and handle, and the number of tanks in which they can be tested is limited, we believe that the widespread sharing of the results of leading groups will promote the development of numerical analysis techniques in the future. As for theoretical analysis, it is noteworthy that hydroelasticity was discussed based on the momentum exchange between fluid and flat plate. This could lead to practical methods for FSI problems in ships and offshore structures.

Research on the *added resistance* and speed-power predictions seems to focus on four main areas:

1. Development of new semi-empirical formulae with the accumulation of more model test data for the rapid estimation of added resistance, including various wave headings and hull shapes
2. Novel data-driven models utilizing deep learning techniques to estimate added resistance in waves
3. Various numerical methods, including potential-flow and CFD methods, to directly evaluate the added resistance acting on ships in waves
4. Model tests for the added resistance of ships in various wave conditions or with coupling effects

CFD is now a popular tool in seakeeping applications. Commercial SIMCENTER STAR-CCM+ and open-source OpenFOAM solvers are widely used in recent scientific productions, but other codes and in-house solvers, often based on Finite-Volume Method with overset capabilities, are also successful. Seakeeping CFD studies now commonly include uncertainty quantification and comparison to experimental results, and confidence in the calculations is expected to increase in the next years. Simulations of self-propelled sailing ships in complex wave systems exist but there is no widely used methodology to perform this kind of applications. This is expected to change in the next years.

Research on the seakeeping of *High-Speed Marine Vehicles* seems to focus on three main areas:

1. Experimental and numerical predictions of motions and loads
2. Novel predictive methods for motions and loads, including machine learning/ AI-based methods.
3. Ride Control Systems (RCS) to improve passenger comfort and to actively reduce slamming and the resulting structural loads.

Over the past years the most investigated types of high-speed marine vehicles were wave-piercing catamarans and trimarans.

11.2 Recommendations to the full conference

During the 30th term the procedures below have been updated with minor modifications. The Seakeeping Committee recommends to:

1. Adopt the updated procedure No. 7.5-02-07-02.1 (Seakeeping Experiments).

2. Adopt the updated procedure No. 7.5-02-07-02.2 (Prediction of Power Increase in Irregular Waves from Model Tests).

3. Adopt the updated procedure No. 7.5-02-07-02.3 (Experiments on Rarely Occurring Events).

4. Adopt the updated procedure No. 7.5-02-07-02.5 (Verification and Validation of Linear and Weakly Non-linear Seakeeping Computer Codes).

5. Adopt the updated procedure No. 7.5-02-07-02.6 (Global Loads Seakeeping Procedure).

6. Adopt the updated procedure No. 7.5-02-07- 02.7 (Sloshing Model Tests).

7. Adopt the updated procedure No. 7.5-02-07- 02.8 (Calculation of the Weather Factor fw for Decrease of Ship Speed in Wind and Waves).

8. Adopt the updated procedure for high-speed marine vehicles No. 7.5-02-05-04 (HSMV Seakeeping Tests).

9. Adopt the updated procedure for high-speed marine vehicles No. 7.5-02-05-04.1 (Excerpt of ISO2631, Seasickness and Fatigue).

10. Adopt the updated procedure for high-speed marine vehicles No. 7.5-02-05-06 (HSMV Structural Loads).

11.3 Proposals for future work

11.3.1 Benchmarking data for added resistance in oblique waves

The 31st Seakeeping Committee should make the recently collected data from the "benchmarking experimental campaign on added resistance" (ToR 7 for SKC of 30th ITTC) accessible online. This repository should include the post-processed time-averaged data and possibly also the raw time histories of the measurements (some participating organisations have agreed to share the data). Such an online repository of measured time series of motions and other signals would be very valuable for Verification and Validation of CFD calculations and other purposes.

11.3.2 Number of wave encounters required for model tests in irregular waves

ITTC procedure 7.5-02-07-02.1 (Seakeeping Experiments) recommends a total number of wave encounters of N=50 as a lower limit for seakeeping experiments and states that N=200 or above is considered "excellent practice". The next seakeeping committee should check "experimental convergence" of motion and added resistance values to back-up or refute this statement. Recent experience by several members of the 30th Seakeeping committee has indicated that the required number of wave encounters for convergence could be higher. Liaise with the Full-Scale Ship Performance Committee on the topic.

11.3.3 Weather factor fw for small ships

As pointed out in Section 8.2, experimental data for small ships in fw-conditions is rare. It is recommended that the next Seakeeping Committee uses simulations to investigate the topic of 'voluntary' speed reduction for vessels smaller than 100 m in length. If required, such simulations can also be used to develop alternative "milder" sea states for small ships.

11.3.4 Investigate special topics related to the drafted minimum power guideline

The ITTC "Guideline on determining Minimum Propulsion Power to Maintain the Manoeuvrability of Ships in Adverse Conditions" that was drafted by the 30th Seakeeping Committee is a technical interpretation of IMO MEPC.1/Circ.850/Rev.3. During the preparation of the guideline several issues with the IMO Circular became apparent. The 31st Seakeeping Committee should investigate these in detail and update/improve the draft procedure accordingly:

- The IMO guideline appears to be contradictory on what range of peak wave periods TP should be used in the minimum power assessment (step 16 of the IMO assessment contradicts the TP values listed under the spectrum definitions by IMO). Discuss and resolve this issue with IMO.
- The IMO circular gives "default conservative" estimates for thrust deduction factor and wake fraction. These values are based on a single source of information (MEPC 72-5-9

submission by China) and on difficult to conduct experiments for one single ship.

As illustrated by the work of the 30th Seakeeping Committee, power predictions based on the IMO default values are not necessarily conservative for a full-block ship.

The 31st Seakeeping Committee should continue to investigate this topic by e.g. collection of available data on the behaviour of propulsive factors of different types of ships at low speeds (ideally in waves). In this context hull efficiency, ηH, as a measure for the combined effect of wake fraction and thrust deduction, should also be considered.

The minimum power guideline developed by the 30th Seakeeping Committee should be updated with the findings from such a study.

- Investigate whether the IMO-suggested 3% thrust increase to account for rudder action in waves is realistic.

11.3.5 Wind loads

The work of the current SKC and discussions with other committees have shown that there is a need to address a significant number of issues related to wind loads on ships. The below list of tasks could either be distributed between existing committees or a new specialist committee could be installed:

- Include wind load coefficients for side force, yawing moment and roll moment in the new guideline on "Wind Loads on Ships".
- Improve this guideline, make it more comprehensive and turn it into an ITTC procedure
- Survey state of the art in describing atmospheric boundary layer profiles (ABL) and natural turbulence spectra of the wind over the sea. Unify equations to describe ABL profiles across all ITTC procedures.
- Make recommendations how to measure wind speed and direction in the disturbed flow around a moving ship.
- Develop ITTC guidelines on wind tunnel testing of ships.
- Investigate the question whether Wind Tunnel Facilities working with ships, marine structures and wind propulsion technologies should be invited to join ITTC.

The current committee drafted a wind loads guideline based on the Annex F of ITTC procedure 7.5-04-01-01.1 Preparation, Conduct and Analysis of Speed/Power Trials. This draft guideline, along with a list of suggested modifications to other ITTC procedures, will be passed to the next Committee.

11.3.6 Verification and Validation of CFD methods for seakeeping

Continue to create a guideline on Verification and Validation (V&V) of the CFD methods for seakeeping analysis, taking into account the findings and recommendations of the 30th Seakeeping Committee. Collaborate with the Specialist Committee on Combined CFD/EFD Methods and taking existing procedures for verification and validation of CFD methods into account.

The work of the current (30th) Seakeeping committee has shown that drafting a guideline for V&V of CFD methods for seakeeping is a substantial task involving many complex issues.

11.3.7 On-board and real time data collection

Continue to monitor the state of the art for the acquisition and analysis in on-board and/or real-time seakeeping data. Assess the implications on ITTC activities, including future issues related to autonomous vessels.

12. REFERENCES

Acharya, A., De Chowdhury, S., Peerali Paloth, F. and Datta, R., 2023, "Numerical investigation of bottom slamming using one and two way coupled methods of S175 hull", Applied Ocean Research.

Ahn, I-G. and Jung, B-H., 2022. "Hydroelastic Effect on the Ultimate Strength Assessment of Very Large Ore Carrier based on the Segmented Model Test", International Journal of Offshore and Polar Engineering, 3 (4), pp. 487-494.

Ahn Y. and Kim Y., 2021, "Data Mining in Sloshing Experiment Database and Application of Neural Network for Extreme Load Prediction," Marine Structures, 80, 103074.

Ahn Y., Lee J., Park T. , Kim Y., Kwon C. S. ,. Jung J. H, Gwan Choi M., and Kim S.-Y., 2023, "Long-term Approach for Assessment of Sloshing Loads in LNG Carrier, part I: Comparison of short- and long-term Approaches," Marine Structures, 89, 103381.

Ahn Y., 2023, "Sloshing Loads Estimation using a Genetic Programming", OMAE2023 Melbourne, Australia, OMAE2023-104632.

Almallah, I., Ali-Lavroff, J., Holloway, D. and Davis, M., 2021, "Slam Load Estimation for High-Speed Catamarans in Irregular Head Seas by Full-Scale Computational Fluid Dynamics", Ocean Engineering, 234, 109160.

Almallah, I., Ali-Lavroff, J., Holloway, D. and Davis, M., 2022. "Estimation of Torsional and Global Loads for a Wave-Piercing High-Speed Catamaran at Full-Scale in Irregular Bow Quartering Seas Using CFD Simulation", Ocean Engineering, 266, 113006.

Antolik, J. T., Belden, J. L., Speirs, N. B. and Harris, D. M., 2023, "Slamming forces during water entry of a simple harmonic oscillator", Journal of Fluid Mechanics, 974, A23.

Barabadi, S., Iranmanesh, A., Passandideh-Fard, M. and Barabadi, A., 2023, "A numerical study on mitigation of sloshing in a rectangular tank using floating foams", Ocean Engineering, 277, 114267.

Cepowski, T., 2023, "The use of a set of artificial neural networks to predict added resistance in head waves at the parametric ship design stage", Ocean Engineering, 281, 114744.

Chatzimarkou, E., Michailides, C. and Onoufriou, T., 2022. "Performance of a coupled level-set and volume-of-fluid method combined with free surface turbulence damping boundary condition for simulating wave breaking in OpenFOAM." Ocean Engineering 265, 112572.

Chen, B., Sun, S., Incecik, A., Hou, X. and Ren, H., 2023. "Investigation on wave-body interactions by a coupled High-Order Spectrum method with fully nonlinear Rankine source method". Ocean Engineering 288, 115941.

Chen, D., Feng, X., Hou, C. and Chen, J.-F., 2022. "A coupled frequency and time domain approach for hydroelastic analysis of very large floating structures under focused wave groups". Ocean Engineering 255, 111393.

Chen, D., Yao, X., Huang, D. and Huang, W., 2024. "A multi-resolution smoothed particle hydrodynamics with multi-GPUs acceleration for three-dimensional fluid-structure interaction problems". Ocean Engineering 296, 117017.

Chen, H.-C. and Chen, C.-R., 2023. "CFD Simulation of a container ship in random waves using a coupled level-set and volume of fluid method". Journal of Hydrodynamics 35 (2), 222-231.

Chen, J., Duan, W., Ma, S. and Li, J., 2021. "Time domain TEBEM method of ship motion in waves with forward speed by using impulse response function formulation". Ocean Engineering 227, 108617.

Chen, X. and Wu, Y., 2021, "Model Experimental Research of Wave and Slamming Load of Ship Hull with Bottom Sonar Opening", Proc. ISOPE Rhodes, Greece.

Cho, J. H., Lee, S. H., Oh, D., and Paik, K. J. (2023). "A numerical study on the added resistance and motion of a ship in bow quartering waves using a soft spring system". Ocean Engineering, 280, 114620.

Coslovich, F., Kjellberg, M., Ostberg and M., Janson C.E., 2021, "Added resistance, heave and pitch for the KVLCC2 tanker using a fully nonlinear unsteady potential flow boundary element method", Ocean Engineering, 229, 108935

Dempwolff, L.-C., Windt, C., Bihs, H., Melling, G., Holzwarth, I. and Goseberg, N., 2024. "Hydrodynamic coupling of multi-fidelity solvers in REEF3D with application to ship-induced wave modelling". Coastal Engineering 188, 104452.

Di Mascio, A., Marrone, S., Colagrossi, A., Chiron, L. and Le Touzé, D., 2021. "SPH–FV coupling algorithm for solving multi-scale three-dimensional free-surface flows". Applied Ocean Research 115, 102846.

Diez, M., Serani, A. and Stern, F., 2022, "A Data Clustering Approach to Identifying Slamming Types in Irregular Waves", Proc. 9th International Conference on Hydroelasticity in Marine Technology, Rome, Italy.

Dogrul, A., Kahramanoglu, E. and Cakici, F., 2021, "Numerical prediction of interference factor in motions and added resistance for Delft catamaran 372", Ocean Engineering, 223, 108687

Duan, W., Tang, S. and Chen, J., 2022a. "Power and speed prediction of KVLCC2 in head waves based on TEBEM." Ocean Engineering 249, 110811.

Duan, W., Yang, K., Huang, L., Jing, Y. and Ma, S., 2022b, "A DFN-based method for fast prediction of ships' added resistance in heading waves", Ocean Engineering, 245, 110484

Duan, F., Ma, N., Gu, X., and Zhou, Y., 2023. "An Improved Method for Predicting Roll Damping and Excessive Acceleration for a Ship With Moonpool Based on Computational Fluid Dynamics Method." Journal of Offshore Mechanics and Arctic Engineering, 145 (5), 051401.

van Essen, S.M., Monroy, C., Shen, Z., Helder, J., Kim, D.H., Seng, S. and Ge, Z., 2021. "Screening wave conditions for the occurrence of green water events on sailing ships", Ocean Engineering, 234, 109218.

Faltinsen, O.M. and Timokha, A.N., 2021. "Coupling between Resonant Sloshing and Lateral Motions of a two-dimensional Rectangular Tank", Journal of Fluid Mechanics, 916, p. A60.

Feng, S., Zhang, G., Wan, D., Jiang, S., Sun, Z. and Zong, Z., 2021. "On the treatment of hydroelastic slamming by coupling boundary element method and modal superposition method", Applied Ocean Research, 112, 102595.

Ferro, P., Landel, P., Pescheux, M. and Guillot, S., 2022. "Development of a free surface flow solver using the Ghost Fluid Method on OpenFOAM". Ocean Engineering 253, 111236.

Fu., Z., Li, Y., Gong, J. and Dai, K., 2021a. "Study on Pitch-Roll Coupled Motion Characteristics of Trimaran in Oblique Stern Wave", Proc ISOPE, Rhodes, Greece.

Fu, Z., Li, Y., Gong, J., Zhang, D. and Li, A., 2021b. "Effect of sailing directions on the coupled motion and stability of trimaran in waves", Ocean Engineering, 240, 109955.

Gerhardt F.C. and Kjellberg, M., 2017. "Determining the EEDI 'Weather Factor' fw" RINA, Influence of EEDI on Ship Design and Operation, London, UK.

Gilbert, C., Javaherian, M. J., Woolsey, C. and Shepheard, M., 2023, "Virginia tech advanced towing carriage", Journal of Engineering for the Maritime Environment, IMechE.

Hanssen, F.-C.W. and Greco, M., 2021. "A potential flow method combining immersed boundaries and overlapping grids: Formulation, validation and verification". Ocean Engineering 227, 108841.

Hasheminasab, H., Zeraatgar, H., Malekmohammadi, J. and Azizi, A., 2022. "Analysis of slamming loads on a catamaran section with a centre-bow appended by spray rail", Ships and Offshore Structures.

He, J., Yang, C.-J., Zhu, R.-C., Noblesse, F., 2023. "Alternative flow models, vector Green functions and boundary integral flow representations in ship and offshore hydrodynamics". Ocean Engineering 270, 113630.

Himabindu, A. and Groper, M., 2023. "Speed–Wave Height Operational Envelope for High-Speed Planing Craft in Seaways: Theoretical vs. Empirical Methods", Ship Technology Research, 70 (1): 46–55.

Hong, Y., Heo, K. and Kashiwagi, M., 2021. "Hydroelastic analysis of a ship with forward speed using orthogonal polynomials as mode functions of Timoshenko beam", Applied Ocean Research, 112, 102696.

Hosseinzadeh, S. and Tabri, K., 2021. "Hydroelastic effects of slamming impact Loads During free-Fall water entry", Ships and Offshore Structures,. 16, 68-84.

Htay, W. N., Magari, A., and Toda, Y., 2021. "A Study on the Performance of Rudder Bulb Fins System of KVLCC2 in Regular Head Waves". Proc. ISOPE.

Huang, S., Jiao, J., and Chen, C., 2021a. "CFD prediction of ship seakeeping behavior in bi-directional cross wave compared with in uni-directional regular wave". Applied Ocean Research, 107, 102426.

Huang, W., He, T., Yu, J., Wang, Q., and Wang, X., 2021b. "Direct CFD Simulation and Experimental Study on Coupled Motion Characteristics of Ship and Tank Sloshing in Waves". OMAE2021-63775.

Igbadumhe J.-F., Bonoli J., Dzielski J., and Fürth M., 2023. "Coupled FPSO Roll Motion Response and Tank Sloshing in a pair of two Row Cargo Tanks," Ocean Engineering, 278, 114273.

IMO, 2012, "Interim Guidelines for the Calculation of the Coefficient f_w for Decrease in Ship Speed in a Representative Sea Condition for Trial Use", IMO Circular MEPC.1/Circ.796.

Irannezhad, M., Eslamdoost, A., Kjellberg, M. and Bensow, R.E., 2022. "Investigation of ship responses in regular head waves through a Fully Nonlinear Potential Flow approach". Ocean Engineering 246, 110410.

Islam, H., and Soares, C. G., 2022. "Head Wave Simulation of a KRISO Container Ship Model Using OpenFOAM for the Assessment of Sea Margin". Journal of

Offshore Mechanics and Arctic Engineering, 144(3), 031902.

Jagite, G., Bigot, F., Derbanne, Q., Malenica, Š., Le Sourne, H. and Cartraud, P., 2021. "A parametric study on the dynamic ultimate strength of a stiffened panel subjected to wave- and whipping-induced stresses", Ships and Offshore Structures, 16 (9), 1025-1039.

Jain, U., Novaković, Bogaert, H. and van der Meer, D., 2022 "On wedge-slamming pressures", Journal of Fluid Mechanics, 934, A27.

Javanmard, E., Mehr, J., Ali-Lavroff, J., Holloway, D. and Davies, M. 2023. "An experimental investigation of the effect of ride control systems on the motions response of high-speed catamarans in irregular waves". Ocean Engineering, 281, 114899.

Jawa, S. and Minoura, M., 2023. "Validation of short-term prediction of added resistance in head seas considering wave steepness nonlinearity with probability density function method", Ocean Engineering, 278, 114353

Jiao, J., Huang, S., Tezdogan, T., Terziev, M. and Soares, C.G., 2021a. "Slamming and green water loads on a ship sailing in regular waves predicted by a coupled CFD–FEA approach". Ocean Engineering 241, 110107.

Jiao, J., Huang, S., Wang, S. and Soares, C.G., 2021b. "A CFD–FEA two-way coupling method for predicting ship wave loads and hydroelastic responses". Applied Ocean Research 117, 102919.

Jin, S., Tosdevin, T., Hann, M. and Greaves, D., 2022. "Experimental study on short design waves for extreme response of a floating hinged raft wave energy converter", 37th International Workshop on Water Waves and Floating Bodies, Giardini Naxos, Italy.

Katayama, T., Yamaguchi, K., Nanami, T., Umeda, J., Ozeki, S., Soga, M. and Watanabe, T., 2022, "Calculation of Hydrodynamics Forces Acting on Prismatic Planing Surface by CFD", Proc. PRADS, Dubrovnik, Croatia.

Kim, B.W., Kim, H-S., Lee. K., Hong, S.Y., 2023a. "Comparison of Wave Force Calculation Methods in Time Domain Hydro-elastic Analysis of Floating Body", Proc. ISOPE, pp. 19-23.

Kim, S., Bouscasse, B., Ducrozet, G., Delacroix, S., De Hauteclocque, G. and Ferrant, P., 2023b. "Experimental investigation on wave-induced bending moments of a 6,750-TEU containership in oblique waves", Ocean Engineering, 284, 115161.

Kim, T., Yoo, S. and Kim, H.J., 2021. "Estimation of added resistance of an LNG carrier in oblique waves", Ocean Engineering, 231, 109068.

Kim, Y.R., Esmailian, E. and Steen, S., 2022. "A meta-model for added resistance in waves", Ocean Engineering, 266, 112749

Kobayashi, H., Kume, K., Orihara, H., Ikebuchi, T., Aoki, I., Yoshida, R. and Mizokami, S., 2021. "Parametric study of added resistance and ship motion in head waves through RANS: Calculation guideline". Applied Ocean Research, 110, 102573.

Koo B., Auburtin E. and Kim H., 2021. "Sloshing Effects on FLNG and LNGC side-by-side Offloading", OMAE2021-63778.

Koop, A., Crepier, P., Loubeyre, S., Dobral, C., Yu, K., Xu, H. and Huang, J. 2021. "Development and Verification of Modeling Practice for CFD Decay Calculations to Obtain Roll Damping of FPSO". OMAE2021-62411.

Korobkin, A.A. and Khabakhpasheva, T.I., 2022. "Three-Dimensional Hydroelastic

Impact onto a Floating Circular Plate", Proc. 9th Int. Conference on Hydroelasticity in Marine Technology, pp.79-88.

Lau, C.Y., Ali-Lavroff, J., Holloway, D., Dashtimanesh, A. and Mehr, J., 2023a. "Ride-Control Systems Geometries on a High-Speed Catamaran Using a CFD Forcing Function Method", Proc. 13th Symp. on High Speed Marine Vehicles, Progress in Marine Science and Technology, IOS Press.

Lau, C.Y., Ali-Lavroff, J., Holloway, D., Mehr, J. and Thomas, G., 2023b. "Influence of an active T-foil on motions and passenger comfort of a wave-piercing catamaran based on sea trials in oblique seas", Proc. Institution of Mechanical Engineers, Part M: Journal of Engineering for the Maritime Environment, 237 (1), 83-95,

Lau, C.Y., Ali-Lavroff, J., Holloway, D., Shabani, B., Mehr, J. and Thomas, G., 2022. "Influence of an Active T-Foil on Motions and Passenger Comfort of a Large High-Speed Wave-Piercing Catamaran Based on Sea Trials", Journal of Marine Science and Technology, 27 (2).

Lee, J., Kim, Y., Ahn, Y., 2022a. Hydroelastic Responses of LNG CCS due to Sloshing Loads I: Hydrodynamic Impact due to Different Liquids and Gases, Proc. of 9th International Conference on Hydroelasticity in Marine Technology, pp. 63-70.

Lee, J., Kim, Y., Kim, B.S., Gerhardt, F., 2021a. "Comparative study on analysis methods for added resistance of four ships in head and oblique waves", Ocean Engineering, 236, 109552.

Lee, S. H., Paik, K. J., Hwang, H. S., Eom, M. J., and Kim, S. H., 2021b. "A study on ship performance in waves using a RANS solver, part 1: Comparison of power prediction methods in regular waves". Ocean Engineering, 227, 108900.

Lee, S. H., Paik, K. J., and Lee, J. H., 2022b. "A study on ship performance in waves using a RANS solver, part 2: Comparison of added resistance performance in various regular and irregular waves". Ocean Engineering, 263, 112174.

Lee, J. and Kim, Y., 2023. "Development of enhanced empirical-asymptotic approach for added resistance of ships in waves", Ocean Engineering, 280, 114762.

Li, A., Yan, F. and Zhang, Y., 2023a. "Influence of Wave Amplitude on the Characteristics of Coupled Motion of a Trimaran Equipped with T-Foil in Oblique Head Waves", Proc. ISOPE, Ottawa, Canada.

Li, C., Duan, W.-y. and Zhao, B.-b., 2022a. "Breaking wave simulations for a high-speed surface vessel with hybrid THINC and HRIC schemes". Applied Ocean Research 125, 103257.

Li, J., Duan, W., Chen, J., Ma, S. and Zhang, Y., 2022b. "A study on dynamic trim optimization of VLCC oil tanker in wind and waves", Ocean Engineering, 253, 111270.

Li, M., Pan, S., Cheng, Y., Yuan, Z.-M. and Tao, L., 2023b. "Time-domain numerical simulation for multi-ships moving in waves with forward speed". Ocean Engineering 290, 116325.

Li, Z., Bouscasse, B., Ducrozet, G., Gentaz, L., Le Touzé, D. and Ferrant, P., 2021. "Spectral wave explicit navier-stokes equations for wave-structure interactions using two-phase computational fluid dynamics solvers". Ocean Engineering 221, 108513.

Li, J., Liu, L., Zhang, Z., Wang, L., and Yao, X., 2022c. "Numerical Study on Vertical Motions of a Destroyer With Different Speeds in Extreme Seas". OMAE2022-78652.

Li, J., Chen, J., Yu, J., Liu, L., and Zhang, Z., 2023c. “CFD prediction for the extreme roll motion of ONR Tumblehome in beam waves”. Proc. ISOPE.

Liang, S., Gou, Y. and Teng, B., 2023. “The nonlinear wave interaction with a two-dimensional large-scale floating elastic plate”. Ocean Engineering 282, 115046.

Liao, K., Duan, W., Ma, Q., Ma, S. and Yang, J., 2021. "Numerical Simulation of Green Water on Deck with a Hybrid Eulerian-Lagrangian Method”", Journal of Ship Research.

Lin, Z., Qian, L., Bai, W., Ma, Z., Chen, H., Zhou, J.-G. and Gu, H., 2021. “A finite volume based fully nonlinear potential flow model for water wave problems”. Applied Ocean Research 106, 102445.

Liu, D., Li, F. and Liang, X., 2022a. “Numerical study on green water and slamming loads of ship advancing in freaking wave”. Ocean Engineering, 261, 111768.

Liu, H., Xiong, Y., Xu, H. and Gao, S., 2021a. “Experimental and Numerical Investigation of Slamming on Wedges with Different Stiffened Panels”, Proc. ISOPE, Rhodes, Greece.

Liu, K., Liu, Y., Li, S., Chen, H., Chen, S., Arikawa, T. and Shi, Y., 2023a. “Coupling SPH with a mesh-based Eulerian approach for simulation of incompressible free-surface flows”. Applied Ocean Research 138, 103673.

Liu, L., Feng D., Wang X., Zhang Z., Yu J., and Chen M., 2022b. “Numerical Study on the Effect of Sloshing on Ship Parametric Roll,” Ocean Engineering, 247, 110612.

Liu, S. and Papanikolaou, A., 2020. “Regression analysis of experimental data for added resistance in waves of arbitrary heading and development of a semi-empirical formula”. Ocean Engineering, 206.

Liu, S. and Papanikolaou, A., 2023. “Improvement of the prediction of the added resistance in waves of ships with extreme main dimensional ratios through numerical experiments”, Ocean Engineering, 273, 113963.

Liu, W.-T., Zhang, A.-M., Miao, X.-H., Ming, F.-R. and Liu, Y.-L., 2023b. “Investigation of hydrodynamics of water impact and tail slamming of high-speed water entry with a novel immersed boundary method”, Journal of Fluid Mechanics, 958, A42.

Liu Z., Yuan K., Liu Y., Andersson M., and Li Y., 2022c. “Fluid Sloshing Hydrodynamics in a Cryogenic Fuel Storage Tank under Different Order Natural Frequencies,” Journal of Energy Storage, 52, 104830.

Lu, L., Ren, H., Li, H., Zou, J., Chen, S. and Liu, R., 2023a. “Numerical method for whipping response of ultra large container ships under asymmetric slamming in regular waves”, Ocean Engineering, 287, 115830.

Lu, X., Dao, M.H. and Le, Q.T., 2022a. “A GPU-accelerated domain decomposition method for numerical analysis of nonlinear waves-current-structure interactions”. Ocean Engineering 259, 111901.

Lu, Y., Shao, W., Gu, Z., Wu, C., and Li, C., 2022b. “Study on the influence of cross wave on ship motion characteristics based on computational fluid dynamics”. Proc. ISOPE.

Lu, L., Ren, H., Li, H., Zou, J., Chen, S. and Liu, R., 2023b. “Numerical method for whipping response of ultra large container ships under asymmetric slamming in regular waves”. Ocean Engineering, 287, 115830.

Lyu, W., el Moctar, O. and Schellin, T.E., 2022. "Ship motion-sloshing interaction with forward speed in oblique waves", Ocean Engineering, 250, 110999.

Ma C., Xiong C., and Ma G., 2021. "Numerical Study on Suppressing Violent Transient Sloshing with Single and Double Vertical Baffles", Ocean Engineering, 223, 108557.

Ma, S., Duan, W., Cao, Z., Liu, J., Zhang, M., Li, X. and Liu, D., 2023. "Experimental study on the drop test on wet deck slamming for a SWATH segment model", Ocean Engineering, 285, 115377.

Ma, Y. and Zhu, Q., 2022. "Fast Trimaran Anti-Longitudinal Motion Control System Based on Active Disturbance Rejection Control with Controller Tuning", Journal of Marine Science and Technology, 27 (2).

Mahfoze O.A., Liu W, Longshaw S.M., Skillen A. and Emerson D.R., 2022. "On the Efficiency of Turbulence Modelling for Sloshing", Applied Sciences. 12 (17):8851.

Mai, T.L., Vo A.K., Cho, A. and Yoon, H.K., 2023. "Experimental Study of Wave-Induced Motions and Loads on Catamaran in Regular and Irregular Waves", Proc. ISOPE, Ottawa, Canada.

Malas, B., Creasey, L., Buckland, D., and Turnock, S. R., 2024. "Design, Development and Commissioning of the Boldrewood Towing Tank – A decade of endeavour", Int. J. Maritime Engineering, RINA.

Marin-López, J.R., Villamarín, E., Mendoza, J., Paredes, R. and Datla, R., 2021. "Conceptual Design Recommendations to Improve Seakeeping of Small High-Speed Craft Providing Interisland Transportation in Galápagos", SNAME Int. Conf. Fast Sea Transportation (FAST), Providence, Rhode Island, USA,

Marlantes, K. and Maki, K., 2022. "A Neural-Corrector Method for Prediction of the Vertical Motions of a High-Speed Craft", Ocean Engineering, 262, 112300.

Martinez-Carrascal J. and Gonzalez-Gutierrez L., 2021. "Experimental Study of the Liquid Damping Effects on a SDOF Vertical Sloshing Tank," J. Fluids and Structures, 100, 103172.

Mittendorf, M., Nielsen, U.D., Bingham, H.B. and Liu, S., 2022. "Towards the uncertainty quantification of semi-empirical formulas applied to the added resistance of ships in waves of arbitrary heading", Ocean Engineering, 251, 111040.

Mittendorf, M., Nielsen, U.D., Bingham, H.B. and Dietz, J., 2023, "Assessment of added resistance estimates based on monitoring data from a fleet of container vessels", Ocean Engineering, 272, 113892

Molaemi, A. H., Bredmose, H., Ghadirian, A. and Kristiansen, T., 2023. "Cylinder water entry on a perturbed water surface", Journal of Fluid Mechanics, 965, A16.

Nielsen, U. D., Brodtkorb, A. H., Iseki, T., Jensen, J. J., Mittendorf, M., Mounet, R. E. G., Sørensen, A. J. and Takami, T., 2023. "Estimating Waves Through Measured Ship Responses", International Workshop on Water Waves and Floating Bodies.

Nordforsk, 1987, "Assesment of Ship Performance in a Seaway", The Nordic co-operative project: Seakeeping Performance of Ships, ISBN 87-982637-1-4.

Pal, S.K., Ono, T., Takami, T., Tatsumi, A. and Iijima, K., 2022. "Effect of springing and whipping on exceedance probability of vertical bending moment of a ship", Ocean Engineering 266, 112600.

Paredes, R., Gaona, A., Toala, A., Marín López, J., Datla, R., and Pratt, J., 2022. "Zero-Emission Small High-Speed Craft Conceptual Design using NSGA-II Algorithm for Galapagos Interisland Service", HIPER 2022, Cortona, Italy.

Park, C., Lee, J. and Kim, Y.. 2022. "Hydroelastic Responses of LNG CCS due to Sloshing Loads II: Structural Responses due to Different Impact Patterns", Proc 9th International Conference on Hydroelasticity in Marine Technology, pp. 71-78.

Park, H.J. and Nam, B.W., 2023. "Prediction of Green Water Events for FPSO in Irregular Waves using ANN Model", Int. Workshop on Water Waves and Floating Bodies.

Park, M. and Lee, P-S., 2022. "Non-matching Mesh Treatment in Hydro-elastic Analysis", Proc. 9th Int. Conference on Hydroelasticity in Marine Technology, pp. 359-365.

Park, M. and Lee, P-S., 2023. "Integrated hydrostatic and hydrodynamic analysis of flexible floating structures", Ocean Engineering, 288, 114945.

Park, Y., Hwangbo, S.M., Yu, J.W., Cho, Y., Lee, J.H. and Lee, I., 2023. "Development of a small-sized tanker with reduced greenhouse gas emission under in-service condition based on CFD simulation", Ocean Engineering, 286, 115588.

Qian, Y. and Teng, B., 2023. "A finite element-scaled boundary finite element coupled method for corner singularities in 2D second-order radiation problems". Ocean Engineering 281, 114910.

Remmerswaal, R.A., Veldman, A.E.P. Ronald A. R. and Arthur E. P. V., 2022. "On Simulating Variability of Sloshing Loads in LNG Tanks", OMAE2022-81105.

Riesner, M. and el Moctar, O., 2021. "A numerical method to compute global resonant vibrations of ships at forward speed in oblique waves", Applied Ocean Research, 108, 102520.

Saincher, S. and Sriram, V., 2022. "A three-dimensional hybrid fully nonlinear potential flow and Navier Stokes model for wave structure interactions". Ocean Engineering 266, 112770.

Salis, N., Hu, X., Luo, M., Reali and A., Manenti, S., 2024. "3D SPH analysis of focused waves interacting with a floating structure". Applied Ocean Research 144, 103885.

Sanada, Y., Kim, D. H., Sadat-Hosseini, H., Stern, F., Hossain, M. A., Wu, P. C., and Grigoropoulos, G., 2022. "Assessment of EFD and CFD capability for KRISO Container Ship added power in head and oblique waves". Ocean Engineering, 243, 110224.

Sebhatleb, G., Holloway, D. and Ali-Lavroff, J., 2023. "Slam and Wave Load Response Reconstruction in High Speed Catamarans Using Transmissibility on Full Scale Sea Trials", Ocean Engineering, 271, 113822.

Shi, K.-y. and Zhu, R.-c., 2023. "A fully nonlinear approach for efficient ship-wave simulation". Journal of Hydrodynamics 35 (6), 1027-1040.

Silva, D.F.C., Menezes, F.G.T., Schmidt, D. and Mello, P.C., 2023. "Slamming Effects on FPSO Balconies: Numerical and Experimental Analysis of Alternative Configurations for Impact Attenuation", OMAE2023-105066.

Smith J.R., Gkantonas S. and Mastorakos E., 2022. "Modelling of Boil-Off and Sloshing Relevant to Future Liquid Hydrogen Carriers". Energies. 15 (6):2046.

Song, X., Zhang, X. and Beck, R.F., 2022. "Numerical study on added resistance of ships based on time-domain desingularized-Rankine panel method". Ocean Engineering 248, 110713.

Spinosa, E. and Iafrati, A., 2022. "Analysis of the Fluid-Structure Interaction during the Water Entry of a Flat Plate at High Horizontal Speed", Proc. 9th Int. Conference on Hydroelasticity in Marine Technology.

Spyrou, I. T. and Papadakis, G., 2021. Numerical investigation on the effect of bilge keels in ship roll damping, Proc. 1st Int. Conference on the Stability and Safety of Ships and Ocean Vehicles, Glasgow, Scotland, UK. Proc. 1st Int. Conference on the Stability and Safety of Ships and Ocean Vehicles, Glasgow, Scotland, UK.

Stern, F., Sanada, Y., Park, S., Wang, Z., Yasukawa, H., Diez, M., Quadvlieg, F. and Bedos, A., 2022. "Experimental and CFD Study of KCS Turning Circles in Waves", 34 th Symp. on Naval Hydrodynamics, Washington, DC, USA.

Subramaniam, S., Umeda, N., Matsuda, A. and Maki, A., 2021. "Experimental study on the water-on-deck effect for an offshore supply vessel running in regular and irregular stern quartering waves", Proc. 1st Int. Conference on the Stability and Safety of Ships and Ocean Vehicles, Glasgow, Scotland, UK.

Sun, J. Y., Sun, S. L., Sun, S. Z., and Ren, H. L. 2023. "The impact of piston and sloshing motions on added resistance from moonpool configurations". Ocean Engineering, 267, 113179.

Suzuki, K, Iwashita, H., Kashiwagi, M., Wakahara, M., Iida, T. and Minoura, M., 2023. "Temperature interference in improved FBG pressure sensor for towing tank test", Journal of Marine Science and Technology, 28:351, 369.

Takami, T., Fujimoto, W., Houtani, H. and Matsui, S., 2023. "Combination of HOSM and FORM for extreme wave-induced response prediction of a ship in nonlinear waves". Ocean Engineering 286, 115643.

Tao, Y., Zhu, R., Gu, J., Li, Z., Zhang, Z., and Xu, X. 2023. "Experimental and numerical investigation of the hydrodynamic response of an aquaculture vessel". Ocean Engineering, 279, 114505.

Tang, S.Q., Zhang, Y., Sun, S.L. and Ren, H.L., 2021a. "Experimental Study on the Double-Slamming of a Trimaran Cross Section in Vertical Free Fall Motion". Proc. ISOPE, Rhodes, Greece.

Tang, Y., Sun, S.-L. and Ren, H.-L., 2021b. "Numerical investigation on a container ship navigating in irregular waves by a fully nonlinear time domain method". Ocean Engineering 223, 108705.

Tang, Y., Sun, S. L., Yang, R. S., Ren, H. L., Zhao, X. and Jiao, J. L., 2022. "Nonlinear bending moments of an ultra large container ship in extreme waves based on a segmented model test", Ocean Engineering, 243, 110335.

Tao, Y., Zhu, R., Gu, J., Li, Z., Zhang, Z. and Xu, X., 2023, "Experimental and numerical investigation of the hydrodynamic response of an aquaculture vessel", Ocean Engineering,. 279, 114505.

Tavakoli, S., Babanin, A., and Hirdaris, S., 2023a. "Hydroelastic Analysis of Hard Chine Sections Entering Water—Observations for Use in Preliminary Design Stage", Journal of Offshore Mechanics and Arctic Engineering, 145 (5), 051901.

Tavakoli, S., Mikkola, T. and Hirdaris, S., 2023b. ”A fluid–solid momentum exchange method for the prediction of hydroelastic responses of flexible water entry problems”, J. Fluid Mech, 965, A19.

Tian C, Si H. L., Zhou Q. Y., Lu Y., Cheng X. M., Ye Y. L. and Wu Y. S., 2022. “Investigation on Modal Characteristics of Test Models of Ultra Large Containership for Hydroelastic Responses”, Proc. 9th International Conference on Hydroelasticity in Marine Technology, pp.29-40.

Vijith P.P. and Rajendran, S., 2023. “Hydroelastic effects on the vertical bending moment of a container ship in head and oblique seas”, Ocean Engineering, 285, 115385.

Wang, A., Pan Wong, K., Yu, M., Kiger, K. T. and Duncan, J. H., 2022a. "The controlled impact of elastic plates on a quiescent water surface", Journal of Fluid Mechanics, 939, A4.

Wang, G., Wu, Q., Chen, M., Xie, Y. and Yu, H., 2022b. “Investigation on the Slamming of Wedge-Shaped Body with Oblique Free Entry into Water” Proc. ISOPE, Shanghai, China.

Wang, H., Chen, J., Duan, W. and Shan, M, 2022c. “Time-domain TEBEM for Hydroelastic Responses of a Container Ship with Forward Speed”, Proc. PRADS, pp. 1884-1895.

Wang, H., Duan, W., Chen, J., Ma, S., 2023a. “A numerical method to compute flexible vertical responses of containerships in regular waves”, Ocean Engineering, 266, 112828.

Wang, J., Wang, W., and Wan, D. 2023b. “Study of Self-Propulsion Performance of a Single-Screw Ship in Waves Based on Improved Propeller Body Force Model”. Proc. ISOPE.

Wang, S., Kim, B., Zhu, Z., and Kim, Y. 2022d. “CFD Predictions on Ship Performance in Waves Using OpenFOAM Solver”. Proc. ISOPE.

Wang, S., Kim, B. S., Zhu, Z., Choi, J. H., and Kim, Y. 2023c. “OpenFOAM-Based Computation of Added Resistance in Head and Oblique Seas”. Proc. ISOPE.

Wang, W., Pákozdi, C., Kamath, A. and Bihs, H., 2021a. “A fully nonlinear potential flow wave modelling procedure for simulations of offshore sea states with various wave breaking scenarios”. Applied Ocean Research 117, 102898.

Wang, Y., Jiang, S. and Zhou, T., 2023d. “Experimental Investigation On Response Of Ship Rolling Motion Coupled With Liquid Sloshing”, OMAE2023-104423.

Wang Z., Jiang M., and Yu Y., 2021b, “Nonlinear Behaviours of Three-Dimensional Sloshing in the LNG Elastic Tank”, OMAE2021-61679.

Wei, Y., Incecik, A., Tezdogan, T., 2023. “A hydroelasticity analysis of a damaged ship based on a two-way coupled CFD-DMB method”. Ocean Engineering 274, 114075.

Wei, Y. and Tezdogan, T., 2022. “A Fluid-Structure Interaction Model on the Hydroelastic Analysis of a Container Ship Using preCICE”, OMAE2022-78131.

Wu, J., Sun, Z., Jiang, Y., Zhang, G. and Sun, T., 2021. "Experimental and numerical study of slamming problem for a trimaran hull", Ships and Offshore Structures, 16 (1), 46-53.

Wu, S., Liu, L., Wang, X., Chen, J., and Wang, L. 2022. “Study of wavelength effect on the parametric roll in head waves”. Proc. ISOPE.

Xie, C.-M., Yang, J.-C., Sun, P.-N., Lyu, H.-G., Yu, J. and Ye, Y.-L., 2023. “An accurate and

efficient HOS-meshfree CFD coupling method for simulating strong nonlinear wave–body interactions". Ocean Engineering 287, 115889.

Xu, W., Zhang, J. and Zhong, M., 2023a. "A Sliding Mode Predictive Anti-Pitching Control for a High-Speed Multihull", Ocean Engineering 285, 115466.

Xu, Y., Bingham, H.B., Shao, Y., 2023b. "A high-order finite difference method with immersed-boundary treatment for fully-nonlinear wave–structure interaction". Applied Ocean Research 134, 103535.

Yang, K., Duan, W., Huang, L., Zhang, P., Ma, S., 2022. "A prediction method for ship added resistance based on symbiosis of data-driven and physics-based models", Ocean Engineering, 260, 112012.

Yasukawa, H. and Enui, K., 2021. "Effect of Pitch Moment of Inertia on Added Resistance of Container Ship in Waves", Journal of the Japan Society of Naval Architects and Ocean Engineers, 33.

Yu, J., Yao, C., Liu, L., Feng, D., and Wang, X., 2023a. "Application of virtual disk propulsion model for self-propelled surface ship in regular head wave". J. of Marine Science and Technology, 28(2), 471-495.

Yu, J., Yao, C., Wang, J., Liu, L., Dong, G., and Zhang, Z., 2023b. "Numerical study on motion responses and added resistance for surge-free KCS in head and oblique waves based on the functional decomposition method". Ocean Engineering, 285, 115300.

Yu, J.W., Kim, S.G., Jeong, W., Kim, Y.I., Choi, J.E. and Lee, I., 2022. "Prediction of resistance and propulsion performances using calm-water and resistance tests in regular heave waves of a 1,800 TEU container ship", Int. J. Naval Architecture and Ocean Engineering, 14, 100458

Zhang, H., Yuan, Y., Tang, W., Xue, H., Liu, J. and Qin, H., 2021a. "Numerical analysis on three-dimensional green water events induced by freak waves", Ships and Offshore Structures.

Zhang, J., Liu, Z., Dai, X. and Li G., 2021b. "Robust Decoupled Anti-Pitching Control of a High-Speed Multihull", Journal of Marine Science and Technology, 26 (4), 1112–25.

Zhang, N., Yan, S., Ma, Q. and Zheng, X., 2021c. "A QSFDI based Laplacian discretisation for modelling wave-structure interaction using ISPH". Applied Ocean Research 117, 102954.

Zhang, N., Yan, S., Ma, Q., Guo, X., Xie, Z. and Zheng, X., 2023a. "A CNN-supported Lagrangian ISPH model for free surface flow". Applied Ocean Research 136, 103587.

Zhang, Y., Reliquet, G., Bouscasse, B., Gentaz, L. and Le Touzé, D., 2021d. "Numerical investigation on the added resistance and seakeeping performance of KVLCC2 with the SWENSE method". Journal of Ship Research 65 (04), 362-379.

Zhang, X., Gu, X., and Ma, N., 2021e. "Comparative Study on Eddy Roll Damping with Experimental Results Using a High-order Fractional Step Finite Volume Solver". International Journal of Offshore and Polar Engineering, 31 (02), 199-209.

Zhang, X., Song, X. and Beck, R.F., 2023a. "Numerical investigations on seakeeping and added resistance in head waves based on nonlinear potential flow methods". Ocean Engineering 276, 114043.

Zhang, Z., Ma, N., Lin Y., Gu, X. and Shi, Q., 2022. "Experimental Study on Non-Linear Wave Loads of a Ship Model with Variable

Cross-section Backbone in Irregular Waves", Proc. ISOPE, pp. 2315-2322.

Zhang, Z., Yang, J., Zhang, H., Zou, Z. and Zhang, X., 2023b. "Numerical study on mean wave drift forces and moment of ships using Rankine panel method in frequency domain". Ocean Engineering 283, 114986.

Zhang, Z.-L., Sun, S.-L., Chen, B.-Y. and Ren, H.-L., 2024. "Numerical investigation of a semi-submersible platform interacting with steep waves using a fully nonlinear method". Ocean Engineering 294, 116755.

Zhao, J., Zhu, R. and Zhou, W., 2022. "Implementation of a velocity decomposition method coupled with volume-of-fluid method for simulating free-surface flows". Ocean Engineering 263, 112339.

Zheng, Jh., Xue, M.A. and Dou, P., 2021a. "A Review on Liquid Sloshing Hydrodynamics". J Hydrodynamics 33, 1089–1104.

Zheng, L., Liu, Z., Zeng, B., Meng, H. and Wang, X., 2023b. "Experimental and Numerical Study on Heave and Pitch Motion Calculation of a Trimaran", J. Marine Science and Technology, 28 (1):136–52.

Zheng, M., Ni, Y., Wu, C. and Jo, H., 2021b." Experimental investigation on effect of sloshing on ship added resistance in head waves", Ocean Engineering, 235, 109362.

Zheng, Y., Yiew, L., Jin, Y., Ravindra, K., and Magee, A. R., 2023c. "Experimental and numerical study on seakeeping performance of a benchmark ASD tug in head seas". Ocean Engineering, 272, 113800.

Zhong, S.-Y., Sun, P.-N., Peng, Y.-X., Liu, N.-N., Lyu, H.-G. and Huang, X.-T., 2023. "An SPH study of slamming and splashing at the bow of SYSU vessel". Ocean Engineering 269, 113581.

Zhong, W.-j., Wang, W.-t. and Wan, D.-c., 2022. "Coupling potential and viscous flow models with domain decomposition for wave propagations". J. Hydrodynamics 34 (5), 826-848.

Zhu, Z., Lee, J., Kim, Y., Lee, J. and Park, T., 2021, "Experimental measurement and numerical validation of sloshing effects on resistance increase in head waves". Ocean Engineering, 234.

Zhuang, Y. and Wan, D.-c., 2021. "Parametric study of a new HOS-CFD coupling method". Journal of Hydrodynamics 33, 43-54.